Università degli Studi di Firenze

DOTTORATO DI RICERCA IN
"*Spettroscopia atomica e molecolare*"

CICLO XXIV

COORDINATORE Prof. Francesco Pavone

Absorption Enhancement by Light Scattering for Solar Energy Applicaions

Settore Scientifico Disciplinare FIS /03

Dottorando
Dott. Mupparapu Rajeshkumar

Tutore
Prof. Wiersma Diederik

Anni 2009/2013

Contents

Abstract

In this thesis, I discuss few novel approaches to enhance the light-matter interaction, which have applications in solar energy. Enhancement of absorption/fluorescence is a topic of immense interest in recent years for its importance in various fields: bio-sensing and diagnostics, solar energy, imaging, forensics, etc.. Often, applications involving fluorescence are quite low efficient, and which is mainly attributed to poor fluorescence from constituent fluorescent molecules. Enhancing fluorescence of molecules can enable to realize very efficient applications. And, one such application which needs attention is Luminescent solar concentrator, which is a main topic of discussion in this thesis. Luminescent solar concentrators (LSCs) are polymer slabs filled with fluorescent molecules which absorb incoming sunlight and emit fluorescence inside the slab, and which is partially guided to the edges where photovoltaic cells are attached.

Poor absorption/fluorescence of organic molecules is due to their intrinsic chemical structure, due to which either they display huge non-radiative decay losses or poor absorption efficiency, etc.. It is well know that the amount of light emitted by molecules also depends on their surrounding medium properties. Modifying the surrounding environment very close to the molecules can actually modify the intrinsic fluorescence properties of molecules. This idea has been applied quite a lot to modify the properties of molecules close to metallic nanostructures/nanoparticles. When it comes to enhance the fluorescence of molecules embedded in polymer slabs like LSCs all existing approaches fail to work. In thesis, I discuss elaborately, in particular answering following questions: *why existing approaches fail to work, essentially what kind of approaches are needed, and how they should be implemented.*

The basic structure of my thesis is organized as follows:

Chapter 1 : Light-matter interaction is introduced at first, particularly light scattering is discussed with three different perspectives: Light scattering in disordered media, ordered media and with metal nanoparticles. Light scattering behaviour in a collection of particles which are either arranged in order or in disorder can give some interesting phenomena, and have relevance in approaches to enhance the absorption of fluorescent molecules in a bulk volume. Furthermore, light-matter interaction at nanoscale using plasmonic nanostructures is discussed.

Chapter 2 : In this chapter, at first, properties of fluorescent molecules are discussed elaborately. Working principle of luminescent solar concentrators

is introduced, and followed by a broad discussion on its efficiency. Various issues which lower the efficiency of LSCs and some very well known strategies pursued to enhance the absorption of fluorescent molecules are discussed.

Chapter 3 : This chapter is devoted to discuss on experimental and numerical results of the enhancement of UV absorption by using resonant scattering of aluminum nanoparticles. In this chapter, a novel approach is proposed by using path length enhancement of light in a UV absorbing media using resonant scattering of aluminum nanoparticles. This was realized in a way to keep the transparency of the system at a high value and achieve the enhancement effect over a bulk volume. This approach is simple, cost effective, and scalable. This approach can help to realize transparent luminescent solar concentrators.

Chapter 4 : This chapter discusses elaborately on the path length enhancement approach demonstrated in the chapter 3. Numerical and analytical results of path length enhancement studied in different scattering regimes are presented. A simple theory formulated using probability distribution functions to estimate the maximum path length enhancement that can be obtained in a weakly scattering regime is presented, and which found to validate the results of Monte Carlo simulations. Similarly, results of Monte Carlo simulations in diffusive regime were compared with a known diffusion theory, which found to have a good agreement.

Chapter 5 : In this chapter, I discuss a novel approach to engineer the dispersion of an LSC slab patterned with a design of fractal in a way that its absorption is enhanced and its transport properties are improved. This approach mainly tries to achieve the increment of photons coupling in to an LSC slab in a spectral region where fluorescent molecules absorb, and decrement of photons coupling out of the slab in a spectral region where fluorescent molecules emit. Results of frequency domain calculations are presented which reveal the presence of defect states, strong confinement of fields at frequencies of the defect modes. Furthermore, results of mode dynamics in k-space for various frequencies are presented.

1

Introduction to Light scattering

Interaction of wave with matter is a omnipresent process. In particular, light interaction with matter is something we come across every day in our lives. Understanding, and ability to control light-matter interaction is a topic of tremendous interest in various fields. Interaction of light with matter occurs mainly in two forms: scattering and absorption. In this chapter, light scattering with matter consisting of particles arranged in different geometries is introduced.

Interaction of light with matter occurs all around. Light coming from the sun is lost in thick clouds, low visibility during the winter due to fog and smoke affects all forms of traffic, change in colour of opals and butterfly wings with the angle of observation, colours of flowers and vegetation, etc., and all these phenomenon are some simple manifestations of light scattering and absorption by matter that we come across in our daily lives. Light attenuation through any medium with inhomogeneities occurs by scattering and absorption, and together referred as extinction. The study of light extinction and its applications is a vast field, and has been pursued with many perspectives in various fields including astronomy, atmospheric science, oceanography, biomedical diagnostics, photonics, solar energy, etc..

1.0.1 Scattering

Light extinction in a medium with inhomogeneities can be better described by looking at an elementary picture of light interaction with a single inhomogeneity/object. The interaction of light with a single particle may be very complicated. To a first approximation an object of arbitrary shape and size

is conceptually divided into smaller regions. Applying electric field induces a dipole moment in each of those small regions. Thereby, each smaller region acts as a source of secondary wavelets and emits secondary radiation in the new form of electromagnetic radiation in all directions. The interaction between electromagnetic field and inhomogeneity can be either elastic or non-elastic, whereas in elastic interaction no frequency change occurs, while in a non-elastic interaction some amount of light may be converted in the form of heat or in to other forms of energy. This elementary picture of single scattering can be extended to explain the extinction of light with objects like dust grain, blood, metallic object, smog, water molecules, particulate in ocean, etc.. and whose knowledge has significant relevance in many fields. Since the laws of electromagnetic waves can be scaled, so the theories and principles of transport of waves of any wavelength can be relevant for light transport or vice versa.

The size of the scatterer is an important aspect in the study of single scattering phenomenon, since it is crucial to know whether the light with a certain wavelength is able to resolve the object in its path. Theories of Rayleigh scattering [1] and Mie scattering [2, 3] can explain the scattering properties of particles of dimensions smaller and comparable to the wavelength of light.

The Rayleigh scattering theory is valid for the particles of dimensions much smaller than the wavelength of light. The amount of Rayleigh scattering that occurs for a beam of light mainly depends on the size of the particles and the wavelength of light. The intensity scattered from the dipole scatterers at a particular wavelength towards an observer is given by

$$I = I_0 \left(\frac{8\pi^4 N a^6}{\lambda^4 r^2} \right) \left| \frac{m^2 - 1}{m^2 + 2} \right|^2 (1 + cos^2\,\theta), \tag{1.1}$$

where I_0 is the incident intensity of light received by the particle, r is the distance between the particle and the observer, θ is the scattering angle, m is the refractive index of the particle, a is the diameter of the particle, and N is the number of particles. The Rayleigh scattering intensity clearly indicates a strong dependence on the wavelength(λ) of light and the size of the particle.

The extinction properties of particles with dimensions smaller, or larger or comparable to the wavelength of light can be accurately determined by the Mie solutions to the Maxwell's equations solved for spherical particles [2, 3]. Mie scattering theory has been applied also to study the extinction properties of stratified spheres [4], and infinite cylinders [3], etc..

Using the theories of Rayleigh and Mie scattering, it is possible to explain various aspects related to the sky. The particles present in the atmo-

sphere have dimensions much smaller than the visible light wavelengths, so their scattering can be accurately described by Rayleigh scattering. Since the Rayleigh scattering is more effective at shorter wavelengths, blue light is strongly scattered in the atmosphere towards the earth than the rest of the wavelengths in the visible range, which tells why the sky appears blue in colour. While at the sunset, sun rays make a long path through the atmosphere, light of all shorter wavelengths is scattered out, except the red portion of the sunlight remains less scattered and reaches the earth surface. Another noticeable aspect of light scattering in the sky is the whiteness of clouds. Clouds constitute of water droplets of dimensions comparable to the visible light wavelengths, so according to the Mie scattering theory, scattering efficiency of water droplets follow a smooth wavelength dependence, which gives them a white appearance.

The scattering properties of particles of dimensions much larger than wavelengths can be explained by the principles of ray optics. Inside the particle, light beam can be approximated as a ray. This approximation explains many phenomenon like the formation of rainbows to the whispering gallery modes in a microsphere [5].

1.1 Light interaction with disordered media

Nature of light scattering in a disordered medium can be explained by the scale of observation. Two parameters are considered as yardsticks for the scale of observation: size of the scatterer(R), and wavelength(λ). When the size of the scatterer is very small compared to the wavelength ($R \ll \lambda$), light propagating through the medium can not resolve the scatterer in its path, hence undergo weak scattering or no scattering. Whereas, if the size of the scatterer is comparable to the wavelength ($R \leq \lambda$), so the wave can resolve the scatterer and undergo scattering. However locally it appears that scattering might be weak, but the direction of light will be randomized over a large distance of travel due to the multiple scatterings with other scatterers in its path.

1.1.1 Single scattering

In a collection of particles, if particles are randomly separated by very long distances, such that each particle is located in the far field of the other particles and no systemic phase relation exists between their scattered fields, so the field exposed by a particle from the rest of the particles is negligible compared to the incident field. This also implies that the light propagating

in the medium is scattered only once with a single particle before exiting out the system. This is known as single scattering approximation [6]. The field detected in the far-field is simply the incident field.

1.1.2 Multiple scattering

When the collection contains many more particles closely packed enough, single scattering approximation is no longer valid. The light undergoes multiple scattering with different particles, eventually escapes out of the collection. The scattering in such medium is typically defined by a characteristic length called scattering mean free path l_s, which is an average distance travelled by light between two scattering events, which is meaningful only if defined with respect to the size of the system. If the scattering mean free path is extremely small compared to the size of the system, then the scattering would be very strong in such medium, where light hardly travels in the forward direction. If scattering mean free path is longer than the system size, then the scattering is considered as weak scattering. The light multiply scattered from different particles interfere constructively and destructively, generates a far field known as speckle that fluctuates in space and time. Explicit measurements of speckle are quite complicated to take into account of the fluctuations of space and time, hence spatial and temporal properties are measured over a interval of time longer than the time scale over fluctuations occur, and over many disorder realizations. In general, average behaviour of the transport of light intensity is considered in terms of random walk to describe the multiply scattered light instead of highly complex wave transport.

Strength of the disorder on an average can be decided by a characteristic length called transport mean free path l_t, which is an average distance travelled by photons in a disordered medium before their direction is being randomized and light looses correlation with its initial characteristics completely. Transport mean free path is given by:

$$l_t = \frac{l_s}{1 - \langle cos\,\theta \rangle}, \tag{1.2}$$

where $\langle cos\,\theta \rangle$ is the average cosine of the scattering angle, typically referred as anisotropy factor(g). If the anisotropy factor is positive it implies that maximum scattering occurs in the forward direction, if negative it occurs in the back ward direction. For an isotropic scattering, anisotropy factor becomes zero so the transport mean free path is same as the scattering mean free path.

Coherent light illuminated on a disordered medium spreads slowly with time inside the medium and completely loses correlation with its initial di-

rection of propagation, this is known as a diffusive transport. The concept of diffusion is familiar to us from the fields of transport of gases and heat, etc.. Light propagation through the clouds, opaque media, milk are some every day examples where we come across light diffusion.

It is possible to express the diffusive transport in simple terms like energy density(ρ) at a position $\mathbf{r}$ in space and at time t. The diffusion equation is given by

$$\frac{d\rho(\mathbf{r},t)}{dt} = D \bigtriangledown^2 \rho(\mathbf{r},t), \tag{1.3}$$

where D is the diffusion constant, measured in m^2/s and is related to the parameters of the microscopic transport of light in a three dimensional disordered medium by the following equation:

$$D = \frac{1}{3} v l_t, \tag{1.4}$$

where v is the velocity of energy transport [7]. Taking Fourier transform($\mathfrak{F}$) of the (1.3) with respect to spatial coordinates gives

$$\frac{\partial \mathfrak{F}}{\partial x}\left[\rho(\mathbf{r},t)\right] = -D\mathbf{k}^2 \mathfrak{F}\left[\rho(\mathbf{r},t)\right]. \tag{1.5}$$

Simplifying the expression (1.5) we get

$$\mathfrak{F}[\rho(\mathrm{r},\mathfrak{t})] = Ae^{-D\mathfrak{t}\mathbf{k}^2}, \tag{1.6}$$

where A is an arbitrary constant to be determined by applying boundary conditions. Transforming the Fourier transform in (1.6) back in to the real space, and imposing the boundary condition $\rho(\mathbf{r}, t=0) = \rho_0 \delta(r)\delta(t)$, and we get

$$\rho(\mathrm{r},t) = \rho_0 \frac{1}{\sqrt{4\pi D t}} e^{-\frac{\left|\mathrm{r}^2\right|}{4Dt}}. \tag{1.7}$$

Hence obtained propagator(probability amplitude) of the energy density follows Gaussian distribution function, whose width is given by the mean square displacement $\langle x^2(t)\rangle$ of photons at a given point of time(t). The cloud of photons propagating through a diffusive medium spreads linearly with time:

$$R \simeq \langle \mathbf{r}^2(t)\rangle = \int \mathbf{r}^2 \rho(\mathbf{r},t)\ \mathrm{d}\mathbf{r} = 2\rho_0 D t. \tag{1.8}$$

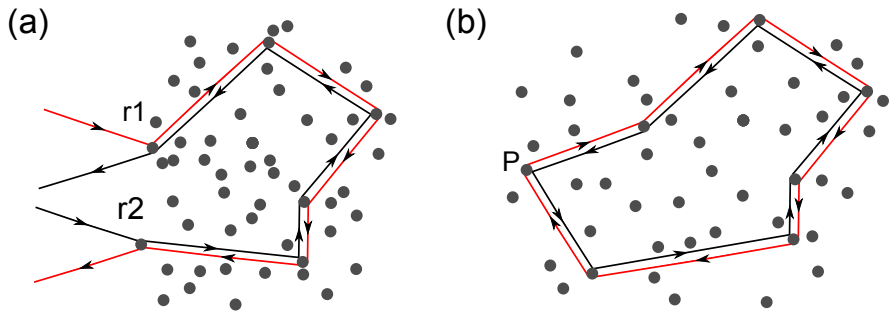

Figure 1.1: (a) Illustration of enhanced back scattering effect. Optical paths entering at **r1** and exiting at **r2**(red path), and vice versa(black path) respectively, interferes constructively leading to a enhanced back scattering effect. (b) Illustration of Anderson localization: Photons making time reversal reciprocal paths in a strongly scattering medium interfere constructively, thus create a localized state.

As mentioned earlier, multiply scattered light interfere constructively and destructively that generates a speckle pattern in the far field, clearly indicating the preserved coherence upon multiple scattering. The speckle pattern depends on the arrangement of particles, however during the averaging process all the inferences are averaged out, and the interference contribution only in the backward direction survives. The light following reciprocal multiple scattering paths in the collection of particles interference constructively and cause a enhanced back scattering, so called as coherent back scattering effect [8]. Illustration of reciprocal loops which give back scattering effect is shown in the Fig. 1.1(a). The average intensity in the back scattering is observed to be twice the diffused intensity.

When the scattering mean free path relative to the system size is decreased, photons tend to return to their initial position. Increase of the return probability of photons essentially reduces the net transport in the forward direction, as a result the diffusion constant decreases. Normally return probability is very small. When the disorder is further increased beyond a limit(decreasing the scattering mean free path relative to the size of the system), light tends to return to its initial position and interferes constructively with the counter propagating waves, due to which light is localized strongly inside system, thus brings the transport of light to a complete halt, this effect is known as Anderson localization. Mechanism of localization by time reversal loops in a 3D system is illustrated in the Fig. 1.1(b). Enhanced back scattering effect discussed in the previous paragraph, is a precursor of Anderson localization, so it is also called as weak localization.

Localization was hypothesized by P.W. Anderson actually in electronic

systems [9]. Anderson predicted that transition from metal to insulator occurs due to the interference of electronic waves in disordered metallic lattice, thereby suppressing the diffusion completely. Localization creates exponentially confined modes randomly across the medium. The same effect was later demonstrated in other spectral ranges like ultra sound [10], light [11]. Demonstrating the localization effect is bit lesser complicated in optical range since photons do not interact with each other unlike in electrons. In contrary, obtaining the same scattering strength in dielectric materials as in electronic case is a challenge.

To obtain the localization in a three dimensional sample, transport mean free path must be of the order of the wavelength of light in the medium, subject to Ioffe-Regel criterion [12]

$$kl_t \leq 1, \tag{1.9}$$

where k is the wave vector. In the Anderson localization regime, all the waves are localized in an infinite medium. For a finite sized system, modes leak out of the system, as a result diffusion constant scales with the size of the system.

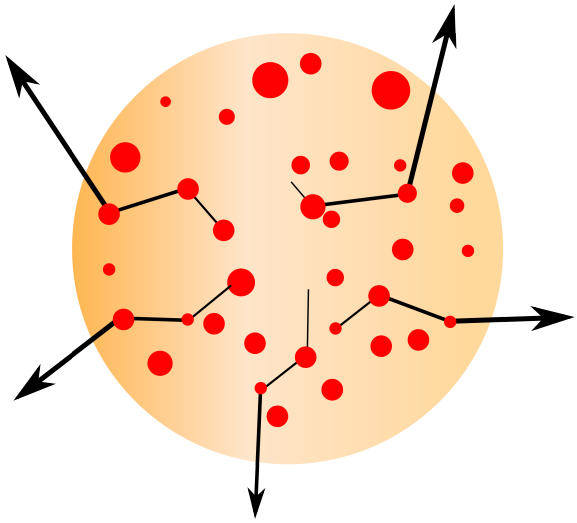

Figure 1.2: Random laser action in a disordered active medium. In random laser, multiple light scattering provides the necessary optical feedback into the gain medium.

One of the most fascinating application of multiple scattering of light is random lasing. Unlike in conventional lasers, a random laser uses optical feedback provided by the multiple scattering in the random media [13],

whose general mechanism is illustrated in the Figure. 1.2. The speckle pattern obtained as a result of interferences in a random media determines the mode structure of random laser. Above the threshold, emission of a random laser narrows down and starts showing narrow spikes, and the modes with a maximum gain obtain maximum intensity. Random lasing was found in a materials of different scattering strengths, with kl_t values ranging from 10 to 10^4 [14, 15, 16], which suggests that both extended and localized modes in random media can support random lasing. Random lasing is a phenomenon that shows how the rich the physics of disordered media.

Local density of states (LDOS) describes the available modes supported by a index modulated structure. The spontaneous emission of emitters placed in a disordered medium is decided by its local density of states, which varies from position to position in the medium, as a result strong fluctuations can be observed in the spontaneous emission of emitters [17]. And, these fluctuations in spontaneous emission can be used as a tool to probe the local environment [18].

1.2 Light interaction with periodic media

Controlling the transport of electrons in the semiconductors has enabled to create wonders of electronics, where the band gap is manipulated in a desired manner. The band gap of semiconductors is attributed to the periodic potential of the lattice structure. In the advent of photonics field, there is a strong interest in recreating efficient photonic devices similar to the counterparts of electronic devices. Periodic potential can be realized also for photons by modulation of refractive index at a scale where light can resolve. Periodic arrangement of objects like sphere, cylinder, and rods of dimensions of the order of wavelengths can give a collective response very different from their individual Mie scattering behaviour. In fact such an arrangement of fundamental scattering units result into complex photonic structures called "Photonic crystals". Light makes multiple reflections and refractions inside the periodically index modulated structures, hence undergoes destructive interference which affect the propagation of electromagnetic waves through them. The properties of the photonic crystals are quite similar to the semiconductors, so the concepts of condensed matter physics are usually extended to explain the geometry and light behaviour in such systems.

Depending on the direction of index modulation, photonic crystals of one, two and three dimensions can be constructed. The illustration of the periodic arrangement of scattering units(combination of high and low index objects)in one, two and all the three directions is shown in the Fig. 1.3. In a

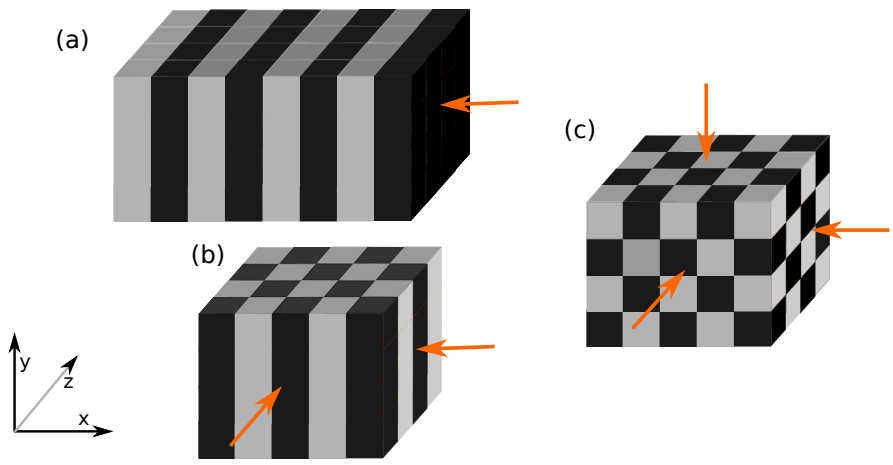

Figure 1.3: The illustration of the scattering units arranged in one, two and three directions.(a) One dimensional photonic crystal (b) two dimensional photonic crystal (c) three dimensional photonic crystal.

one dimensional photonic crystal, when the period is half of the wavelength of light in the medium, Bragg diffraction occurs. The incident light along the periodicity direction will be reflected back with nearly 100% efficiency. One of the key consequence of Bragg diffraction is the iridescence from photonic crystals, on account of which, their colour changes sharply for different angles of observation.

Similarly, in two and three directions, if the refractive index contrast is big enough and the absorption is negligible, the scattering at the dielectric interface can lead to the formation of frequency ranges where the propagation of light is inhibited in some particular directions. Those frequency ranges are called as photonic band gaps(PBGs), analogous to the electronic band gaps of the semiconductors.

Three dimensional photonic crystals provide much greater flexibility to control the light propagation in all three directions. If the refractive contrast is large enough, three dimensional photonic crystals can have a complete photonic band gap, in a frequency range where the light is forbidden to propagate in any direction. The first example of a complete band gap material was reported by Yablonovitch *et al.* in the microwave wavelengths [19]. In order to shift the band gap to optical and telecom wavelengths, structures must be modulated at a sub-micron scale which require sophisticated fabrication techniques. Woodpiles and Opal structures of silicon are two such robust geometries of 3D photonic crystals which were shown to demonstrate complete band gap in optical wavelengths [20, 21].

Opals are fabricated by a self assembly of polymer spheres. This method involves aggregation of nano spheres, which after being driven to the growing surface by gravity, relax to attain a minimum potential energy. Thus obtained structures display a face centered cubic geometrical ordering. In order to increase the refractive index contrast, initially opals are fabricated with polymer nano spheres, later, either its voids are replaced with silicon and then followed by removing spheres, or polymer is replaced with silicon, using multi step chemical processing technique. Opals suffer from various kinds of disorder effects like formation of domains, cracks, polydispersity of spheres, void defects, etc.. Low cost fabrication makes opals as more promising photonic crystals.

Woodpiles structure was first proposed by Ho *et al* [22]. The geometry of the woodpiles facilitates to tune the band gap in a desired manner. The band gap of woodpiles is expected to be quite robust against the intrinsic disorder due to its connected structure. Woodpiles structure have been fabricated with techniques like layer by layer assembly [23], and Direct laser writing(DLW) [24], out of which latter is most suited for the current geometry.

Figure 1.4: Photonic crystal geometries found in nature:(start from top-left: clockwise) (a) butter fly, (b) peacock feather, (c) opal, (d) Chrysochroa vittata.

Light can be alternatively confined in three dimensions using 2D photonic crystals which are fabricated on a slab. These slab structures consists of a 2D photonic crystal at the core, and surrounded by layers of lower refractive index. Light is confined in the slab by index guiding in the third dimension, and in plane by photonic band gap due to the photonic crystals. Photonic crystal slab configuration reduces the need for a periodicity in the third dimension [25].

Understanding of periodic geometry's ability to mold the light propagation can not be simply explained from the Mie scattering of individual scatterers, instead requires a rigorous approach. Of course starting point lies with the Maxwell's equations. As presented in the [26], a very general master equation

$$\bigtriangledown \times \left[\frac{1}{\epsilon(\mathbf{r})} \bigtriangledown \times \mathbf{H}\right] = \frac{w^2}{c^2}\mathbf{H}(\mathbf{r}) \tag{1.10}$$

can be derived for a macroscopic medium, with a position dependent dielectric constant $\epsilon(\mathbf{r})$. The master equation represents an eigenvalue problem where the operator $\bigtriangledown \times \frac{1}{\epsilon(\mathbf{r})} \bigtriangledown \times$ is an hermitian and positive definite quantity(for real $\epsilon > 0$).

Photonic crystals display discrete translational symmetry due to the periodicity, so their dielectric function corresponds to $\epsilon(\mathbf{r}) = \epsilon(\mathbf{r} + \mathbf{R})$ for any primitive lattice vector $\mathbf{R}$ that is an integral multiple of lattice constant a. Which is called as Bloch state. Bloch theorem states that the Bloch states with wave vector k and $k+m2\pi/a$ are identical and therefore same frequency $w(k) = w(k + 2m\pi/a)$. Hence, the dispersion diagram is periodic in the k direction with a period equal to the reciprocal vector of the lattice $\mathrm{G} = 2\pi/a$. To investigate the dispersion properties of photonic crystals, we can restrict ourselves to one period, called as irreducible Brillouin zone. For an each value of the wave vector k inside the Brillouin zone, there exist an eigenstate of Θ with frequency $w(\mathrm{k})$ and an eigenvector $\mathrm{H_k}$ of the form

$$\mathbf{H_k}(\mathbf{r}) = e^{i(\mathbf{k}.\mathbf{r})}.\mathbf{u_k}(\mathbf{r}), \tag{1.11}$$

where $\mathbf{u_k}(\mathbf{r})$ is a periodic function on the lattice: $\mathrm{u_k}(\mathbf{r}) = \mathrm{u_k}(\mathbf{r} + \mathbf{R})$ for all primitive lattice vectors $\mathbf{R}$.

For each value $\mathbf{k}$, we can expect infinite set of modes with discretely separated frequencies, which are referred as bands. As $\mathbf{R}$ varies continuously, its frequency also vary continuously. The family of continuous functions $w(\mathbf{k})$ arranged in the increasing order of frequency for different values of $\mathbf{k}$ with in the irreducible Brillouin zone is called as band structure.

Photonic band structure contains complete information of expected optical properties of photonic crystals. A gap with in the frequency bands at a particular wave vector **k** is called as pseudo gap, whereas a gap in the bands for all wave vectors is called as complete photonic band gap.

Photonic crystals constitute a perfect platform where light can be molded and controlled at will by proper engineering of its geometry. Introducing structural defects like cavity inside the photonic crystal can create a defect state inside the photonic band gap. It is possible to confine light in a single defect plane in one dimension, in a line defect in two dimensions, and localize in a small volume at a single point defect in three dimensions. The light associated with the frequency and wave vector of the defect state confine spatially at the position of the defect. By proper engineering of the geometry of the cavity, it is possible to modify the strength of the light confinement in the cavity. The efficiency of a cavity is characterized by the quality factor $Q = w/\Delta w$, and the mode volume of the cavity. Maximal mode volume of the order of cubic wavelength can be obtained for a cavity.

In the vicinity of band gaps strong deviation of dispersion can be observed. The bands become flatter close the band edge, which results in a decrease of group velocity in effect light propagation slows down. Slow light has numerous applications which include enhancement of linear and non-linear effects(higher harmonic generation [27], wave mixing [28]), and also enable to realize controllable optical delay lines [29], etc..

A photonic band structure is geometrically represented by its iso frequency curves. Iso frequency curves for a normal dielectric medium are spherical in shape, while for the photonic crystals they are bit distorted in shape. Normal to the iso frequency curves represent the direction of group velocity. Self collimation occurs where the iso frequency curves are flat [30]. Another important feature of the photonic crystals is super prism effect [31], which occurs where the iso frequency curves are sharply curved.

1.3 Light interaction with plasmonic nanostructures

The optical properties of the noble metals are governed by their conduction electrons and can be well described by their complex dielectric function. The interaction of electromagnetic waves with the metal surfaces causes collective oscillation of their spatially bounded surface electrons called surface plasmons. The coupling state of photons with the surface plasmons is so called as surface plasmon polaritons(SPPs) [32].

Strong electron density oscillations that occur on the metal-dielectric interface leads to a strong enhancement of the electric field close to the metal surface, and those electric fields stay confined very close to the surface. Where as in metal nanoparticles, electron gas is strongly confined in the three dimensions and exhibit localized surface plasmon resonances(LSPR). As a result of the interaction of external field with the electrons inside the metal nanoparticle, an opposite field is created to cancel the effect of external electric field, in such manner dipole moment is induced. The resonance condition with the external radiation is attained when the frequency of photons matches with the natural frequency of the plasmons acted upon by the restoring force due to the induced dipole moment. Creation of surface plasmons in metal nanoparticles depend upon the geometrical parameters of the nanoparticles.

Propagation and behaviour of the SPPs in metals is mainly decided by their complex permittivity and of their surroundings. LSPR of metal nanoparticles generally occur when the real part of the complex permittivity of metal ε_m is equal to $-2\,\varepsilon_s$, where ε_s is the real permittivity of the surrounding medium. Usually three different noble metals are considered, namely silver, gold and aluminum. Complex permittivities of gold, silver and aluminum calculated using a freely available code based on the model described in [33] are shown in the Figure. 1.5, suggesting that plasmon resonances of gold, silver occur in the visible range at 535 nm, 420 nm and aluminum in the ultra-violet range at 192 nm.

Extinction properties of nanoparticles: Mie theory

The scattering of a plane wave with a homogeneous sphere can be well described by the formal solutions of Maxwell's equations solved with the appropriate boundary conditions [2, 3]. The formal solutions of the scattering problem are derived by considering the incident and scattered fields as radiating spherical wave functions, incident field as regular wave functions and using proper boundary conditions for the tangential and normal components of the fields at the interface of the sphere. The Mie scattering coefficients a_n and b_n of a sphere of radius R embedded in a medium of refractive index n_s, are given by

$$a_n = \frac{\psi_n'(y)\psi_n(x) - m\psi_n(y)\psi_n'(x)}{\psi_n'(y)\zeta_n(x) - m\psi_n(y)\zeta_n'(x)}, \tag{1.12}$$

$$b_n = \frac{m\psi_n'(y)\psi_n(x) - \psi_n(y)\psi_n'(x)}{m\psi_n'(y)\zeta_n(x) - \psi_n(y)\zeta_n'(x)}, \tag{1.13}$$

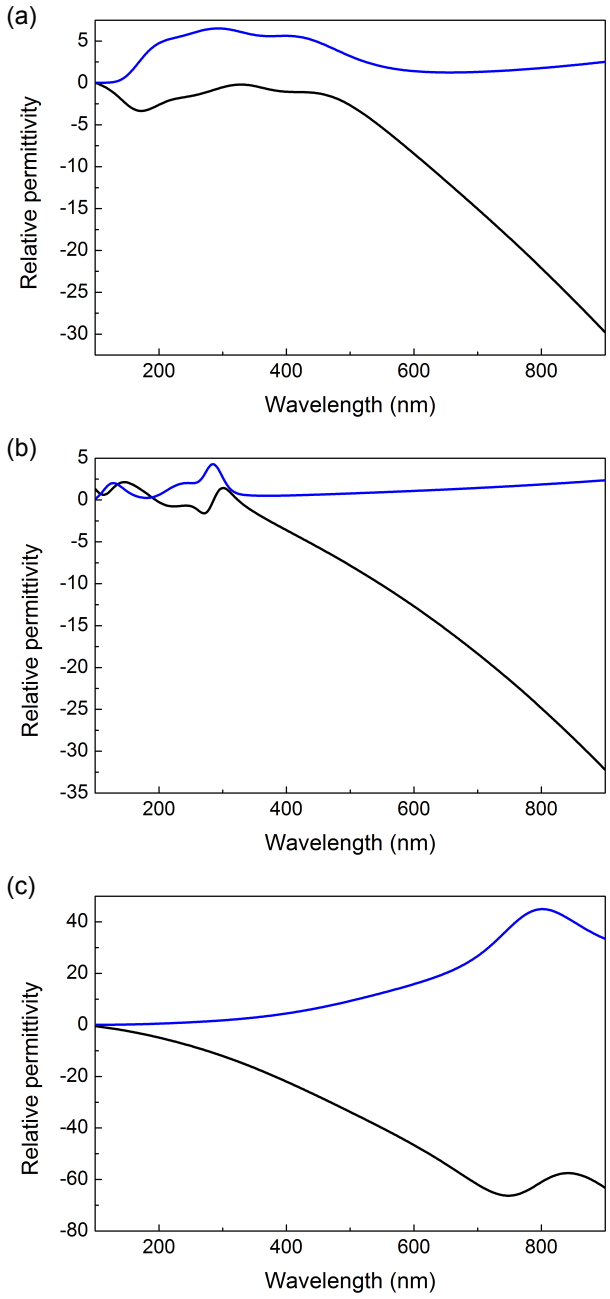

Figure 1.5: Real (black) and imaginary (blue) permittivities of noble metals (a) gold, (b) silver, and (c) aluminum. Surface plasmon resonant frequency range of these metals is determined by finding the frequency at which the real part of complex permittivity of a metal is equal to the -2 times the permittivity of the surrounding medium.

where ψ_n and ζ_n are Ricatti-Bessel functions, m = n_i/n_e, x = kR, y = mkR and **k** is the free space wave vector. The extinction, scattering, and absorption efficiencies of the spherical nanoparticles, represent the ratios of effective cross-section and geometric cross-section of the particle(πR^2)and refractive index n_i, embedded in a medium of refractive index n_e:

$$Q_{ext} = \frac{2}{x^2}\sum(2n+1)[\Re(a_n + b_n)], \tag{1.14}$$

$$Q_{sca} = \frac{2}{x^2}\sum(2n+1)[|a_n|_2 + |b_n|_2], \tag{1.15}$$

$$Q_{abs} = Q_{ext} - Q_{sca}. \tag{1.16}$$

Spectral properties of metal nanoparticles of diameter 20 nm in vacuum are calculated using Mie theory, see in Fig. 1.6. It can be inferred from the figures that the extinction of gold and silver nanoparticles is dominated by their absorption component over the scattering component, while the aluminum nanoparticles have strong extinction, and also have equal contribution from both scattering and absorption. The relative contribution of absorption and scattering depends on the metal and on the size of the nanoparticles. Plasmon resonances of larger nanoparticles shift towards the longer wavelengths, and their extinction is significantly dominated by scattering component. The scattering component is measure of the extent to which the plasmons can radiate into the far field.

1.4 Conclusions

Light interaction with matter results in to various forms of energy like scattering, absorption, heat, luminescence, etc.. and which depends on the size of the particles, material, local environment, arrangement of particles, etc.. In particular, scattering by particles of dimensions comparable to the wavelengths of light holds the key to control the light in a desired way by their arrangement, whether it is disorder or order. Surface plasmon resonances of nanostructures/nanoparticles take the light interaction to much smaller scale, confine the light strongly in a small volume, thus provide the route to enhance the interaction of light with matter.

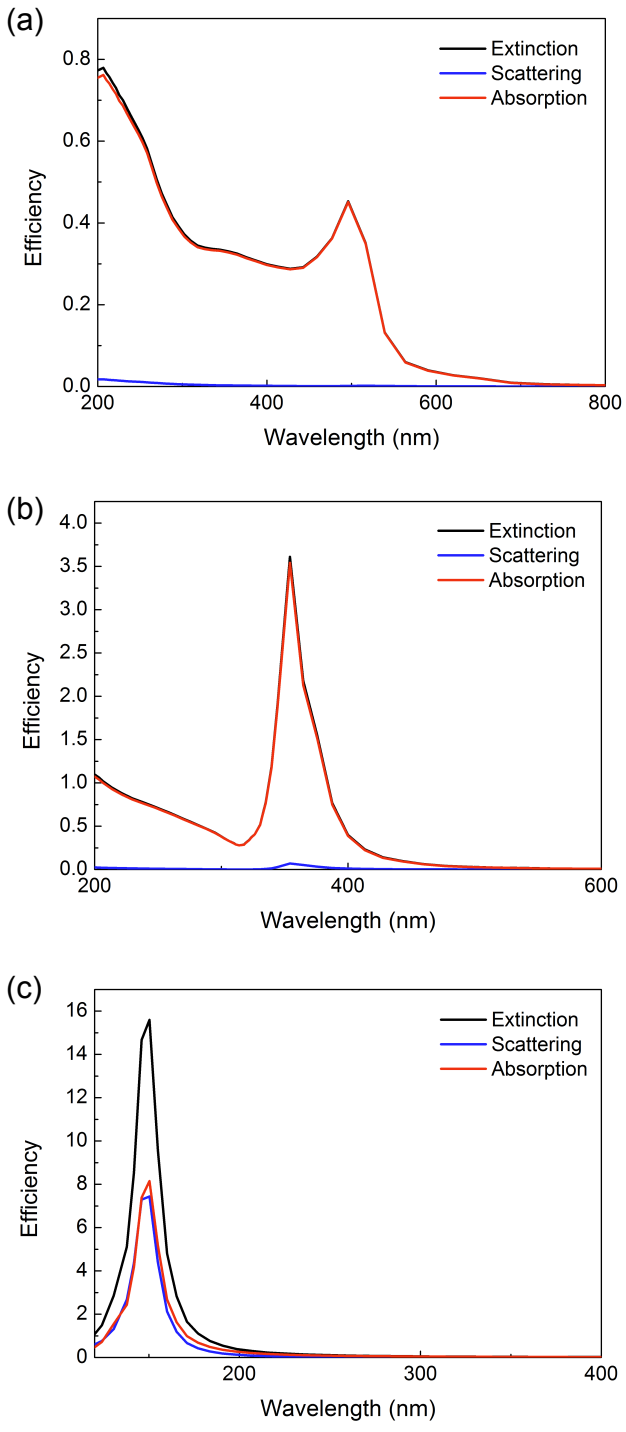

Figure 1.6: Extinction properties of (a) gold (b) silver and (c) aluminum nanoparticles of diameter 20 nm.

REFERENCES

[1] JW Strutt. On the light from the sky, its polarization and colour. *Philosophical Magazine Series 4*, 41(271):107–120, February 1871.

[2] Craig F. Bohren and Donald R. Huffman. *Absorption and scattering of light by small particles*. Wiley, 1983.

[3] H. C. van de Hulst. *Light scattering by small particles*. Dover Publications, 1981.

[4] Arthur L. Aden and Milton Kerker. Scattering of electromagnetic waves from two concentric spheres. *Journal of Applied Physics*, 22(10):1242, 1951.

[5] M.L. Gorodetsky and A.E. Fomin. Geometrical theory of whispering-gallery modes. *IEEE Journal of Selected Topics in Quantum Electronics*, 12(1):33 – 39, February 2006.

[6] Michael I. Mischenko, Larry D. Travis, and Andrew A. Lacis. *Scattering, Absorption, and Emission of Light by Small Particles*. Cambridge University Press, 2002.

[7] Meint P. van Albada, Bart A. van Tiggelen, Ad Lagendijk, and Adriaan Tip. Speed of propagation of classical waves in strongly scattering media. *Physical Review Letters*, 66(24):3132–3135, June 1991.

[8] Pierre-Etienne Wolf and Georg Maret. Weak localization and coherent backscattering of photons in disordered media. *Physical Review Letters*, 55(24):2696–2699, December 1985.

[9] P. W. Anderson. Absence of diffusion in certain random lattices. *Physical Review*, 109(5):1492–1505, March 1958.

[10] Hefei Hu, A. Strybulevych, J. H. Page, S. E. Skipetrov, and B. A. van Tiggelen. Localization of ultrasound in a three-dimensional elastic network. *Nature Physics*, 4(12):945–948, 2008.

[11] Diederik S. Wiersma, Paolo Bartolini, Ad Lagendijk, and Roberto Righini. Localization of light in a disordered medium. *Nature*, 390(6661):671–673, December 1997.

[12] AF Ioffe and AR Regel. Non-crystalline, amorphous, and liquid electronic semiconductors. *Prog. Semicond.*, 4:237–291, 1960.

[13] Diederik S. Wiersma. The physics and applications of random lasers. *Nature Physics*, 4(5):359–367, 2008.

[14] R. C. Polson, A. Chipouline, and Z. V. Vardeny. Random lasing in π-conjugated films and infiltrated opals. *Advanced Materials*, 13(10):760–764, 2001.

[15] Sushil Mujumdar, Marilena Ricci, Renato Torre, and Diederik S. Wiersma. Amplified extended modes in random lasers. *Physical Review Letters*, 93(5):053903, July 2004.

[16] G. Strangi, S. Ferjani, V. Barna, A. De Luca, C. Versace, N. Scaramuzza, and R. Bartolino. Random lasing and weak localization of light in dye-doped nematic liquid crystals. *Optics Express*, 14(17):7737–7744, August 2006.

[17] M. D. Birowosuto, S. E. Skipetrov, W. L. Vos, and A. P. Mosk. Observation of spatial fluctuations of the local density of states in random photonic media. *Physical Review Letters*, 105(1):013904, July 2010.

[18] V. Krachmalnicoff, E. Castanié, Y. De Wilde, and R. Carminati. Fluctuations of the local density of states probe localized surface plasmons on disordered metal films. *Physical Review Letters*, 105(18):183901, October 2010.

[19] E. Yablonovitch, T. J. Gmitter, and K. M. Leung. Photonic band structure: The face-centered-cubic case employing nonspherical atoms. *Physical Review Letters*, 67(17):2295–2298, October 1991.

[20] Susumu Noda, Katsuhiro Tomoda, Noritsugu Yamamoto, and Alongkarn Chutinan. Full three-dimensional photonic bandgap crystals at near-infrared wavelengths. *Science*, 289(5479):604–606, July 2000.

[21] Yurii A. Vlasov, Xiang-Zheng Bo, James C. Sturm, and David J. Norris. On-chip natural assembly of silicon photonic bandgap crystals. *Nature*, 414(6861):289–293, November 2001.

[22] K.M. Ho, C.T. Chan, C.M. Soukoulis, R. Biswas, and M. Sigalas. Photonic band gaps in three dimensions: New layer-by-layer periodic structures. *Solid State Communications*, 89(5):413–416, February 1994.

[23] Li Wang, Sasa Zhang, Qingpu Wang, Jiaqi Chen, Wei Jiang, and Ray T. Chen. Fabrication of three-dimensional (3D) woodpile structure photonic crystal with layer by layer e-beam lithography. *Applied Physics A*, 95(2):329–334, May 2009.

[24] Markus Deubel, Georg von Freymann, Martin Wegener, Suresh Pereira, Kurt Busch, and Costas M. Soukoulis. Direct laser writing of three-dimensional photonic-crystal templates for telecommunications. *Nature Materials*, 3(7):444–447, 2004.

[25] Masayuki Fujita, Shigeki Takahashi, Yoshinori Tanaka, Takashi Asano, and Susumu Noda. Simultaneous inhibition and redistribution of spontaneous light emission in photonic crystals. *Science*, 308(5726):1296–1298, May 2005.

[26] John D. Joannopoulos, Steven G. Johnson, Joshua N. Winn, and Robert D. Meade. *Photonic Crystals: Molding the Flow of Light (Second Edition)*. Princeton University Press, February 2008.

[27] B. Corcoran, C. Monat, C. Grillet, D. J. Moss, B. J. Eggleton, T. P. White, L. O'Faolain, and T. F. Krauss. Green light emission in silicon through slow-light enhanced third-harmonic generation in photonic-crystal waveguides. *Nature Photonics*, 3(4):206–210, 2009.

[28] Juntao Li, Liam O'Faolain, Isabella H. Rey, and Thomas F. Krauss. Four-wave mixing in photonic crystal waveguides: slow light enhancement and limitations. *Optics Express*, 19(5):4458–4463, February 2011.

[29] Rodney S. Tucker, Pei-Cheng Ku, and Constance J. Chang-Hasnain. Slow-light optical buffers: Capabilities and fundamental limitations. *Journal of Lightwave Technology*, 23(12):4046, December 2005.

[30] Hideo Kosaka, Takayuki Kawashima, Akihisa Tomita, Masaya Notomi, Toshiaki Tamamura, Takashi Sato, and Shojiro Kawakami. Self-collimating phenomena in photonic crystals. *Applied Physics Letters*, 74(9):1212–1214, March 1999.

[31] Hideo Kosaka, Takayuki Kawashima, Akihisa Tomita, Masaya Notomi, Toshiaki Tamamura, Takashi Sato, and Shojiro Kawakami. Superprism phenomena in photonic crystals. *Physical Review B*, 58(16):R10096–R10099, October 1998.

[32] Lukas Novotny and Bert Hecht. *Principles of Nano-Optics*. Cambridge University Press, June 2006.

[33] Aleksandar D. Rakic, Aleksandra B. Djurišic, Jovan M. Elazar, and Marian L. Majewski. Optical properties of metallic films for vertical-cavity optoelectronic devices. *Applied Optics*, 37(22):5271–5283, August 1998.

2

Absorption enhancement for efficiency improvement of downconversion based applications

Enhancement of absorption and luminescence has been studied extensively in the last few years on account of their immense importance in many applications. Many light emitting molecules are either poor absorbers or poor emitters, in effect the performances of applications rely on fluorescence are severely effected, therefore enhancing the spectral properties of luminescent molecules is strongly needed. In this chapter, a downconversion based application called luminescent solar concentrator is introduced, and issues related to its efficiency are discussed elaborately. Finally, some previously studied approaches to enhance the fluorescence are discussed, which have relevance for this thesis.

Interaction of light with matter is a vast subject of interest, and it has been studied extensively since many years. Light interacting with a matter(matter is made up of fundamental particles like electrons, molecules, atoms, etc..) can end up with two possible consequences. First, light may be emitted as secondary radiation of the same frequency as of the incident field, and this process is called as scattering. Second, incident light may be partially or fully converted into other forms of energy through the absorption process. Further, the energy absorbed by the particles in the matter is emitted into other forms of energy, which is solely determined by their energy level diagram. The combined effect of scattering and absorption is to reduce the amount of energy contained in the incident wave.

Electrons in molecules, atoms, nanostructures(quantum dots) absorb en-

ergy and emit the electromagnetic radiation of slightly lower energy in the form of light with a very high efficiency, is called as fluorescence. Among all emitters, organic molecules are earliest class of fluorescence emitters. The fluorescence from organic molecules is a result of transition of electrons between energy states, whose mechanism is usually described by Jablonski diagram, whose illustration is shown in the Fig. 2.1. To a first approximation a molecule is excited to a higher vibration level of either **S1** or **S2** state. Molecule in the excited state quickly relaxes back to the lowest vibration level state of **S1**, which is called as internal conversion, then makes a transition to the ground state with an emission of photon.

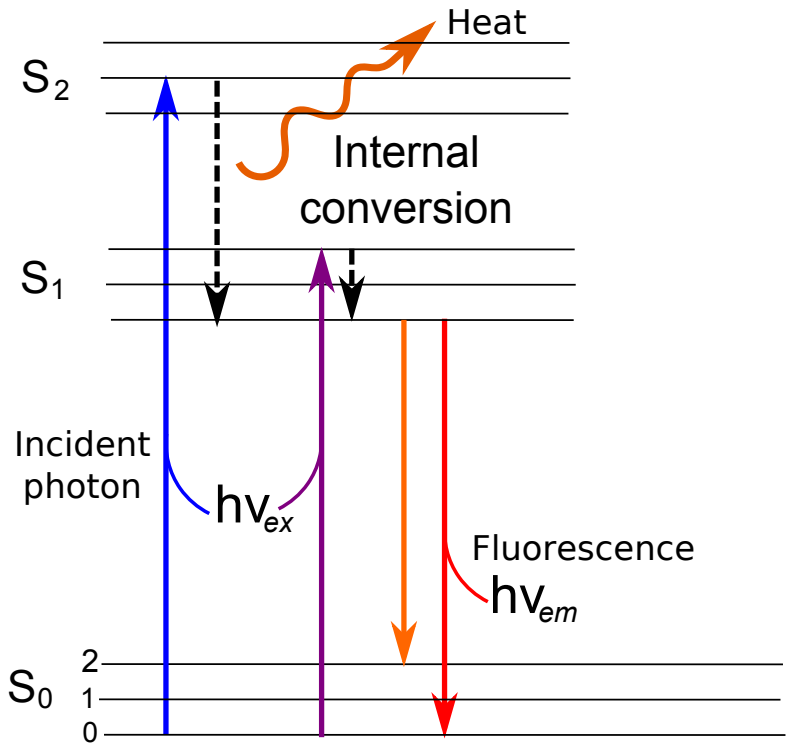

Figure 2.1: A Jablonski diagram of electronic energy states of molecules and transitions between them.

$$\textbf{Absorption:} S_0 + h\nu_{ex} \rightarrow S_1$$
$$\textbf{Fluorescence:} S_1 \rightarrow S_0 + h\nu_{em} + \text{heat}$$

2.0.1 Characteristics of fluorescent molecules

The molecules which can emit fluorescence are also referred as fluorophores, which display a number of characteristics.

Stokes shift

As mentioned earlier, molecule excited to the highest vibration level of either S1 or S2 relaxes rapidly to the lowest vibration level of S1 state, and then makes a transition to the any of the vibration levels of the ground state. And, the difference between the energies associated with absorption and fluorescence processes is called as Stokes shift. The cause of Stokes shift is due to the non-radiative decay process to the lowest level of the excited state. Furthermore, electrons in the lowest vibration level state of S1 may also relax to the highest level of the ground state, in effect much more energy is lost in the form heat.

Quantum yield and life times

Quantum yield Φ is a parameter that quantify the efficiency of a fluorophore. Essentially, it is a ratio of photons emitted relative to the number of photons absorbed. The maximum quantum yield of a fluorophore can be 1.0(100%). Quantum yield can be defined also in another way from the rates of excited state decay:

$$\Phi = \frac{\mathbf{k}_f}{\sum_i \mathbf{k}_i}, \tag{2.1}$$

where $\mathbf{k}_f$ is the rate of spontaneous emission, can be also called as radiative decay rate, $\sum_i \mathbf{k}_i$ is the sum of all the excited state decay rates including radiative decay rate and non radiative decays rates from processes such as dynamic collisional quenching, near-field dipole-dipole interaction (or resonance energy transfer), internal conversion, and inter system crossing, etc..

Another important characteristic of fluorophores is their life time. Life time of a fluorophore is the average time the molecule stays in its excited state before emitting a photon. Depopulation of molecules in a excited state occurs through radiative and non radiative processes, hence the total decay rate Γ_{total} is given by

$$\Gamma_{total} = \Gamma_{rad} + \Gamma_{nrad}, \tag{2.2}$$

where Γ_{rad} is the radiative decay rate, and Γ_{nrad} is the non radiative decay rate.

2.0.2 Applications of fluorescence

Fluorescence phenomenon has immense applications in many fields, which either use the fluorescence in direct form, or to sense the objects which emit it. To begin with, simplest example for fluorescence is a incandescent lamp which every one use in households. The common fluorescent lamp relies on the fluorescence of the phosphor material on the walls of the tube. An electric discharge in the tube causes mercury atoms to emit UV light, and phosphor deposited on the walls absorb the UV light and emit white light. In the same way, mixture of phosphors in LEDs absorb the blue light and emit fluorescence of different colors from green to red, and the net effect of which gives a white light emission.

Fluorescence is used in biology to track and analyze the biomolecules in a non-invasive manner. Labeling of biomolecules, detection of bio-molecular interactions that manifest themselves by influencing the fluorescence life times, bio sensors, study of protein interactions, cell sorting, DNA detection are few fluorescence based applications [1]. Forensics is another area where fluorescent materials are used to detect the finger prints. Forensic experts also look for traces of body fluids like blood, urine, etc. at the crime scene, since which contain fluorescent molecules.

Fluorescence phenomenon is widely used in solar energy applications like dye sensitized solar cells, quantum dot solar cells, organic solar cells, luminescent solar concentrators, etc., and the advantage of using downconversion process is that it can be effectively concentrated. Among all these applications, luminescent solar concentrator(LSC) finds significant attention in recent years due to their simple architecture. This thesis is devoted to discuss the various strategies pursued to enhance the absorption of fluorescent molecules and thereby their fluorescence, towards the improvement of LSCs efficiency.

2.1 Luminescent solar concentrators(LSCs)

Photovoltaics has gained a tremendous attention in recent years for its potential to cater the future energy needs. Conventional semiconductor solar cells are the most popular among all other kind of solar cells, on account of their higher efficiency than others. However, in order to make solar energy more socially acceptable, cost of the solar energy technology has to be brought down and its technology has to be much simplified. Luminescent solar concentrators(LSCs) [2] are one such kind of solar cells which have enormous potential to be socially accepted owing to their simple architecture

and cost-effectiveness. Unlike the earlier years of LSCs invention, they are not considered any more as an alternative solution to semiconductor based photovoltaic cells, rather as a parallel solution on account of their specific advantages.

A luminescent solar concentrator is a plastic or glass planar wave guide doped with fluorescent molecules(see the illustration of an LSC in the Figure. 2.2(a)). The fluorescent molecules in the polymer slab absorb incoming light of shorter wavelengths, emit at longer wavelengths. The light emitted is partially guided to the edges of the slab by total internal reflection, and where it will be absorbed by the photovoltaic cells. The principle of the LSC was first proposed by Weber *et al* in the year 1976 [3], immediately followed by some more comprehensive works [4, 5]. Similar to the parabolic concentrators, luminescent solar concentrators concentrate the sunlight collected over a large area into a very small area, but in a simple way, occupying less space, and does not require tracking of sunlight as it can capture both direct and diffused sunlight.

Luminescent solar concentrators can be useful as windows and roofs for the buildings, and in particular desirable for urban infrastructure. In order to be used as windows, LSCs should act transparent to the visible radiation and should harness only ultraviolet and infra-red spectral regions. Since the luminous intensity in these wavelength ranges in solar spectrum is quite low, hence these spectra must be harnessed at a full capacity.

2.1.1 Efficiency of an LSC

The efficiency of an LSC is mainly governed by several factors related to fluorescent molecules and the host medium. The optical efficiency of an LSC can be simply expressed as

$$\eta_{\text{opt}} = (1 - R)\, \mathrm{P}_{\text{TIR}}\ \eta_{\text{abs}}\ \eta_{\text{PLQY}}\ \eta_{\text{stokes}}\ \eta_{\text{host}}\ \eta_{\text{TIR}}\ \eta_{\text{self}}, \tag{2.3}$$

where R is the Fresnel reflection coefficient of the host medium, P_{TIR} is the total internal reflection efficiency in the slab, η_{abs} is the absorption efficiency of the fluorescent molecules, η_{PLQY} is the quantum yield of the fluorophore, η_{stokes} is the energy lost due to the non-radiative processes such as heat, η_{host} is the transport efficiency of the guided photons through the slab, η_{TIR} is the reflection efficiency of the slab determined by the smoothness of the slab surface, and η_{self} is the efficiency of the guided photons related to re-absorption of the emitted photons by another fluorophore [5]

Even three decades after the invention of LSCs, highest efficiency achieved in these devices stands still at a low value i.e $\sim 7\%$ [6] on account of various

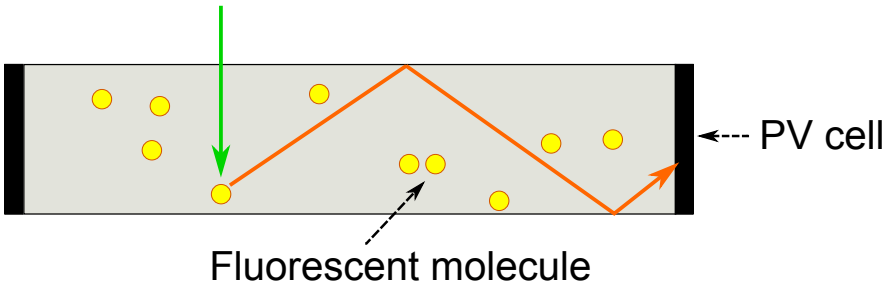

(a) Illustration of a luminescent solar concentrator. Incoming light(green arrow) is absorbed by fluorescent molecules, and emit fluorescence(orange arrow), which is guided to the edges of the slab by total internal reflection. Photovoltaic cells are attached to the edges of the slab, which capture the fluorescence and convert into electricity.

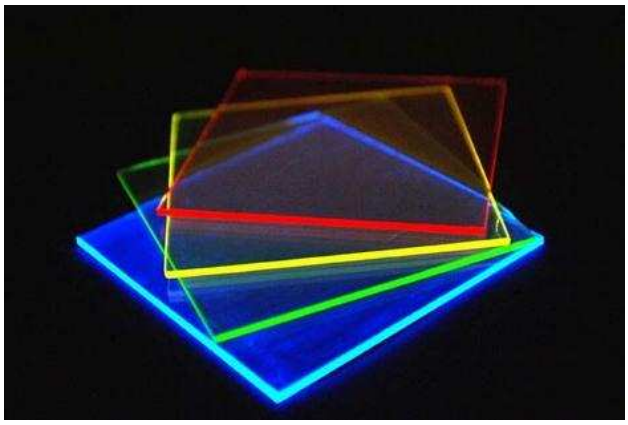

(b) An image of LSCs with different emissions(Courtesy: M. Baldo, MIT).

Figure 2.2: Luminescent solar concentrator.

issues related to dye and light transport in the host medium. Poor efficiency of LSCs is attributed to various kinds of losses [2], which are discussed below in a detailed manner:

Light transport in an LSC: Light emitted by the fluorescent molecules in an LSC is partially guided by the total internal reflection towards the edges, while photons which make angles less than the critical angle simply escape out of the slab. Loss due to the escape of light in a slab of refractive index n is given by the relation

$$L = 1 - \frac{\sqrt{n^2 - 1}}{n},$$

where n is the refractive index of the host medium. Typically polymers are chosen as host medium due to their low cost. For a polymer of refractive index equal to $n = 1.5$, the fractional amount of loss of light in the loss cone is $L = 0.2546$, which is a quite significant loss.

Self absorption: Many of the organic dyes loose their significant amount of emission due to their intrinsic property called re-absorption. The physical mechanism of self absorption can be better understood from the energy states diagram of molecules as shown in the Fig. 2.1. Electrons in an excited fluorescent molecule undergoes transition to the excited electronic state and quickly relax to the meta stable electronic state through a non-radiative decay process such as heat, then come back to the ground state releasing fluorescence. The stokes shift, difference between the energy of the electronic excitation state and meta stable emission state, which depends on a fluorescent molecule and its local environment. Small stokes shift between absorption and emission energies causes an overlap of spectral bands, implying that molecules absorb fraction of their own emission. On the other hand, molecules with large stokes shift exhibit non-radiative decay losses in the form of heat, as a result display poor quantum yield. This can be better understood from the expression given by

$$Q = \frac{\Gamma}{\Gamma + k_{nr}}, \tag{2.4}$$

where Q is the quantum yield of the fluorescent molecules, Γ is the radiative decay rate of the electrons in a electronic excited state, and k_{nr} is the non radiative decay rate of the electrons. Luminescent molecules dissolved in solvents of different refractive index and polarity will have different non-radiative decay rates, hence different quantum yields [1]

Photo-stability: Most of the fluorescent molecules such as organic dyes decompose on exposure to the UV radiation as a result their absorption and emission efficiency decreases and in effect their life span shortens. The fluorescent molecules in a host media also undergo degradation by the interaction with the remains of active species from the photo-decomposition of polymer or singlet oxygen [7].

Fluorescence efficiency The efficiency of LSCs is mainly dictated by the performance of fluorescence emitters which include organic dyes, quantum dots, rare earth complexes, and inorganic phosphors, etc.. An optimal emitter for an LSC should display following characteristics: Large spectral width in absorption, large stokes shift, high quantum efficiency, high absorption

efficiency over the entire absorption spectrum, high photo-stability, narrow spectral width in emission, and good solubility in a host matrix.

Organic dyes were considered as fluorophores in the initial works on LSCs due to their very broad spectral widths in absorption, high quantum efficiency, and their solubility in solvents. Organic dyes have some limitations such as their low photo-stability, self absorption, broad spectral widths in emission which makes them less preferable for LSCs.

Quantum dots outperform over the organic dyes due to their large stokes shift, broad absorption band, high photostability, high absorption efficiency, etc.. Some works tried to compare the efficiencies of LSCs with quantum dots and organic dyes, and found quantum dot concentrators had comparable efficiency as that of organic dye concentrator, which they attribute to the low quantum efficiencies of Quantum dots [8]. Typical quantum dots are toxic in nature, and can pose a severe harm to the environment, which is their major drawback.

Each of these fluorescent molecules have their own advantages and disadvantages. In this framework, rare earth complex dyes can become good alternatives to the organic dyes and quantum dots due to their low self absorption, broad absorption band, sharp emission band and strong photostability [2]. Particular europium complex dyes also display a very broad absorption band, and very narrow emission band, thus provide an opportunity to control the fluorescence in LSC at will [9, 10]. Nevertheless, it is known that RECs absorb very weakly, hence require a few millimeters thick propagation length to absorb the incident light completely, that will require enormous quantity of dye and as well the host material. Henceforth, enhancing the absorption of dye over a bulk volume is strongly needed.

There are also other minor problems such as polymer matrix losses, surface scattering losses, etc. which can be minimized at production stage.

Another important issue in LSCs is the loss of fluorescent light through the escape cone of the slab. There have been so many efforts in recent years which have tried to address the problem using wavelength specific reflective filters. Reflective filters are chosen such that their reflection band matches spectrally with the emission band of the dye, and act as transparent to the absorption band of the dye. The illustration of emitted light propagation in a LSC with and without wavelength reflective filters is shown in the Figure. 2.3. Wavelength specific reflective filters such as rugate filters [11, 12], photonic crystals [12], and organic cholesteric liquid crystal filters [13] can be used to confine the light emitted by the fluorescent molecules inside the slab and transport it efficiently to the edges.

Several organic molecules are dichroic in nature, owing to which they efficiently absorb the light of certain polarization, and emit light only in certain

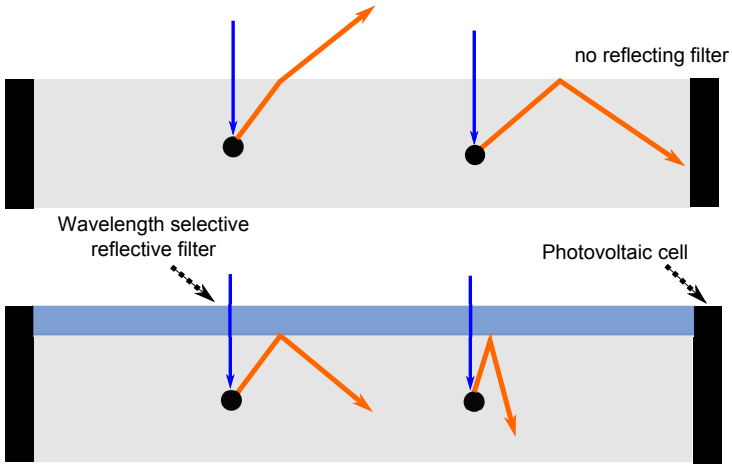

Figure 2.3: Illustration of fluorescence propagation in LSCs covered without any wavelength specific reflective filters(top figure), with filters(bottom figure). Bottom surface of the LSC slab can be attached with another filter(not shown in the figure) or can be attached with a scattering layer. Fluorescence in an LSC covered with wavelength specific reflective filter allow the incident light from the top surface, and reflect the fluorescence back in to the slab, thus efficiently transport the fluorescence to the edges of the slab,

directions. This opens a new possibilities in controlling the fluorescence inside an LSC slab by aligning the molecules, and this was investigated before by using the alignment of liquid crystal molecules [14, 15, 16, 17], using self aligning nano rods [18]. In these works, alignment of fluorescent molecules was shown to redirect the significant amount of fluorescence into the guided modes of the slab. Alignment of molecules with liquid crystal ordering not only effects the anisotropy of fluorescence, also absorption, essentially decreases the absorption efficiency of molecules.

2.2 Light-matter interaction enhancement strategies

Quite often, spectral properties like absorption and emission of the matter/molecules are weak and undetectable, either due to poor interaction of light with them or their poor intrinsic absorbance and quantum yield. Fundamental science has grown independently in the fields of chemistry and physics to address poor interaction of light with molecules or to enhance the intrinsic spectral strengths of the molecules. Variety of tools and techniques

to enhance the efficiency of luminescent molecules and interaction of light with matter have been demonstrated in the last two decades, and still this is considered as a challenging topic.

Enhancement of light absorption and emission has gained importance in recent years owing to their immense potential in many applications. If fluorescence of molecules is enhanced significantly, it could be possible to realize efficient sensing applications and solar concentrators, improve the quality of images, etc.. The modification of spectral properties of fluorescent molecules has been studied using phenomena related to nanophotonics and plasmonics fields.

The relaxation of an atom/molecule in a higher energy level to the ground state commonly occurs by spontaneous emission process. Spontaneous emission rate of an atom is directly proportional to the available density of electromagnetic states of the spatial environment. The density of electromagnetic modes can be described as the number of channels through which molecular emission can radiate. Modifying the refractive index, solvent polarity, and temperature of the surrounding medium of the fluorescent molecules can actually effect little or not at all on the emission of the molecules.

In the year 1940, E. Purcell discovered that the spontaneous emission rate of emitters can be enhanced by coupling its emission to the resonance of a cavity. There after several studies have demonstrated the modification of spontaneous emission decay rates, for instance, the enhancement of spontaneous emission decay rate in a photonic crystal cavities owing to the absence of electromagnetic modes in its band gap [19], in a strongly scattering disordered media due to strong fluctuations in its local density of states [20], and in the proximity of metal surfaces, nanostructures and nanoparticles etc. [21]. Bringing metallic surfaces or nanoparticles close to the fluorescent molecules can alter the free space conditions of the molecules there by leads to the modification of radiative properties of latter significantly [22]. Changes in the free space conditions can be defined in terms of the photonic mode density which is the number of channels through which emission of the molecules can radiate.

First observation of the effect of metal surfaces on the fluorescence of the molecules was reported in the works of Drexhage [23] in the early seventies. In this report, it was shown that fluorescent molecules in the proximity (nearly $\geq 100nm$) of a metal surface displayed oscillation of their life times with the variation of the distance from the metal surface. The effect of metal surfaces on the fluorescence of molecules could either result in an increase or decrease of latter's life times depending on their distance from the metal surfaces.

As discussed in the previous section, strong electron density oscillations on metallic surfaces results in a large enhancement of electric field near to

their surface. Placing molecules close to the metallic surface can undergo any of the three processes: (1) molecules can experience strong increase of the excitation field there by they tend to absorb more light and emit more fluorescence, (2) as explained in the above paragraphs, molecules can experience the increase of photonic density of modes close to the metallic surfaces there by under go an increase of their intrinsic radiative decay rate, (3) metal can damp the dipole oscillations of the molecules thus it can quench the fluorescence of the molecules. This third process occurs typically very close to a metals surface.

Metallic nanoparticles (NPs) are of particular interest compared to planar surfaces. Since the resonant properties of small objects strongly depend on their shape (sphere, rod, ...) and size, metallic NPs make it possible to tune localized surface plasmon resonances (LSPRs) over a large range of wavelengths (from UV to near-infrared). Several materials are currently available, the most common ones being silver (Ag) and gold (Au), which exhibit LSPRs in the visible range.

Metallic nanoparticles display remarkable properties like strong extinction and large enhancement of their near-field on account of their LSPRs. As discussed above on the mechanisms of enhancement of fluorescence using metallic surfaces, similarly, some works have demonstrated enhancement of fluorescence either by making use of intense electric fields close to the nanoparticles to increase the absorption of the dye [24] or by modifying the radiative decay rate of fluorescent molecules in the proximity of nanoparticles [25].

2.3 Conclusions: Right strategy for the enhancement of an LSC's efficiency

Though there have been various strategies to enhance the efficiency of LSCs using different kinds of fluorescence emitters, filters, alignment, nanoparticles, etc.. But it is still a difficult task to judge which is the best approach. The approaches to enhance the absorption do not consider effects on fluorescence propagation, whereas the approaches which try to confine the light to the slab diminish fluorescent molecules absorption efficiency. Therefore, any improvement strategy relevant to an LSC device can be better judged by looking at the increment of light which couple in to the system and decrement of light which couple out of the system.

REFERENCES

[1] Joseph R. Lakowicz. *Principles of Fluorescence Spectroscopy*. Springer, February 2009.

[2] Wilfried G.J.H.M. van Sark, Keith W.J. Barnham, Lenneke H. Slooff, Amanda J. Chatten, Andreas Bächtemann, Andreas Meyer, Sarah J. McCormack, Rolf Koole, Daniel J. Farrell, Rahul Bose, Evert E. Bende, Antonius R. Burgers, Tristram Budel, Jana Quilitz, Manus Kennedy, Toby Meyer, C. De Mello Donegá, Andries Meijerink, and Daniel Vanmaekelbergh. Luminescent solar concentrators - a review of recent results. *Optics Express*, 16(26):21773–21792, December 2008.

[3] W. H. Weber and John Lambe. Luminescent greenhouse collector for solar radiation. *Applied Optics*, 15(10):2299–2300, October 1976.

[4] J. A. Levitt and W. H. Weber. Materials for luminescent greenhouse solar collectors. *Applied Optics*, 16(10):2684–2689, October 1977.

[5] A. Goetzberger and W. Greube. Solar energy conversion with fluorescent collectors. *Applied physics*, 14(2):123–139, October 1977.

[6] L. H. Slooff, E. E. Bende, A. R. Burgers, T. Budel, M. Pravettoni, R. P. Kenny, E. D. Dunlop, and A. Bächtemann. A luminescent solar concentrator with 7.1% power conversion efficiency. *physica status solidi (RRL) Rapid Research Letters*, 2(6):257–259, 2008.

[7] I. Baumberg, O. Berezin, A. Drabkin, B. Gorelik, L. Kogan, M. Voskobojnik, and M. Zaidman. Effect of polymer matrix on photo-stability of photo-luminescent dyes in multi-layer polymeric structures. *Polymer Degradation and Stability*, 73(3):403–410, 2001.

[8] V. Sholin, J. D. Olson, and S. A. Carter. Semiconducting polymers and quantum dots in luminescent solar concentrators for solar energy harvesting. *Journal of Applied Physics*, 101(12):123114–123114–9, June 2007.

[9] Omar Moudam, Brenda C. Rowan, Mohammed Alamiry, Patricia Richardson, Bryce S. Richards, Anita C. Jones, and Neil Robertson. Europium complexes with high total photoluminescence quantum yields in solution and in PMMA. *Chemical Communications*, (43):6649–6651, October 2009.

[10] Xin Wang, Tongxin Wang, Xiujie Tian, Lijuan Wang, Wenxuan Wu, Yanhua Luo, and Qijin Zhang. Europium complex doped luminescent solar concentrators with extended absorption range from UV to visible region. *Solar Energy*, 85(9):2179–2184, September 2011.

[11] Jan Christoph Goldschmidt, Marius Peters, Armin Bösch, Henning Helmers, Frank Dimroth, Stefan W. Glunz, and Gerhard Willeke. Increasing the efficiency of fluorescent concentrator systems. *Solar Energy Materials and Solar Cells*, 93(2):176–182, February 2009.

[12] Jan Christoph Goldschmidt, Marius Peters, Liv Pronneke, Lorenz Steidl, Rudolf Zentel, Benedikt Blasi, Andreas Gombert, Stefan Glunz, Gerhard Willeke, and Uwe Rau. Theoretical and experimental analysis of photonic structures for fluorescent concentrators with increased efficiencies. *physica status solidi (a)*, 205(12):2811–2821, 2008.

[13] Michael G. Debije, My-Phung Van, Paul P. C. Verbunt, Maud J. Kastelijn, Rudy H. L. van der Blom, Dirk J. Broer, and Cees W. M. Bastiaansen. Effect on the output of a luminescent solar concentrator on application of organic wavelength-selective mirrors. *Applied Optics*, 49(4):745–751, February 2010.

[14] G. H. Heilmeier and L. A. Zanoni. Guest-host interactions in nematic liquid crustals.a new electro-optic effect. *Applied Physics Letters*, 13(3):91–92, August 1968.

[15] R.L. van Ewyk, I. O'Connor, A. Mosley, A. Cuddy, C. Hilsum, C. Blackburn, J. Griffiths, and F. Jones. Anisotropic fluorophors for liquid crystal displays. *Displays*, 7(4):155–160, October 1986.

[16] Rafael Piñol, Johan Lub, Maria Pilar Garcìa, Emiel Peeters, José Luis Serrano, Dirk Broer, and Teresa Sierra. Synthesis, properties, and polymerization of new liquid crystalline monomers for highly ordered Guest-Host systems. *Chemistry of Materials*, 20(19):6076–6086, October 2008.

[17] C. L. Mulder, P. D. Reusswig, A. M. Velázquez, H. Kim, C. Rotschild, and M. A. Baldo. Dye alignment in luminescent solar concentrators: I vertical alignment for improved waveguide coupling. *Optics Express*, 18(S1):A79, April 2010.

[18] Concetta Nobile, Luigi Carbone, Angela Fiore, Roberto Cingolani, Liberato Manna, and Roman Krahne. Self-assembly of highly fluorescent semiconductor nanorods into large scale smectic liquid crystal structures

by coffee stain evaporation dynamics. *Journal of Physics: Condensed Matter*, 21(26):264013, July 2009.

[19] Peter Lodahl, A. Floris van Driel, Ivan S. Nikolaev, Arie Irman, Karin Overgaag, Daniël Vanmaekelbergh, and Willem L. Vos. Controlling the dynamics of spontaneous emission from quantum dots by photonic crystals. *Nature*, 430(7000):654–657, August 2004.

[20] Jordi Martorell and N. M. Lawandy. Spontaneous emission in a disordered dielectric medium. *Physical Review Letters*, 66(7):887–890, February 1991.

[21] Joseph R Lakowicz. Radiative decay engineering 5: metal-enhanced fluorescence and plasmon emission. *Analytical biochemistry*, 337(2):171–194, February 2005. PMID: 15691498.

[22] Chris D. Geddes and Joseph R. Lakowicz. Editorial: Metal-Enhanced fluorescence. *J. Fluoresc.*, 12:121–129–129, 2002.

[23] K.H. Drexhage. Influence of a dielectric interface on fluorescence decay time. *Journal of Luminescence*, 1.2(0):693–701, 1970.

[24] Ondrej Stranik, Robert Nooney, Colette McDonagh, and Brian D. MacCraith. Optimization of nanoparticle size for plasmonic enhancement of fluorescence. *Plasmonics*, 2:15–22, 2006.

[25] Felicia Tam, Glenn P. Goodrich, Bruce R. Johnson, and Naomi J. Halas. Plasmonic enhancement of molecular fluorescence. *Nano Lett.*, 7:496–501, 2007.

3

UV absorption enhancement by resonant scattering of aluminum nanoparticles

In this chapter, I discuss a novel, simple, low cost and scalable approach to enhance the absorption of fluorescent molecules in the Ultraviolet(UV) spectrum. Significant enhancement of UV absorption is demonstrated in a bulk medium with extremely small amount of scatterers while keeping its transparency at a high value. The approach presented in this chapter is aimed to realize transparent luminescent solar concentrators/smart windows.

3.1 Ultraviolet unharnessed yet

Harnessing the ultraviolet spectrum (< 400 nm) has been a key interest in the fields of biology, photo-lithography and solar energy, etc.. Though the UV spectrum accounts a small portion in the solar spectrum, still it is a significant amount for certain solar energy applications. Downconversion of the UV light can be useful to realize applications in solar energy, for instance transparent luminescent solar concentrators(LSCs) which are also called as smart windows. Smart windows can be used as windows or roofs for the houses and buildings at the same to produce electricity. It is possible to realize such transparent LSCs by using fluorescent molecules absorbing in the UV and emitting in the visible range. Realizing such transparent LSCs would create a significant impact on the society because of their scalability, low cost, easy installation and they do not require additional space, etc.. As discussed in the previous chapter, LSCs suffer from various kind of losses which deteriorate their performance, one of them in particular is poor absorption of the dye/fluorescent molecules. In fact using excess concentration of the dye in

a solvent/matrix medium could make it to absorb light completely however which would require an enormous amount of dye and solvent/polymer matrix. Therefore enhancing the absorption of a dye/active media in the UV spectrum is vital and beneficial for realizing efficient transparent LSCs. And, enhancing the light-matter interaction in UV also benefits other applications like bio-sensing, imaging, etc..

3.1.1 Enhancement strategy

As discussed in the previous chapter, plasmonic tools can show a route to enhance the absorption of the dye in any spectral range including the UV. Aluminum nanostructures/nanoparticles have been identified to display plasmon resonances in the ultra-violet range [1, 2, 3, 4], were considered recently to enhance the intrinsic fluorescence of the proteins [5], to enhance the fluorescence of molecules [6, 7], and the light absorption in organic photovoltaic devices [8].

The primary interest of this study is to enhance the UV absorption of fluorescent molecules with out deteriorating the transparency of the configuration. Different approaches discussed in the chapter 2 on enhancement strategies can not be applied directly here as they require a very high concentration of nanoparticles, which can deteriorate the transparency of the system. A completely different strategy based on light scattering by nanoparticles is proposed here. The basic idea is to enhance the path length of light propagating inside the UV absorbing media by making use of the resonant scattering of aluminum nanoparticles(NPs) and at the same time transparency of the system should be kept at a high value. Our strategy of enhancement can be

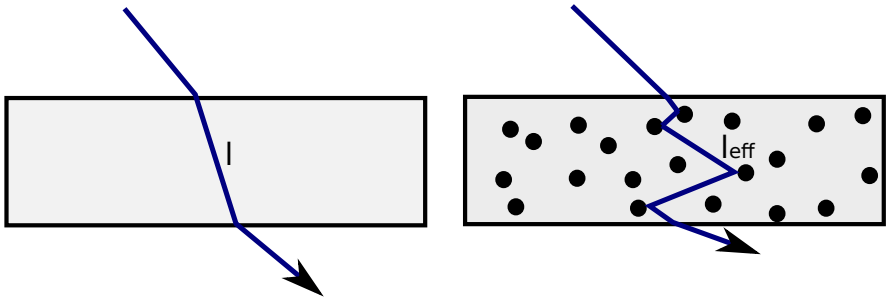

Figure 3.1: Schematic diagram shows how light propagate in samples with and without nanoparticles.

explained by the illustration shown in the Figure. 3.1, where two slabs containing UV absorbing fluorescent molecules are considered. Light inside the

slab without any scatterers propagates ballistically, and escapes out of the slab, thus travels a length equal to l. Where as light in the slab with scatterers undergoes multiple scattering, travels in a zig-zag path and escapes out of the slab, thus light travels much longer distance equal to l_{eff} compared to the distance travelled in the bare slab, essentially increases the chance of absorption of light in an absorbing medium.

Aluminum nanoparticles of size distributed between 50 - 70 nm were chosen as scatterers for this study. Extinction, scattering and absorption efficiencies of aluminum nanoparticles were calculated with Mie theory [9, 10], see in Figure. 3.2. As discussed in the chapter 1, large nanoparticles typically exhibit large scattering component in comparison to absorption component, and resonances over the broad range of wavelengths. 9,10-Diphenylanthracene(DPA), a UV absorbing dye was considered for this study.

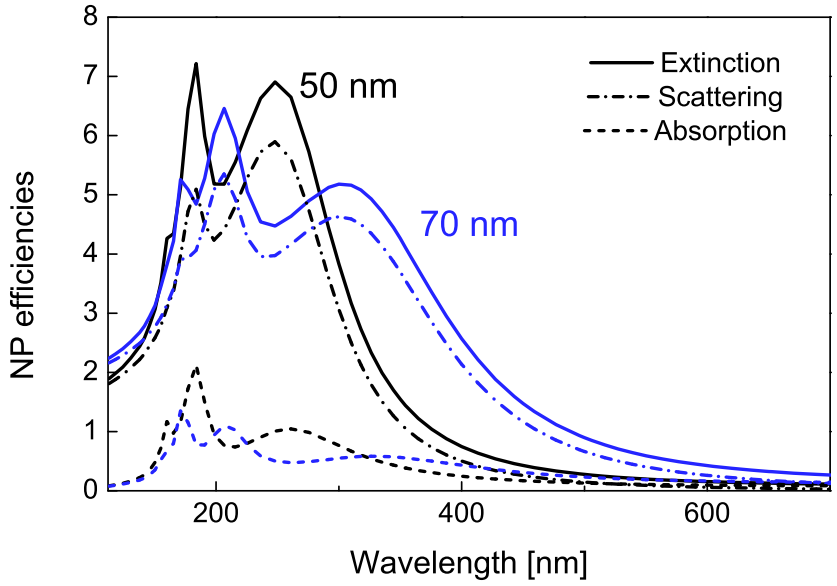

Figure 3.2: Extinction, scattering and absorption spectra of Aluminum nanoparticles of diameter 50 and 70 nm calculated with Mie theory.

3.1.2 Experimental configuration

In order to experimentally verify the enhancement of fluorescence of the DPA by exploiting the plasmon resonances of Al NPs, we decided to work in solution configuration. This configuration makes it possible to vary, in a simple

way, the relative concentration between the DPA and the NPs, and to perform all measurements with a commercial spectrophotometer [Perkin Elmer Lambda950 UV/Vis spectrometer] and a spectro-fluorimeter [Perkin Elmer LS55 Fluorescence-Spectrometer]. To realize prototypes for the experimental measurements, we used solvents with refractive indices close to that of the Polymethylmethacrylate (PMMA) and with limited absorption in the near-UV range. Various organic solvents were tested to disperse the aluminum nanoparticles, among all acetinitrile (spetcrophotometric grade) could able to disperse the nanoparticles in a better manner. Acetonitrile is a polar and aprotic organic solvent, moreover transparent in the spectral region of interest.

The samples were made according to the specifications given above. Spherical Al NPs of diameter ranging between 50 and 70 nm were purchased from IoLiTec GmbH. Al NPs are typically covered by an oxide layer of thickness from 2 to 5 nm, which causes a small red shift of the LSPR. This oxide layer is intentionally passivated in a controlled manner during the production stage in the industry in order to stop further oxidation of the Aluminum NPs. Oxide layer can act as a spacer, thus can help to avoid quenching effects, though the strategy used in our study is not by making use of the near-field enhancement, so this information can be useful else where. A master solution

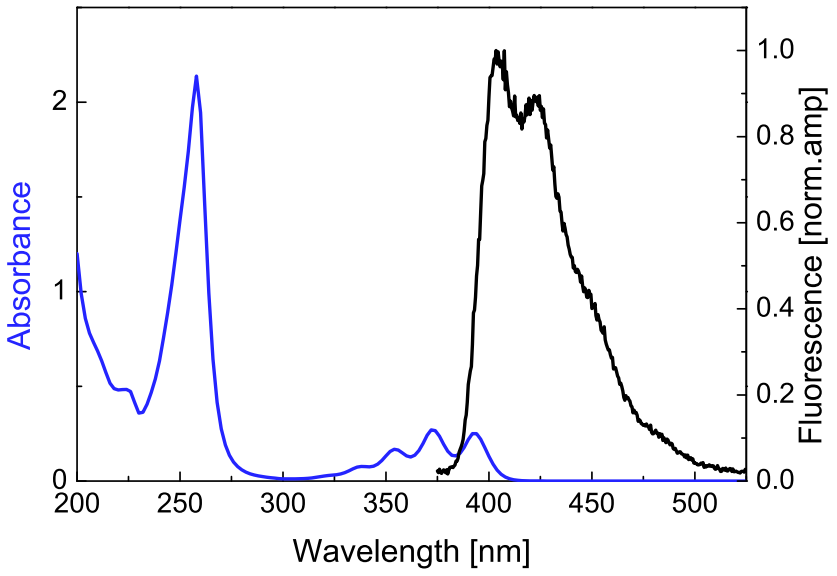

Figure 3.3: Absorption and fluorescence spectra of 9,10-Diphenylanthracene dissolved in the acetonitrile solvent.

of the dye was prepared by dissolving DPA in Acetonitrile with a concentration of 1.189×10^{-4}M. Spectral properties (absorption and emission) of the DPA solution were characterized by UV-Vis spectrophotometer and spectrofluorimeter. DPA absorbs broadly in the in the ultraviolet region and emits in the visible region, see Fig. 3.3. Part of the master solution was used for reference and the other part to disperse the Al NPs. The dispersions were prepared by adding the Al NPs with a concentration of 0.01% in weight in the solution and sonicating it for two hours at room temperature to disaggregate the NPs. A non-fluorescent dispersion of Al NPs in Acetonitrile with the same concentration was realized following the same experimental procedures.

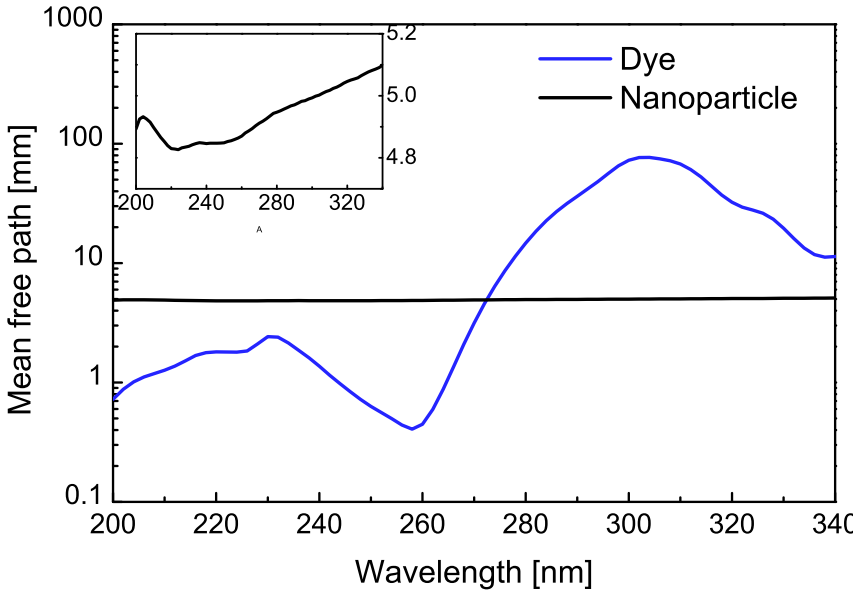

Figure 3.4: Extinction mean free path of the nanoparticles dispersed in Acetonitrile solvent(black curve) and absorption mean free path of the DPA dissolved in Acetonitrile solvent(blue curve).

3.2 Absorption measurements

The dispersion containing the Al NPs only was characterized using a commercial UV-Vis spectrophotometer. The extinction mean free path in the NP dispersion, obtained using Beer-Lambert law, is shown in the Fig. 3.4 and compared with the absorption mean free path of the solution containing

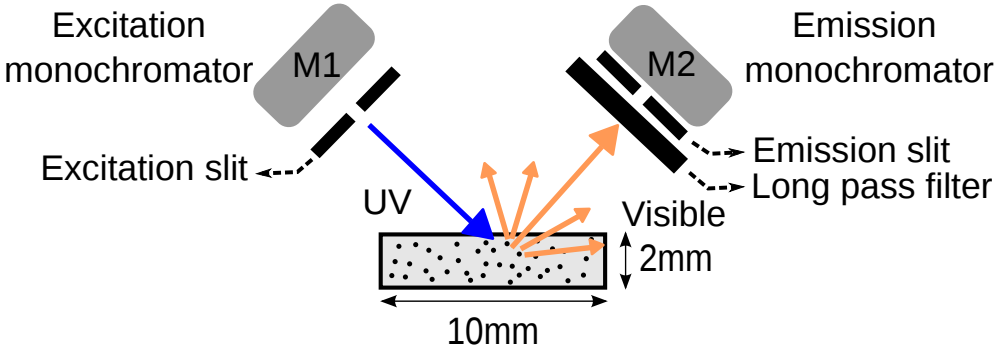

Figure 3.5: Schematic diagram of the experimental set-up used in fluorescence measurements.

fluorescent molecules only. The extinction spectrum of the NP dispersion exhibits very weak resonant features over the entire UV range, yielding an extinction mean free path of about 5 mm in the range 220-380 nm, see inset of the Fig. 3.4. This absence of features might be explained by considering the polydispersity of the Al NPs and the presence of NP aggregates in the solution [11]. First, the polydispersity in the NP diameter is expected to broaden the total extinction efficiency of the NP towards higher wavelengths, see Fig. 3.2. The tail of the LSPR of 70 nm Al NPs clearly enters the visible region and is therefore expected also to affect the visible light transmission. Second, aggregates of resonant NPs (e.g. fractal aggregates are expected to scatter light on a broad range of wavelengths, yielding a rather featureless response in light scattering experiments. As a result, a ballistic transparency of about 68% at normal incidence on the 2 mm-thick solution was found in the visible range. A much higher transparency is expected for monodisperse and non aggregated NPs.

Standard efforts like adding surfactants (oleic acids) to nanoparticle dispersions were carried out to disaggregate the aluminum nanoparticles, however all efforts were vain. It was clear from the literature that the commercially available aluminum nanoparticles in powdered form are synthesized with powder metallurgy techniques, can aggregate easily [12]. Some recent works show that aluminum nanoparticles can be synthesized with a technique using laser ablation of the aluminum targets in the inert atmosphere [13]. This technique was demonstrated to be a safe and superior technique to produce non-aggregated, mono disperse nanoparticles with a precise control on size. Though this is a promising news, but the synthesis of aluminum nanoparticles is beyond the interest of our study.

3.3 Fluorescence measurements

The modification of fluorescence due to the introduction of Al NPs was investigated using a commercial fluorometer with excitation and emission monochromators, making it possible to select accurately the excitation and collection wavelengths. The quartz cuvette containing the fluorescent solution was mounted in front face illumination geometry in the fluorometer, light being incident at 45 degrees with respect to the normal to the surface (Fig. 3.5). Extra measures were taken to avoid detecting any stray or scattered excitation light, like using a long pass filter with a cut off wavelength 350 nm just more than the maximum excitation wavelength used in the experiment, and emission slit was narrowed down to 5 nm to selectively allow the emission with k-vectors from the sample and forbid the stray light. Monochromator/grating at the detection has a very high rejection ratio for the wavelengths not chosen, so avoids detecting stray or excitation light. Fluorescence measurements were characterized by exciting the samples at a particular wavelength and collecting the entire emitted light. Figure 3.6 shows the fluorescence enhancement γ due to the addition of Al NPs as a function of the excitation wavelength. The fluorescence is shown to be enhanced at almost all wavelengths but those close to 260 nm, exceeding 20% in the range 270-340 nm. The absence of fluorescence enhancement at wavelengths close to 260 nm is due to fact that the dye solution already absorbs most of the incident light, leaving no possibility to enhance it further by introducing the NPs. The enhancement of fluorescence for an excitation wavelength of 320 nm due to the addition of Al NPs in the luminescent solutions is evident in the Fig. 3.7.

3.4 Enhancement mechanisms

We now investigate the physical origin of the fluorescence enhancement reported before. The enhancement of absorption due to the presence of metallic NPs could first be attributed to the near-field intensity enhancement in the vicinity of the NPs. It can be calculated using an extended Mie theory generalized to absorbing host media [14]. For dilute dispersions of NPs, the overall absorption enhancement due to the near-field intensity enhancement can be estimated by considering the absorption enhancement in the average volume occupied by a single NP. Mie calculations show that the absorption enhancement expected for NP concentrations as low as 0.01% in weight (about 0.0029% in volume) would not exceed one percent. Although NP aggregates are expected to have somewhat different near-field intensity

patterns, it is reasonable to state that near-field effects do not explain by themselves the fluorescence enhancement observed in our samples.

An alternative explanation for the absorption enhancement is the light scattering induced by the NPs. The increase of light-matter interaction due to multiple scattering is a well-known phenomenon [15]. Multiply-scattered light essentially spends more time interacting with the medium than ballistic light. In our case, we expect scattering to contribute the most to the extinction by the NP dispersion, in spite of the presence of NP aggregates in the solution. With a mean free path of about 5 mm for a cuvette of thickness 2 mm, light transport is clearly not diffusive, yet a single scattering event is already sufficient to increase the optical path length in the absorbing medium and thus, increase the absorption of light by the medium. This hypothesis is verified by means of Monte Carlo simulations that model the transport of photons in scattering media [16]. Algorithm used for Monte Carlo simulations is presented in the appendix (A.1). In the simulations, considering light incident at an angle $\pi/4$ radians on a medium with refractive index 1.35, thickness $L = 2$ mm, scattering mean free path $\ell_s = 5$ mm and assuming isotropic scattering, we find the average optical path length to be $l_{\mathrm{mpl}} = 3.12$ mm, compared with the path length in the bare slab $l = 2.35$ mm. Knowing

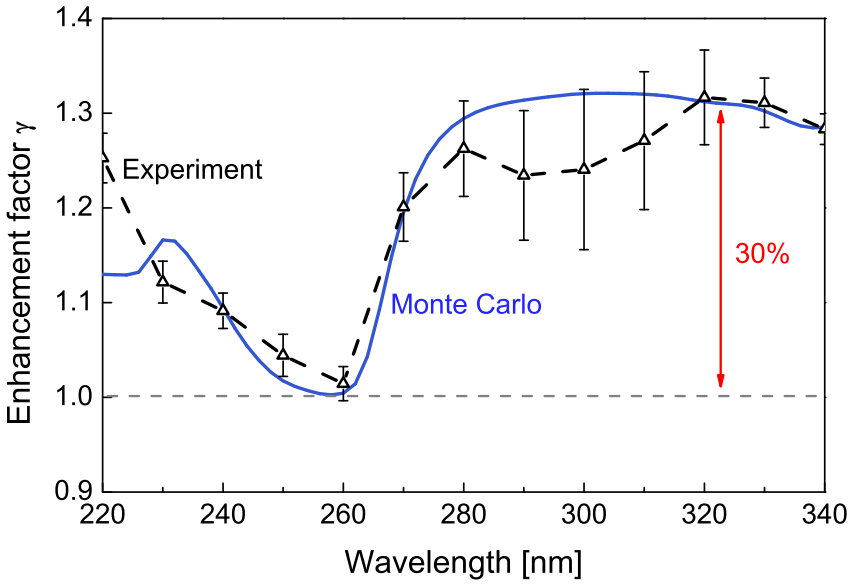

Figure 3.6: Summarized results of fluorescence measurements at various excitation wavelengths.

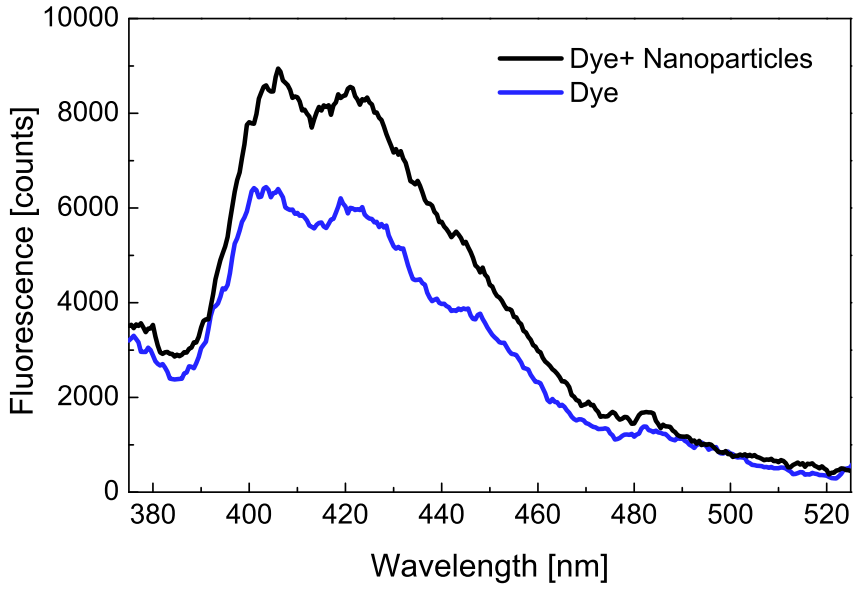

Figure 3.7: Emission spectra of the dye solution dispersed with and without nanoparticles at an excitation wavelength 320 nm.

the absorption mean free path ℓ_i in the dye solution (Fig. 3.4), the absorption enhancement due to scattering in the slab can simply be calculated as $\gamma = (1-\exp[-l_{\mathrm{mpl}}/\ell_i])/(1-\exp[-l/\ell_i])$. Being in a weakly scattering regime at the emission wavelengths, the total amount of emitted light collected by the detector is expected to be proportional to the total amount of light absorbed by the medium. The resulting emission enhancement expected from light scattering effects, shown in Fig. 3.6, is found to be in excellent agreement with the experimental results. The fluorescence enhancement remains higher than 20% at wavelengths above 270 nm and reaches 30%. It is clear from the expression of γ above that larger enhancements are expected when the intrinsic absorption of the dye is weak (i.e. large ℓ_i).

3.5 Conclusions

Fluorescence of solutions containing UV-absorbing molecules is significantly enhanced by adding very small concentration of Al NPs and it is shown that this effect was due to light scattering by Al NPs. This study offers a novel opportunity for enhanced light-matter interaction in the UV range with low interaction at visible wavelengths. Higher fluorescence enhancement and

transparency in the visible range are expected for monodisperse and non-aggregated nanoparticles.

REFERENCES

[1] Paul R. West, Satoshi Ishii, Gururaj V. Naik, Naresh K. Emani, Vladimir M. Shalaev, and Alexandra Boltasseva. Searching for better plasmonic materials. *Laser Photon. Rev.*, 4:795–808, 2010.

[2] Y. Ekinci, H. H. Solak, and J. F. Loffler. Plasmon resonances of aluminum nanoparticles and nanorods. *Journal of Applied Physics*, 104(8):083107 –083107–6, October 2008.

[3] George H. Chan, Jing Zhao, George C. Schatz, and Richard P. Van Duyne. Localized surface plasmon resonance spectroscopy of triangular aluminum nanoparticles. *The Journal of Physical Chemistry C*, 112(36):13958–13963, September 2008.

[4] Christoph Langhammer, Markus Schwind, Bengt Kasemo, and Igor Zorić. Localized surface plasmon resonances in aluminum nanodisks. *Nano Letters*, 8(5):1461–1471, May 2008.

[5] Mustafa H. Chowdhury, Krishanu Ray, Stephen K. Gray, James Pond, and Joseph R. Lakowicz. Aluminum nanoparticles as substrates for metal-enhanced fluorescence in the ultraviolet for the label-free detection of biomolecules. *Anal. Chem.*, 81:1397–1403, 2009.

[6] Krishanu Ray, Mustafa H. Chowdhury, and Joseph R. Lakowicz. Aluminum nanostructured films as substrates for enhanced fluorescence in the ultraviolet-blue spectral region. *Analytical Chemistry*, 79(17):6480–6487, September 2007.

[7] Nuriye Akbay, Joseph R. Lakowicz, and Krishanu Ray. Distance-dependent metal-enhanced intrinsic fluorescence of proteins using polyelectrolyte layer-by-layer assembly and aluminum nanoparticles. *The Journal of Physical Chemistry C*, 116(19):10766–10773, May 2012.

[8] Vladimir Kochergin, Lauren Neely, Chih-Yu Jao, and Hans D. Robinson. Aluminum plasmonic nanostructures for improved absorption in organic photovoltaic devices. *Appl. Phys. Lett.*, 98:133305, 2011.

[9] C. F. Bohren and D. R. Huffman. *Absorption and scattering of light by small particles*. John Wiley & Sons, 1998.

[10] H. C. van de Hulst. *Light scattering by small particles*. Dover Publications, 1981.

[11] John C. Weigle, Claudia C. Luhrs, C. K. Chen, W. Lee. Perry, Joseph T. Mang, Martin B. Nemer, Gabriel P. Lopez, and Jonathan Phillips. Generation of aluminum nanoparticles using an atmospheric pressure plasma torch. *J. Phys. Chem. B.*, 108:18601–18607, 2004.

[12] Dieter Vollath. Plasma synthesis of nanopowders. *Journal of Nanoparticle Research*, 10(1):39–57, December 2008.

[13] C.A. Crouse, E. Shin, P.T. Murray, and J.E. Spowart. Solution assisted laser ablation synthesis of discrete aluminum nanoparticles. *Materials Letters*, 64(3):271–274, February 2010.

[14] I. Wayan Sudiarta and Petr Chylek. Mie-scattering formalism for spherical particles embedded in an absorbing medium. *J. Opt. Soc. Am. A*, 18:1275–1278, 2001.

[15] Akira Ishimaru. *Wave propagation and scattering in random media.* Wiley-IEEE Press, 1999.

[16] Lihong Wang, Steven L. Jacques, and Liqiong Zheng. Mcml–monte carlo modeling of light transport in multi-layered tissues. *Comput. Meth. Prog. Bio*, 47:131–146, 1995.

4

Optical path length enhancement by light scattering in a thin slab

Enhancing the interaction of light in an absorbing medium is of great interest in recent years. There exist many approaches to enhance the absorption or emission of an absorbing medium, and one of them, popular and the simple approach is optical path length enhancement. Path length enhancement strategy using light scattering by nanoparticles has been discussed in the chapter 3. In continuation of the enhancement strategy presented in the chapter 3, path length enhancement using different regimes of scattering are discussed in this chapter. Light scattering in a collection of particles in a thin slab is simulated with the Monte Carlo approach and further validated with a simple analytical theory.

The enhancement of optical path length inside an absorbing medium is a very popular approach, often employed to improve the efficiency of semiconductor solar cells [1, 2]. Earlier in the chapter 3, I have discussed a similar approach to enhance the optical path length in a UV absorbing medium by making use of resonant scattering of aluminum nanoparticles [3]. In fact, in that work only the proof of concept was demonstrated and did not give a quantitative upper limit of the enhancement that can be possible to obtain in such systems. As discussed in the chapter 3, it is possible to simulate such random media with a robust technique called Monte Carlo simulation [4]. Monte Carlo approach is used quite extensively in the atmospheric science [5], biomedical diagnostics [6], light transport in disordered media [7, 8], etc. to extract information such as, path length distribution, total transmission and reflection, time resolved transmission and reflection, etc.. Monte

Carlo simulations are also used in economics to value and analyze investments [9]. In order to better understand about the path length enhancement in configurations similar to those implemented in the aluminum nanoparticles work(chapter 3), Monte Carlo(MC) simulations were performed for various values of scattering mean free paths and then validated with analytical methods.

4.1 Upper limit of the path length enhancement

Increasing the optical path length inside a weakly absorbing medium(absorbing media such as Silicon, GaAs and dye-polymer matrix, etc..) is of primary interest in solar energy applications. There are several ways to increase the optical path length in a slab/wafer, for instance, by making light to under go total internal reflection, which was demonstrated by making the slab of gradient thickness in transverse direction such that light makes multiple passes inside the silicon wafer [2], or patterning grating structures at the rear surface of the silicon wafer [10], etc.. Light entering into a slab with a textured surface whether on one side or on both sides, changes its direction in to random or predetermined directions depending on the shape of the surface, thus travels longer distances in the slab before being absorbed. Lambertian surface roughness [11] and periodic grating structures are popular shapes chosen for the path length enhancement in semiconductor solar cells.

Knowing the maximum optical path length enhancement that can be possible to achieve inside a slab with a rough surface indeed can be a very useful information. Eli Yablonovitch has proposed a statistical ray optics based approach to estimate the maximum of the intensity enhancement(equivalent to path length enhancement) that can occur in a slab with a complicated surface shape [12] and the maximum enhancement limit is so called as Yablonovitch limit. This statistical approach considers an important assumption that the slab medium located in the vacuum is ergodic in behaviour, and this approach is invalid for non-ergodic geometries. Hence, it is crucial at the beginning to understand the concept of ergodicity and ergodic geometries.

The ergodicity, as defined in the statistical mechanics, is a behaviour of a dynamical system averaged spatially and temporally over all its states. Randomization of the phase space is a thumb rule to obtain an average spatial and temporal behaviour over all states in the system. Essentially, the radiation in an ergodic medium undergoes angular randomization, loses memory of its initial direction of propagation. The radiation on undergoing randomization

loses correlation with its initial direction of propagation, typically which can occur to an isotropic radiation either on refraction through the slab or after the first internal reflection or after the second internal reflection, or even due to the motion of the source as it happens with the sunlight. The same hypothesis is also valid for the collimated beam if the radiation undergoes angular randomization inside the slab.

According to the Yablonovitch hypothesis, when the internal radiation in a slab with ergodic geometry approaches equilibrium with the external black body radiation in the vacuum, intensity in the slab becomes n^2 times larger than the incident intensity in the vacuum. Similarly, in a slab with the back reflector, intensity is enhanced by $2n^2$ times of the incident intensity, and absorption is enhanced by $4n^2$ times. It is important to note that, non ergodic geometry is expected to give lower or no intensity enhancement compared to the $2n^2$ limit.

Yablonovitch has presented two complementary approaches to estimate the maximum intensity enhancement: statistical-mechanical approach and geometric ray optics approach, here I discuss in detail only about the geometrical ray optics approach.

4.1.1 Geometrical ray optics approach: Intensity enhancement

The scheme for the geometrical ray optics approach is basically to balance the inflow and outflow of light through an small area element $\mathrm{d}A$, as illustrated in the Fig. 4.1, assuming internal randomization occurs for the incoming light in the medium. Let I_{inc} be the incident light intensity per area element $\mathrm{d}A$. The fraction of incident light transmitted as a function of incident angle ϕ through an area element $\mathrm{d}A$ is denoted by $T_{\mathrm{inc}}(\phi)$, where ϕ is an incident angle. The internal intensity I_{int} on both sides of the area element $\mathrm{d}A$ is given by

$$I_{\mathrm{int}} = \int B_{\mathrm{int}}\, cos(\theta)\, \mathrm{d}\Omega, \tag{4.1}$$

where B_{int} is the intensity per unit solid angle, $cos(\theta)$ is the projection of the intensity due to oblique incidence, and $\mathrm{d}\Omega$ is a small solid angle element. Hence, I_{int} in the medium is given by

$$\begin{aligned} & I_{\mathrm{int}} = 2 \times 2\pi \int_0^{\pi/2} B_{\mathrm{int}} cos(\theta) sin(\theta)\, \mathrm{d}\theta, \\ \implies \quad & I_{\mathrm{int}} = 2\pi\, B_{\mathrm{int}}. \end{aligned}$$

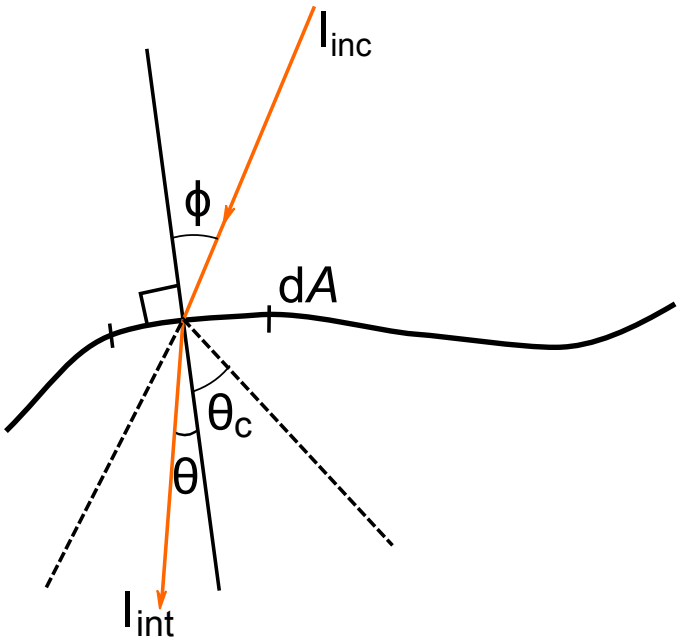

Figure 4.1: Balancing of the energy of incoming and escaping light across the small area element dA. Region below the dashed lines represent the loss cone with a half angle equals to the critical angle in the medium θ_c.

The fraction of power that will escape from the area element dA is

$$I_{\text{esc}} = 2\pi \int_0^{\theta_c} \frac{I_{\text{int}}}{2\pi} T_{\text{esc}}(\theta) cos(\theta) sin(\theta)\, \mathrm{d}\theta. \tag{4.2}$$

In order to simplify the integration in equation(4.2), $T_{\text{esc}}(\theta)$ can be replaced with an average value of transmission $\bar{T}_{\text{esc}}$ over the all angles in the loss cone. For a medium of given refractive index n, the loss cone half angle θ_{c} is defined from the Snell's law by total internal reflection condition:

$$n\, sin(\theta_{\text{c}}) = 1 \Rightarrow \theta_c = sin^{-1}(1/n). \tag{4.3}$$

Substituting the value of critical angle in the equation.(4.2), we get

$$I_{\text{esc}} = I_{\text{int}} \frac{\bar{T}_{\text{esc}}}{2n^2}. \tag{4.4}$$

Balancing the inflow and outflow of power radiation through an area element dA, we have

$$T_{\text{inc}}(\phi) I_{\text{inc}} = I_{\text{int}} \times \frac{\bar{T}_{\text{esc}}}{2n^2}, \tag{4.5}$$

$$\implies \quad I_{\text{int}} = 2n^2 \times \frac{T_{\text{inc}}(\phi)}{\bar{T}_{\text{esc}}} \times I_{\text{inc}}. \tag{4.6}$$

For an isotropic light distribution in the ergodic medium, $\frac{T_{\text{inc}}}{\bar{T}_{\text{esc}}}$ equals to 1, thus intensity inside the slab becomes:

$$I_{\text{int}} = 2n^2 \times I_{\text{inc}}. \tag{4.7}$$

Intensity enhancement in an ergodic slab medium can become greater than the $2n^2$ limit if the ratio $\frac{T_{\text{inc}}}{\bar{T}_{\text{esc}}}$ is more than one, which can only happen if the illumination is angularly selective.

4.2 Path length enhancement in a weakly scattering media

One of the primary interests in this framework is to enhance the absorption of the dye in transparent luminescent solar concentrators/smart windows over the bulk volume without deteriorating their transparency [13]. As discussed in the chapter 3, path length enhancement by resonant scattering of

aluminum nanoparticles of extremely small concentration is sufficient to improve the absorption of a dye significantly. Advantages with such scattering approach are cost effectiveness, scalability, and it can be easily adopted to nanoparticles of different materials, shapes and sizes. In order to explore and understand more about such weakly scattering media, Monte Carlo approach is considered, which gives an opportunity to study such media with a good control over the parameters like concentration of nanoparticles, thickness of the slab, refractive indices of the scatterers and host media, illumination direction, anisotropy of the nanoparticles, etc.. In general, a Monte Carlo approach is considered for simulation of light scattering in random media. Therefore, light scattering in a slab medium sparsely dispersed with scatterers was simulated to retrieve information such as path length distribution in the medium, and which further can give much more information like mean path length, transmission, reflection, absorption, time decay, etc..

4.2.1 Monte Carlo simulations

In order to implement MC simulations, we considered a plane parallel non-absorbing slab of infinite size in the transverse directions and finite in the z-direction, dispersed with strongly scattering and non-absorbing point scatterers. The slab was illuminated with a point source placed at the front surface of the slab, pointing normally in to the slab. The algorithm followed in MC simulations is explained in the appendix (A.2). In the simulation, photons make steps of lengths randomly chosen from the exponential distribution with a mean equals to the predefined scattering mean free path. A photon which crosses the boundary of the slab can be allowed to reflect internally if the angle subtended by it with the surface of the slab is greater than the critical angle. Whereas a photon making a angle less than the critical angle can have a probability to reflect internally based on the Fresnel reflection conditions given by the expressions for S(eq. (4.8a)) and P(eq. (4.8b)) polarizations:

$$R_s = \left(\frac{n_1 \left| uz1 \right| - \sqrt{n_2^2 - n_1^2 + (n_1 uz1)^2}}{n_1 \left| uz1 \right| + \sqrt{n_2^2 - n_1^2 + (n_1 uz1)^2}} \right)^2 , \tag{4.8a}$$

$$R_p = \left(\frac{(n_1/(n_2))\sqrt{n_2^2 - n_1^2 + (n_1 uz1)^2} - n_1 \left| uz1 \right|}{(n_1/(n_2))\sqrt{n_2^2 - n_1^2 + (n_1 uz1)^2} + n_1 \left| uz1 \right|} \right)^2 . \tag{4.8b}$$

In the above expressions, n_1, n_2 are the refractive indices of the slab and air respectively, and $uz1$ is the direction cosine of the trajectory of outgoing photon with the surface of the slab. Hence, if the angle subtended by the

trajectory of a photon with the surface of the slab is less than the critical angle, a random number is generated and checked whether it is less than the average of the S and P Fresnel reflection coefficients:

$$\bar{R}_{s+p} = \frac{R_s + R_p}{2}, \tag{4.9}$$

where $\bar{R}_{s+p}$ is the reflection coefficient for an arbitrary polarization, to know whether it should be internally reflected or escape out of the slab. In a multiple scattering medium, initial polarization scrambles out after few scattering events, hence an arbitrary polarization is considered for every reflection at the surface of the slab.

Monte Carlo simulations were performed for a large range optical thicknesses(slab thickness/scattering mean free paths), and photon path lengths were recorded for each of those optical thicknesses, then their mean path lengths were calculated. Summarized results of the path length enhancements (ratio of the mean path length in a slab with scatterers and the mean path length in a slab with no scatterers) are shown in the Fig. 4.2 for a slab medium with the refractive index $n = 1.525$. It is clear from the results of path length enhancement that even for a weakest concentration of scatterers(smaller optical thicknesses), a significant enhancement can be obtained. Recorded path lengths in the MC simulations suggest that there are few photons which make extremely long path lengths since either which were reflected internally for multiple number of times or scattered multiple times. The probability of occurrence of a scattering event goes to zero only for the scattering mean free path of infinity, therefore for any small value of scatterers concentration there is always a chance of occurrence of aforementioned events and very long path lengths.

In order to gain insight into this impressive path length enhancement in a very weakly scattering and non-absorbing medium, a simple analytical expression is derived. In a slab of thickness L dispersed with few amount of scatterers, the mean path length can be expressed as a weighted sum of the individual mean path lengths of the different orders of scattering events. The weight of each scattering event is equals to the probability of undergoing respective scattering event. The mean path length ($\bar{l}$) derived for weakly scattering regime is given by

$$\bar{l} = P_0\, L(1+r) + P_1\, \overline{l_1} + P_2\, \overline{l_2} + P_3\, \overline{l_3} + ... + P_n\, \overline{l_n}, \tag{4.10}$$

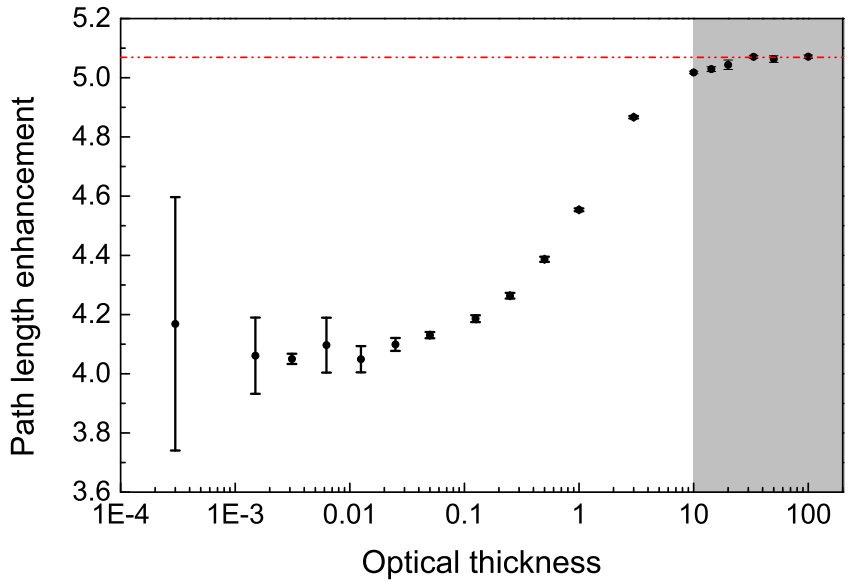

Figure 4.2: The summary of the path length enhancement obtained in a slab dispersed with scatterers, over a long range of optical thicknesses(slab thickness/scattering mean free path) extending from weakly scattering to diffusive regime, where illumination is pointing normally in to the slab. Gray area indicates diffusive regime, and red dashed line indicates the Yablonovitch limit calculated for angularly selective illumination. Error bars were calculated from the standard deviation of mean path lengths obtained for five simulations with each simulation ran for a million random walkers.

where each term in the equation. (4.10) is given by

$$P_0 = e^{\left(\frac{-L}{l_s}\right)}(1+r) \qquad r = \left(\frac{n_1 - n_2}{n_1 + n_2}\right)^2$$

$$P_1 = (1 - P_0)P \qquad \overline{l_1} = \gamma = x_1 + x_2$$

$$P_2 = (1 - P_0 - P_1)P \qquad \overline{l_2} = l_s + \gamma$$

$$P_3 = (1 - P_0 - P_1 - P_2)P \qquad \overline{l_3} = 2\,l_s + \gamma$$

$$P_n = (1 - P_0 - P_1 - P_2 - ....P_{n-1})P \qquad \overline{l_n} = (n-1)\,l_s + \gamma.$$

Majority of photons in weakly scattering regime undergoes ballistic propagation, and whose probability is given by the P_0 and they travel a distance equal to L. While some of those ballistically travelling photons reflect back at the rear surface, and whose probability of occurrence is given by rP_0, and

they travel a distance equals to L, here r is the Fresnel reflection coefficient for normal incidence with the slab-air interface.

In the above equations, P is defined as the escape probability of photons through the loss cone with a half angle equals to the critical angle of the slab θ_c, which is given by $(1 - cos(\theta_c)) \times \bar{T}$, and $\bar{T}$ is a average transmittance in the loss cone angular range. The terms $P_1, P_2, P_3, ..., P_n$ are the probabilities of the occurrence of 1,2,3,..., and n^{th} order scattering events respectively and $\overline{l_1}, \overline{l_2}, \overline{l_3}, ..., \overline{l_n}$ are their respective mean path lengths. Schematic diagram of different orders of scattering events which can occur in a thin slab are illustrated in the Fig. 4.3. As can be seen in the Figure 4.3(b), for instance, the mean path length (l_2) in a double scattering event can be expressed as the sum of the distance travelled by the photon before the first scattering event (x_1) occurs, mean free path of the system (l_s) and the distance travelled by the photon inside the slab before it escapes out of the slab (x_2). In the same manner mean path lengths of all other order scattering events can be explained. In order to investigate the validity of the assumed mean

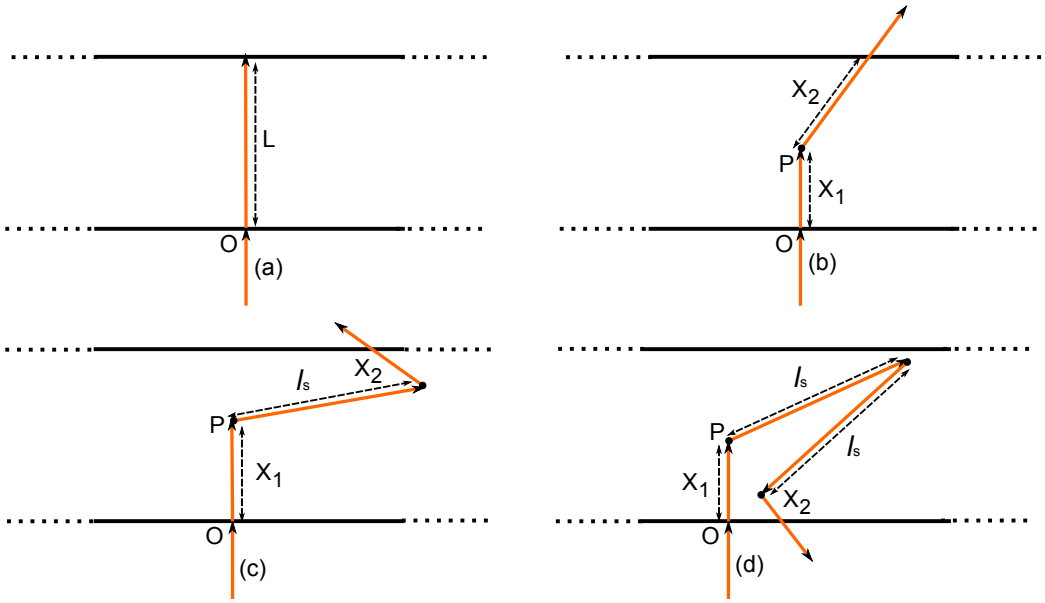

Figure 4.3: Schematic diagrams of different orders of scattering events in a plane-parallel slab (a) ballistic propagation event with the mean path length equals to L, (b) single scattering event with the mean path length equals to $\gamma = x_1 + x_2$, (c) double scattering event with the mean path length equals to $x_1 + l_s + x_2$, (d) triple scattering event with the mean path length equals to $x_1 + l_s + l_s + x_2$.

path lengths for each order of the scattering events considered in the above

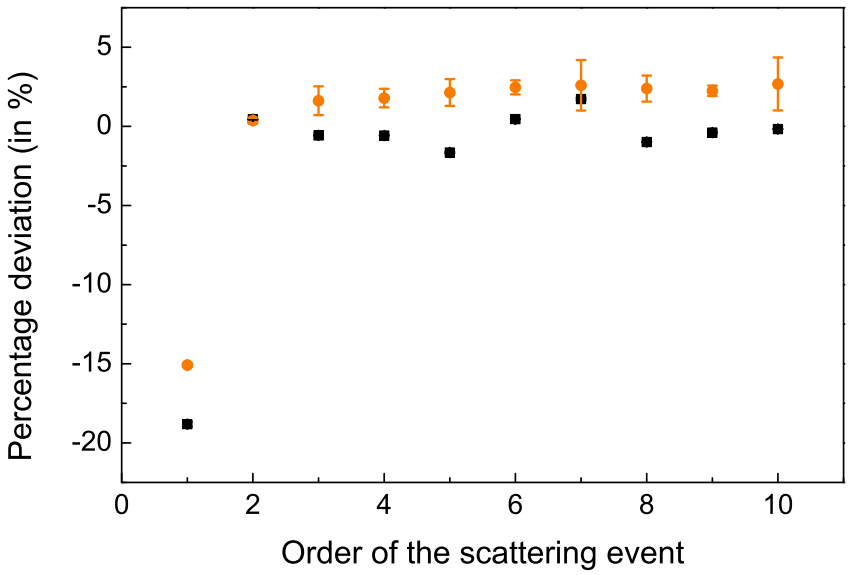

Figure 4.4: Percentage deviation of the analytical mean path lengths with the mean path lengths obtained from MC simulations plotted for scattering events of different orders, for two different values of optical thickness : 0.15 (orange-filled-circles), 0.01 (black-filled-squares).

mentioned derivation, a MC simulation is performed by recording the path lengths and the number scattering events for each photon to determine the mean path length for each order of the scattering event, and for two different values of optical thickness (l_s): 0.15 and 0.01. The mean path lengths considered in the analytical approach are compared with the results of MC simulations for orders of the scattering events from 1 to 10 and their comparison is expressed in terms of percentage deviation, see Fig. 4.4. As can be seen from the Figure. 4.4 that, there is a big negative deviation of nearly 20% for the first scattering event, which comes from the underestimated average value of transmittance in the escape probability. While the small value of percentage error for other scattering events clearly justifies the assumptions considered for the analytical derivation.

As written in the above eq.(4.10), the mean path length (L_{eff}) is a summation of the constant term and a infinite series term, which can be expressed

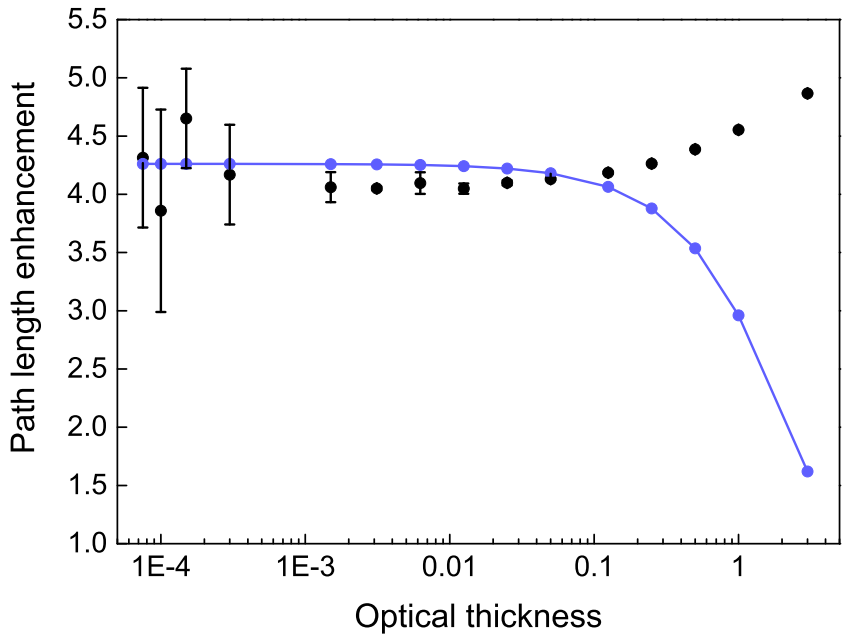

Figure 4.5: Path length enhancements obtained with the analytical approach(blue-filled-circles) are compared with the results of MC simulations(filled-black-circles) for normal incidence case.

as a simplified expression given by

$$L_{\text{eff}} = e^{\frac{-L}{l_s}} L(1+r) + (1 - e^{\frac{-L}{l_s}})(\gamma + l_s \frac{1-P}{P}), \tag{4.11}$$

$$\text{where } \gamma = \frac{l_s - exp(\frac{-L}{l_s})(L + l_s)}{1 - exp(\frac{-L}{l_s})} (1 + (\log|\sec(\theta_c) + \tan(\theta_c)|)/\theta_c). \tag{4.12}$$

The first term of the sum in eq. (4.11) corresponds to the ballistic propagation, and the second term comes from other order scattering events.

Results obtained with the analytical approach are compared with MC simulation results, see Fig. 4.5. In the Figure. 4.5, a good agreement between analytical results and MC simulation results in weakly scattering regime(at smaller values of slab thickness/scattering mean free path) is evident, which validates the theory and correctness of the assumptions considered.

Above approach suggests that a significant enhancement can be obtained even for a weak concentration of scatterers. This approach is perfectly suitable to enhance the efficiency of transparent luminescent solar concentrators,

since a low concentration of scatterers will not effect the emission propagation in an LSC, there by protects its transparency.

4.3 Path length enhancement in a diffusive regime

Light propagating in a random media can lead to a variety of phenomenon with rich physics, and which has found immense applications over the years. In particular, many of the interesting phenomenon such as diffusion [14], random lasing [15], weak localization [16] etc. have been demonstrated to occur in the strongly scattering regime. Scattering strength in a random medium, actually that dictates its optical characteristics. Parameters such as scatterers relative refractive index with the surrounding medium, size, concentrations, and thickness of the slab plays a crucial role in deciding the scattering strength of the medium, also gives an opportunity to tune the scattering strength. Combination of several parameters like large relative refractive index, large concentration of scatterers, scatterers with diameters of the order of the wavelength of light and the slab thickness of few times the transport mean free path [17] are usually considered as figures of merit for the strongly scattering regime. Light in a sufficiently thick strongly scattering random media undergoes spread of light so called as diffusion process. The spread of light in a random media is defined by the mean square displacement of photons cloud which grows linearly with the time.

Consequences of scattering can be very different at different scattering strengths. On the one hand, net transport of light in weakly scattering regime occurs in the forward direction. On the other hand, photons in a strongly scattering regime can have a probability to return back to their initial position[1]. It was predicted that the random medium with a transport mean free path of the order of the wavelength of light can undergo Anderson localization because of the interference of light in counter propagating loops, resulting a complete halt of light propagation.

There have been so many comprehensive studies pursued theoretically and experimentally about the diffusion of light in random/turbid media, in both semi infinite and slab configurations. It was proved that there exist a clear cut-off on the ratio of transport mean free path with the thickness of the slab, for light in it to be diffusive in behaviour [17]. Light transport in

[1]The probability for a photon to return to its initial position or origin decrease with the dimension of the system. The probability to return to origin is 1 for both one and two dimensions, and it is smaller than one in the three dimensions.

the intermediate regime is ubiquitous too. There is no theory to explain the behaviour of light in the intermediate regime between the diffusion limit and weakly scattering regime.

As discussed in the previous section that weak scattering is good enough to enhance the path length significantly. From the Figure. 4.2, it can be observed that the path length enhancement is showing an increasing trend with the increase in the ratio of the slab thickness to the scattering mean free path. Hence, it would be interesting to study the path length enhancement in the diffusive regime, indeed far away from the strongly scattering regime where light localization is predicted to occur. In order to know the path length enhancement in the diffusive regime, Monte Carlo simulations were performed for various values of the scattering mean free path chosen such that the optical thickness (L/l_s) is more than 10. Results are summarized in the Figure. 4.2(gray area), where it can be observed that the enhancement is converging to a constant value as of Yablonovitch limit on increasing optical thickness. Yablonovitch limit is calculated by considering illumination as collimated and angularly selective. Since the illumination is pointing normally in to the slab of refractive index $n = 1.525$, so T_{inc} given by $1 - r$ and which is equals to 0.9568, while the $\bar{T}_{\text{esc}}$ is given by

$$\bar{T}_{\text{esc}} = \frac{1}{(1 - cos(\theta_c))2n^2}, \tag{4.13}$$

where $1/2n^2$ is the probability to escape out of the slab after the single scattering. So for the given medium of refractive index $n = 1.525$, $T_{\text{inc}}/\bar{T}_{\text{esc}}$ is 1.090, indeed which is more than 1, hence the Yablonovitch limit for the given case becomes $2n^2 \times 1.090$, and which is the maximum path length enhancement for a given system and it is represented by red dashed line in the Figure. 4.5.

Internal reflections inside the slab play a major role in enhancing the path length in the given system. Path length enhancement can go much higher for a larger refractive index material.

A comparison of results from the MC simulations with the analytical theory for the given system could validate and provide an intuitive picture of the path length enhancement in the diffusive regime. There exist many approaches that have tried to solve the diffusion equation of light and study their related effects. I find comprehensive theoretical work of Contini *et al* [18] perfectly suits for the given system, and in which they have analytically formulated the static and dynamic propagation of light such as total reflection and transmission, time resolved reflection and transmission through a diffusive slab medium. The mathematical derivation of the time resolved transmittance and reflectance is presented in the appendix (A.3). The final

expressions of the time resolved transmittance$T(t)$ and reflectance$R(t)$ for a slab medium while assuming internal reflection conditions, are given by:

$$R(t) = -\frac{exp(-\mu_a vt)}{2(4\pi Dv)^{1/2}t^{3/2}} \times \sum_{m=-\infty}^{m=\infty} \left(z_{3,m} exp(\frac{z_{3,m}^2}{4Dvt}) - z_{4,m} exp(\frac{z_{4,m}^2}{4Dvt}) \right), \tag{4.14a}$$

$$T(t) = \frac{exp(-\mu_a vt)}{2(4\pi Dv)^{1/2}t^{3/2}} \times \sum_{m=-\infty}^{m=\infty} \left(z_{1,m} exp(\frac{z_{1,m}^2}{4Dvt}) - z_{2,m} exp(\frac{z_{2,m}^2}{4Dvt}) \right). \tag{4.14b}$$

The expressions $R(t)$ and $T(t)$ represent the probability density functions of the reflection and transmittance at a time t. In the above equations (4.14), diffusion coefficient D is given by $1/\mu_s$, v is the velocity of light in the diffusive medium, and $z_{1,m}, z_{2,m} z_{3,m} z_{4,m}$ are given by the expressions in the appendix (A.3). The time distributions obtained from the above equations (4.14a) and (4.14b) can be converted into path length distributions by multiplying with the speed of light in the diffusive medium. As discussed in earlier sections, primary interest in this framework is to estimate the optical path length enhancement in a scattering medium. The path length enhancement in a diffusive medium is given by the ratio of the mean path length in a diffusive medium to the path length in a bare slab ,which is $L(1+r)$, here r is the Fresnel reflection coefficient for the normal incidence, and the contribution from back reflected photons is also accounted. The mean path length $\bar{l}$ can be expressed as a weighted mean of path lengths of photons which are either reflected or transmitted through a diffusive slab medium, and weights are given by their corresponding reflection and transmission probability density functions. Hence, the optical mean path length is given by

$$\bar{l} = \frac{\sum_{i=1}^{n} R(l_i) l_i + \sum_{i=1}^{m} T(l_i) l_i}{\sum_{i=1}^{n} R(l_i) + \sum_{i=1}^{m} T(l_i)}. \tag{4.15}$$

In the summation in (4.15), the upper limits n and m are chosen such that their probability density functions for the corresponding lengths are negligibly small. Using the expressions (4.14), path length distributions are plotted for the transmitted and reflected photons through the slab of thickness 100μ with the scattering mean free paths 10μ(see Fig. 4.6(a) and (b) respectively) and 1μ(see Fig. 4.7(a) and (b) respectively). The results from the diffusion theory are compared with MC simulation results, and it can be inferred that in case of $l_s = 10\mu$, the agreement is not so perfect as it found in the slab with $l_s = 1\mu$. The disagreement is due to fact that the ratio of the slab thickness

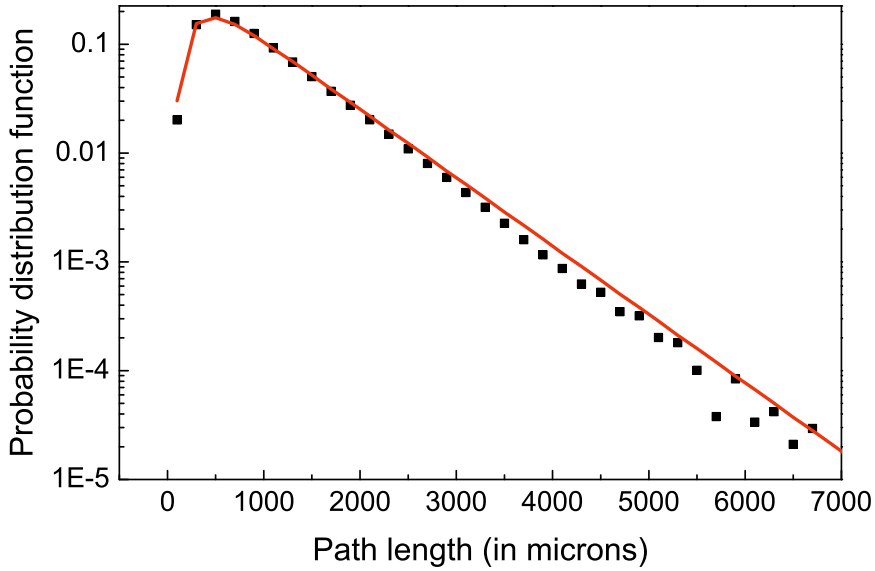

(a) Path length distribution of the transmitted light

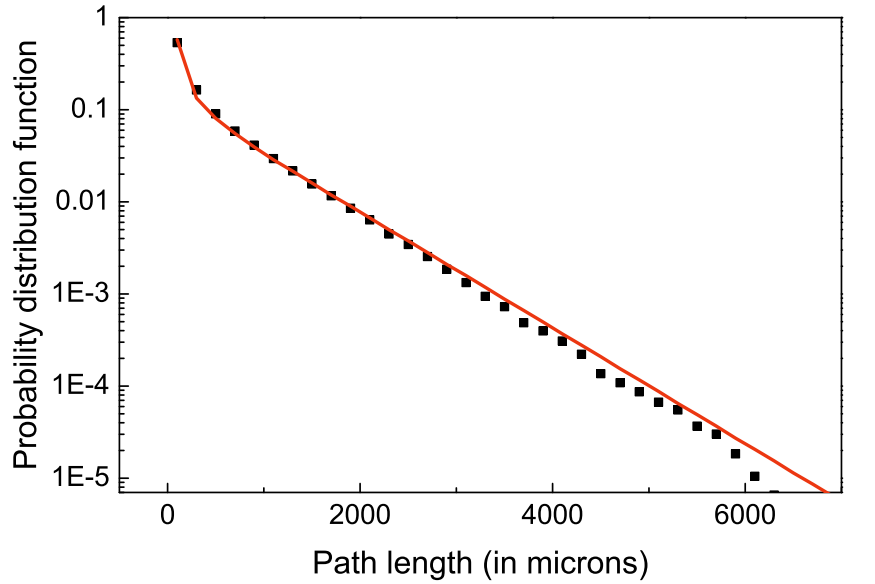

(b) Path length distribution of the reflected light

Figure 4.6: Comparison between the path length distributions of the transmitted and reflected light obtained with the Monte Carlo simulations(black filled square) and analytical expressions from the Contini *et al* work(orange line) [18], through a slab of thickness 100μ with the scattering mean free path of 10μ.

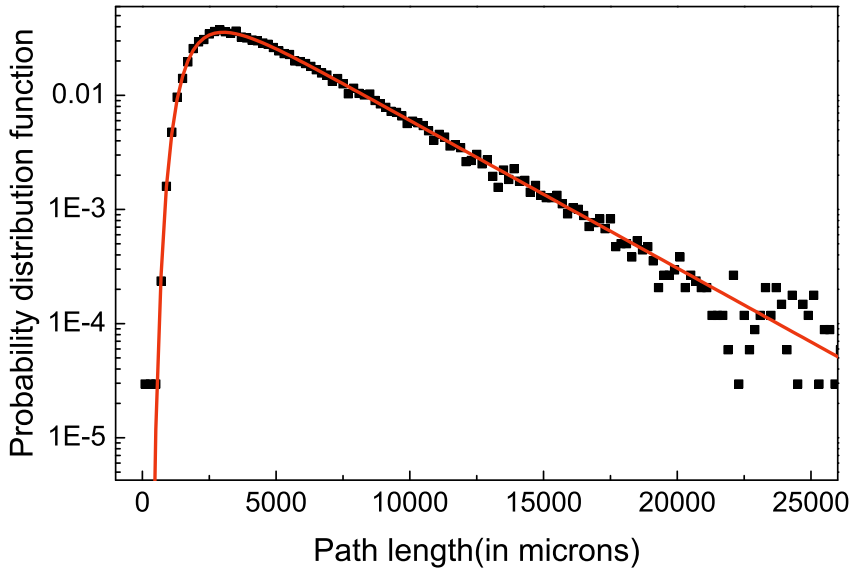

(a) Path length distribution of the transmitted light

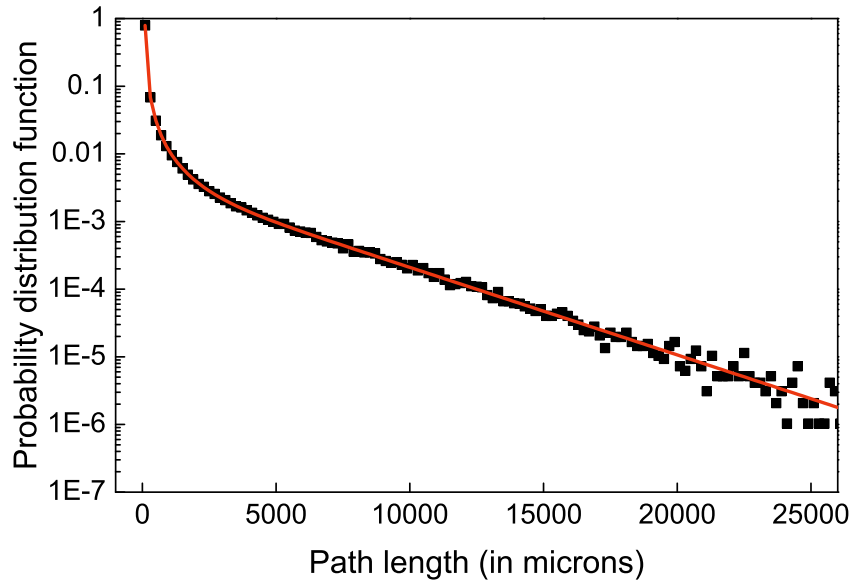

(b) Path length distribution of the reflected light

Figure 4.7: Comparison between the path length distributions of the transmitted and reflected light obtained with the Monte Carlo simulations(black square) and analytical expressions from the Contini *et al* work(orange line), through a slab of thickness 100μ with the scattering mean free path of 1μ.

to the transport mean free path is 10, which falls in the cut-off region where the diffusion just begins to occur [17], hence a small deviation in results of the diffusion theory from the MC simulation is expected, whereas the path length distribution for the slab with the scattering mean free path 1μ is in perfect agreement with the MC simulations.

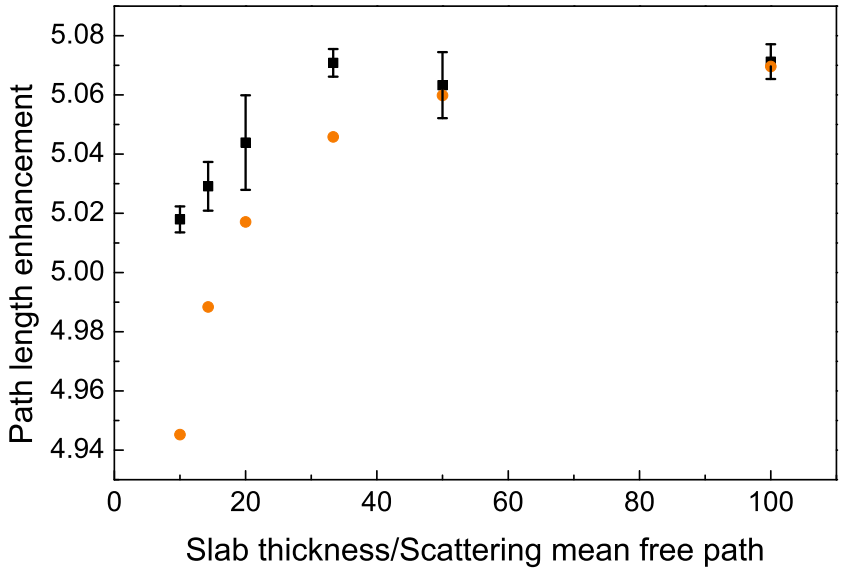

Figure 4.8: Summary of the path length enhancement in the diffusive regime for various values of optical thickness, obtained with MC simulations(black-filled squares) and diffusion theory(red-filled circle).

Similarly, path length distributions are evaluated for various scattering mean free paths in the diffusive regime corresponding to the gray area in the Figure. 4.2, then their mean path lengths are computed. Summarized result of the path length enhancement obtained with the theory and MC simulations is plotted for various values of optical thickness, see in the Fig. 4.8.

The good agreement between MC simulations and diffusion theory in the strongly scattering regime can be observed in the Figure. 4.8, while for slab thickness/scattering mean free path ratios smaller than 20, a partial disagreement is evident, however the deviation of the theory with MC simulations is very small.

4.4 Absorption enhancement

In an absorbing medium, absorption enhancement can be more useful information than the path length enhancement. It was demonstrated in the previous sections that the optical path length can be enhanced significantly even in a weakly scattering and non-absorbing medium. The path length enhancement presented in previous sections can not be directly translated in to the absorption enhancement. In weakly scattering regime, significant contribution to the path length enhancement is attributed to rare events of multiple scattering, and internally reflected events. Since the medium chosen was a non-absorbing, so it means that the events which were making extremely long path lengths probably would have absorbed at a certain shorter path length. In this section, I discuss the absorption enhancement in weakly scattering and strongly scattering regimes.

The absorption of a medium is defined by a characteristic length called absorption mean free path, which is an average distance travelled by a photon before being absorbed. The amount of light absorbed in a medium with a certain optical length L, and the absorption mean free path l_i is given by the Beer-Lambert law:

$$A = 1 - exp(-\frac{L}{l_i}) \tag{4.16}$$

Whereas each photon propagating through a scattering medium makes different path length. From the given sample space of path lengths, path length distribution is constructed by assigning a probability density to each discrete variable. The absorption of light in an absorbing medium can be calculated using the alternative form of (4.16) which includes the path length distribution P(l)

$$A = 1 - \int \mathrm{P}(l)\ exp\left(-\frac{l}{l_i}\right)\ \mathrm{d}l. \tag{4.17}$$

And the absorption enhancement is given by

$$\gamma = \frac{1 - \int \mathrm{P}(l)\ exp\left(-\frac{l}{l_i}\right)\ \mathrm{d}l}{1 - \left[exp\left(-\frac{\mathrm{L}}{l_i}\right)(1-r) + exp\left(-\frac{2\mathrm{L}}{l_i}\right)r\right]}. \tag{4.18}$$

Using the expression (4.18), absorption enhancement is calculated by substituting the path length distributions recorded earlier in MC simulations for a set of scattering mean free paths, for different ratios of the absorption mean

free path to slab thickness (L/l_i= 1, 0.1, 0.01). Calculated absorption enhancement results are plotted in the Figure. 4.9, where it can be observed that absorption is not enhanced at smaller optical thicknesses(weakly scattering regime) for all the three ratios of the slab thickness to the absorption mean free path even though the path length enhancement was significant in weakly scattering regime. Which further validates that the significant enhancement to path length comes from the extremely long path lengths due to the rare multiple scattering events and photons which are reflected inside the slab for multiple times. However, a significant absorption enhancement occurs in a intermediate scattering regime(larger values of optical thickness), which can be called as optimal scattering regime. And, it is worth note that, absorption is enhanced by nearly 30% in optimal scattering regime even though the medium absorbs very strongly without even adding scatterers. Absorption enhancement calculated for scattering mean free paths associated to strongly scattering regime are represented by larger values of optical thickness. As can be observed that the enhancement decreases with the decrease in the scattering mean free path, and even goes less than one. This is due to two reasons: first, light tends to reflect strongly in the backward direction in a strongly scattering media, in effect the distribution of path lengths the medium is shifted towards the smaller path lengths than slab thickness. Second, absorption prevents the propagation of photons deep in to the medium.

In a very weakly absorbing medium ($l \ll l_i$), the exponential term in the expression eq.(4.17) becomes $(1 - \dfrac{l}{l_i})$, so the absorption enhancement becomes

$$\gamma = \frac{1 - [\mathrm{P}(l_1)(1 - \frac{l_1}{l_i}) + \mathrm{P}(l_2)(1 - \frac{l_2}{l_i}) + \mathrm{P}(l_3)(1 - \frac{l_3}{l_i}) + ...]}{1 - (1 - \frac{\mathrm{L}}{l_i})}, \tag{4.19a}$$

$$= \frac{1 - [(\mathrm{P}(l_1) + \mathrm{P}(l_2) + \mathrm{P}(l_3) + ...) - (\frac{1}{l_i})(\mathrm{P}(l_1)l_1 + \mathrm{P}(l_2)l_2 + \mathrm{P}(l_3)l_3 + ...)]}{1 - (1 - \frac{\mathrm{L}}{l_i})}, \tag{4.19b}$$

with,

$$\mathrm{P}(l_1) + \mathrm{P}(l_2) + \mathrm{P}(l_3) + ... + \mathrm{P}(l_n) = 1, \tag{4.20a}$$

$$\text{and} \quad \mathrm{P}(l_1)l_1 + \mathrm{P}(l_2)l_2 + \mathrm{P}(l_3)l_3 + ... + \mathrm{P}(l_n)l_n = \overline{l}. \tag{4.20b}$$

Substituting the expressions (4.20a) and (4.20b) in (4.19b), then what we

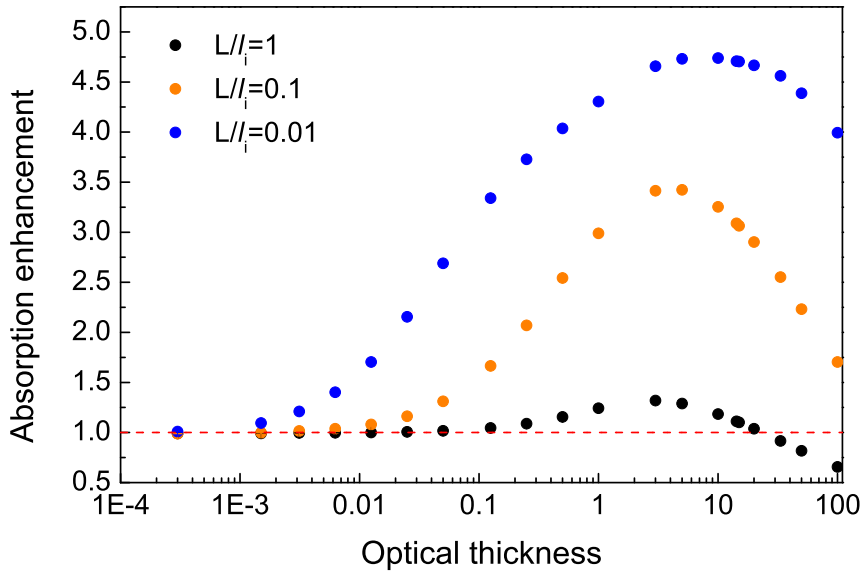

Figure 4.9: Absorption enhancement that can occur in a slab with different amount of absorption defined by L/l_i, due to the light scattering by point scatterers in a slab, and concentration of scatterers is defined by their optical thickness(slab thickness/scattering mean free path). The absorption enhancement at lower values of optical thicknesses are same, so the data points represented by red and black filled circles are not visible in the graph. Optimal scattering regime can be seen for optical thicknesses between 1 to 10, where the maximum absorption is occurring. Light at these values of scattering mean free path is exploring maximum space inside the absorbing medium.

get finally is simply a path length enhancement:

$$\gamma = \frac{\bar{l}}{L}, \tag{4.21}$$

which is indeed the upper limit of the enhancement that can be obtained with the given approach. From the results of the absorption enhancement, it is clear that for any concentration of scatterers, and given a certain amount of absorption, absorption enhancement can be calculated accurately. In sum, a clear and complete picture of the path length enhancement approach is presented in this chapter.

4.5 Conclusions

In conclusion, we have shown that a very weak amount of scattering in a slab is enough to obtain the significant path length enhancement that of Yablonovitch limit. Similarly, the optical path length enhancement is computed in the diffusive regime, which found to be enhancing bit more than the Yablonovitch limit owing to the angular selectivity in the illumination. Finally, the absorption enhancement is computed for different regimes of scattering with different amounts of absorption. Absorption enhancement is negligible in weakly scattering regime for finite amount of absorption, which indicates that weak scattering is not sufficient for enhancing the absorption in an absorbing medium. Maximum absorption enhancement is found for optical thicknesses between 1 to 10, which is identified as an optimal scattering regime.

REFERENCES

[1] E. Yablonovitch and G.D. Cody. Intensity enhancement in textured optical sheets for solar cells. *IEEE Transactions on Electron Devices*, 29(2):300 – 305, February 1982.

[2] David Redfield. Multiple pass thin film silicon solar cell. *Applied Physics Letters*, 25(11):647–648, December 1974.

[3] Rajeshkumar Mupparapu, Kevin Vynck, Iacopo Malfanti, Silvia Vignolini, Matteo Burresi, Petra Scudo, Roberto Fusco, and Diederik S Wiersma. Enhanced downconversion of UV light by resonant scattering of aluminum nanoparticles. *Optics Letters*, 37(3):368–370, February 2012.

[4] Lihong Wang, Steven L. Jacques, and Liqiong Zheng. Mcml–monte carlo modeling of light transport in multi-layered tissues. *Comput. Meth. Prog. Bio*, 47:131–146, 1995.

[5] Gilbert N. Plass and George W. Kattawar. Monte carlo calculations of light scattering from clouds. *Applied Optics*, 7(3):415–419, March 1968.

[6] Qiang Lu, Xiaosong Gan, Min Gu, and Qingming Luo. Monte carlo modeling of optical coherence tomography imaging through turbid media. *Applied Optics*, 43(8):1628–1637, March 2004.

[7] Shlomo Havlin and Daniel Ben-Avraham. Diffusion in disordered media. *Advances in Physics*, 36(6):695–798, 1987.

[8] Diederik S. Wiersma and Ad Lagendijk. Light diffusion with gain and random lasers. *Physical Review E*, 54(4):4256–4265, October 1996.

[9] G.E. Evans and B. Jones. The application of monte carlo simulation in finance, economics and operations management. In *2009 WRI World Congress on Computer Science and Information Engineering*, volume 4, pages 379 –383, April 2009.

[10] F. Llopis and I. Tobias. The role of rear surface in thin silicon solar cells. *Solar Energy Materials and Solar Cells*, 87:481–492, May 2005.

[11] Martin A. Green. Lambertian light trapping in textured solar cells and light-emitting diodes: analytical solutions. *Progress in Photovoltaics: Research and Applications*, 10(4):235–241, 2002.

[12] Eli Yablonovitch. Statistical ray optics. *Journal of the Optical Society of America*, 72(7):899–907, July 1982.

[13] Reisfeld Renata. New developments in luminescence for solar energy utilization. *Optical Materials*, 32:850–856, 2010.

[14] Akira Ishimaru. *Wave propagation and scattering in random media*. Wiley-IEEE Press, 1999.

[15] Diederik S. Wiersma. The physics and applications of random lasers. *Nature Physics*, 4(5):359–367, 2008.

[16] Meint P. Van Albada and Ad Lagendijk. Observation of weak localization of light in a random medium. *Physical Review Letters*, 55(24):2692–2695, December 1985.

[17] K. M. Yoo, Feng Liu, and R. R. Alfano. When does the diffusion approximation fail to describe photon transport in random media? *Phys. Rev. Lett.*, 64:2647–2650, 1990.

[18] Daniele Contini, Fabrizio Martelli, and Giovanni Zaccanti. Photon migration through a turbid slab described by a model based on diffusion approximation. i. theory. *Applied Optics*, 36(19):4587–4599, July 1997.

5

Fractal structures to enhance the efficiency of Luminescent solar concentrators

A novel approach using different dispersion regimes of a fractal geometry is proposed to enhance the efficiency of luminescent solar concentrators. The presence of external light coupling and strong light confinement are investigated in a Sierpinski fractal patterned structure using frequency domain calculations, and dynamics of the modes in the fractal structure is investigated using time domain calculations.

Making use of the light scattering and near-field enhancement of metal nanoparticles(NPs) and nanostructures are popular approaches to enhance the absorption of fluorescent molecules, and which have been pursued also to enhance absorption of fluorescent molecules in luminescent solar concentrators [1]. The enhancement achieved with these approaches is significant, nevertheless has some drawbacks too. On the one hand, near-field enhancement is either considered to enhance the excitation field close to fluorescent molecules, or to modify the radiative and non radiative properties of the molecules, however requires a large concentration of nanoparticles [2]. On the other hand, scattering can be used to enhance the path length in an absorbing medium to enhance the absorption, but scattering by the nanoparticles can effect the fluorescence propagation in the medium [3]. Either of the aforementioned approaches can some how effect the emission propagation in a medium and cause the escape of light, as a result losses would increase in LSCs.

Though so many works in the past have made efforts to achieve a high efficiency in LSCs, however no approach has ever tried address all the issues

together. The best strategy would be here is to achieve an increase of photons which couple in to the slab, and a decrease of photons which couple out of the slab. In order to achieve this goal, engineering of dispersion by creating a pattern with high index material is proposed.

5.1 Strategy: Engineering dispersion

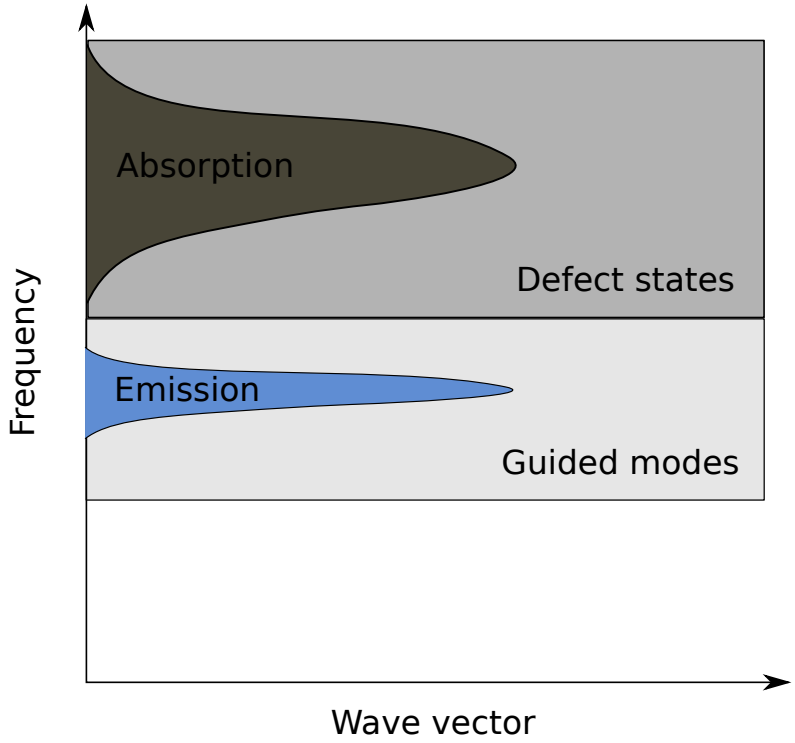

Figure 5.1: Illustration of the scheme to enhance the efficiency of an LSC by making use of two different dispersion regimes supporting either leaky modes or guided modes. The absorption spectrum of fluorescent molecules is matched with the frequencies of leaky modes such that the external excitation light couple efficiently to the slab and interacts sufficiently long time with fluorescent molecules. While the emission spectrum is matched with the frequencies of guided modes of the slab such that emitted light is guided efficiently.

What could be a good strategy for enhancing the efficiency of an LSC is to simultaneously achieve the absorption enhancement and good optical waveguiding. First, absorption in an LSC slab can become maximum only when light from the external medium efficiently couples to the slab, and

interacts sufficiently long time with fluorescent molecules in it. The optimal condition for achieving the maximum absorption enhancement in an LSC is to balance light confinement and out-of-plane coupling with the external medium. Second, fluorescence in an LSC slab can be transported efficiently to the edges if it can couple to the guided modes of the slab waveguide, and at the same time finds no leaky mode to couple out of the slab at that frequency. In a typical bare slab waveguide, it is not possible to achieve both out-of-plane coupling and efficient guided transport at the same time, unless the dispersion of the slab is engineered properly in a way to have two consecutive spectral regimes, where one regime that contains leaky modes, other regime that contains guided modes only. The scheme should be to match the absorption band of fluorescent molecules with the frequencies of the defect modes, and their emission band with the guided modes of the slab. The illustration of the scheme is shown in the Fig. 5.1.

Significant changes in the dispersion occurs only when the index of the slab is modulated over a length scale of the order of wavelength of light. There have been some efforts to engineer the dispersion in semiconductor slabs by patterning the slabs with periodic structures [4], semiconductor nanowires [5],and correlated random structures [6] in order to enhance their absorption. Introducing a defect in a two dimensional photonic crystal can create a defect state, which may even appear in the bandgap. If light is coupled to a defect mode in the band gap, light will be confined strongly in a small volume of the cavity since light can not propagate in xy-plane due to the band gap, however it is evanescent in vertical direction. Since the light-matter interaction in these structures occurs in a small volume in and around the cavity, hence periodic geometries can not be desirable for the absorption enhancement of the bulk medium such as an LSC. On the other hand, correlated random structures are easy to realize, and also support leaky and localized modes at different frequencies. However these approaches were demonstrated to enhance the absorption of the slabs of high index materials like silicon of few nanometers thickness. Indeed these studies provide fundamental ideas to solve the issues in LSCs.

5.2 Fractal geometry for engineering dispersion

Keeping all these issues in purview, I propose to use fractal patterns to engineer the dispersion. The application of fractals geometries in LSCs is genuinely novel and is rather challenging. Fractals display very special ge-

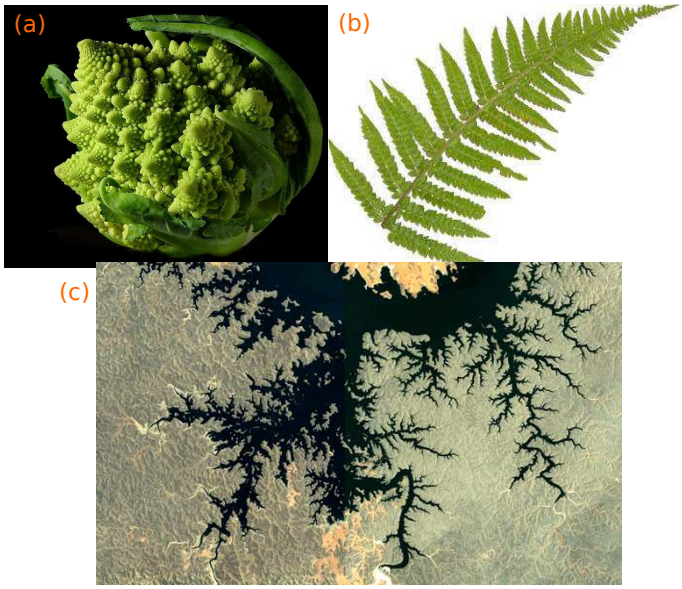

Figure 5.2: Fractals in found in nature (a) Romanesco Broccoli (Image courtesy: Jon Sullivan) (b) Fern plant (c) areal view of vegetation (Image Courtesy: Paul Borke)

ometry which makes them look similar at any scale. Many of the fractal geometries can be simply constructed with the recursion approach, but there are also many fractal geometries which exist in the nature such as in Fig. 5.2. Fractals can be broadly categorized as two major classes depending on their construction approach: deterministic fractals, and random fractals. First, deterministic fractals are those entities which can be constructed with simple mathematical rules and the outcome is always deterministic. Second, random fractals are constructed with probabilistic laws and there can be many or infinite possible outcomes.

Previous studies on the interaction of electromagnetic waves with fractal geometries suggest that self similar features of any multi scale geometry can be reflected in their electromagnetic response, and the response would be broad band [7, 8]. The study on microwaves propagation in three dimensional Menger sponge fractals showed that the waves can be strongly localized inside a fractal cavity, owing to the standing wave formation in the cavities of the fractal and the wave localization was entirely attributed to the fractal geometry [9]. Similarly, giant non-linear optical responses in random fractal cavities were found to strongly enhance the light interaction with the matter [10]. These instances give a strong support to the existence of localized modes and enhanced light-matter interactions inside the fractal cavities.

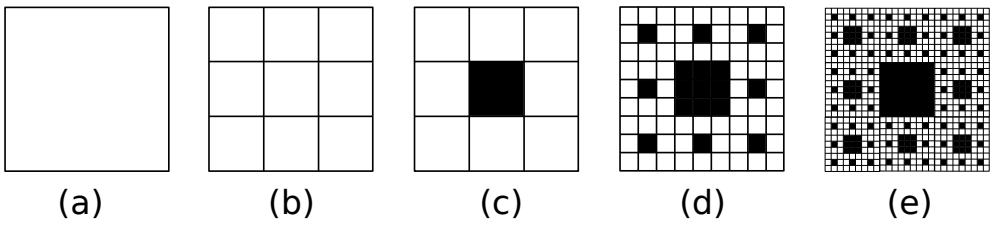

Figure 5.3: Geometries of Sierpinski carpet fractal after different iterations during the construction. The construction begins with a square in (a), then which is divided into 9 subsquares as in (b). Geometries (c),(d), and (e) respectively are Sierpinski carpets obtained after 1,2, and 3 iterations.

However, the fractal geometries considered in these works are difficult to realize because either they are three dimensional structures or random in nature. Sierpinski carpet geometry is chosen for this study to engineer the dispersion of the slab. The application of Sierpinski carpet geometry in the frame work of LSCs is novel, though it has been studied extensively as an antenna in the telecommunications field [7]. Studies on metallic Sierpinski carpets revealed that light can be focused in to a sub-diffraction spot size and confine fields strongly inside the fractal cavities [11]. Sierpinski fractal is a deterministic fractal which can be constructed easily with a recursion approach. Construction begins with a single square(Fig. 5.3(a)), then it is subdivided in to equal sized 9 squares which forms a 3 x 3 grid of small squares(Fig. 5.3(b)), then the one square in the middle is removed thus leaving 8 squares(Fig. 5.3(c)). Again each square in the Fig. 5.3(c) is divided in to 9 subsquares followed by removing one center square, which gives stage 2 Sierpinski carpet as shown in the Fig. 5.3(d)), similarly repeating the method for another time gives stage 3 Sierpinski carpet as shown in the Fig. 5.3(e). This process can be repeated infinite times, however for practical purposes finite number of iterations are considered. In this chapter, I use the convention of calling Sierpinski carpet fractal of n^{th} iteration as stage n Sierpinski carpet.

As a first step, eigenstates supported by the fractal structure were investigated. Studying a fractal patterned LSC slab of thickness of few microns is a computationally difficult task as it would require huge computational cell. Since LSCs are quite thick in the z-direction compared to the geometrical features of the patterns of the order of wavelength of light, by that means the proposed configuration can be approximated as a two dimensional slab, which is an easy configuration to study.

5.3 Band diagrams: Plane wave expansion

Response of any photonic lattice in real space with electromagnetic waves is accurately given by the dispersion relation $w(k)$ in its Fourier space. Dispersion diagram is a map of eigenstates(w) supported by the structure of interest at different wave vectors. Absence of eigenstates or modes at any particular wave vector (k) is typically called as stop gap, while the absence of eigenstates in all directions is called as complete band gap. Any photonic lattice exhibiting a complete band gap would strictly forbid the propagation of light through it in the band gap in any direction. The dispersion calculation of two dimensional Sierpinski carpet structure can provide its complete information of eigenstates, the presence of defect states, leaky modes ,and guided modes, etc.. In general, the dispersion of periodic geometries is calculated using the plane wave expansion method, which is an approach to calculate eigen frequencies out of an eigen value equation. In this study, we used MIT photonic band (MPB) program which implements the plane wave expansion [12] to calculate dispersion diagrams of the two dimensional Sierpinski fractal carpets. In a typical MPB program for any periodic geometry, initially its unit cell in real space and corresponding high symmetry points in the irreducible Brillouin zone are defined, then eigen frequencies are computed at those points. MPB program considers the periodic boundary conditions by default.

As mentioned above, Sierpinski carpet fractals display scale invariant geometry and do not obey translational symmetry. It is not possible to define fractal like single entity with out any periodic boundary conditions in MPB. Henceforth, we use a finite sized approximant of Sierpinski carpet as an unit cell with periodic boundary conditions in MPB. The size of the approximant should be large enough to represent the actual behaviour of the ideal fractal structure. Approximant approach has been studied in quasicrystals which do not display translational symmetry [13]. However the situation in quasicrystals is different, since larger the approximant size closer it represents the ideal quasicrystal. In contrary fractal is a scale invariant geometry, so the approximant of fractal with large number of iterations, closer it represents the ideal fractal. In order to see the changes in the dispersion with an increase in the size of the approximant, we performed dispersion calculations for approximants of different sizes.

Approximant 1 The unit cell of the stage 1 Sierpinski carpet structure is a unit sized square of refractive index as that of polymer 1.5 with one cylinder of finite radius at the center, infinite height in the z dimension, and of refractive index 3.5 as that of silicon, whose illustration is shown in

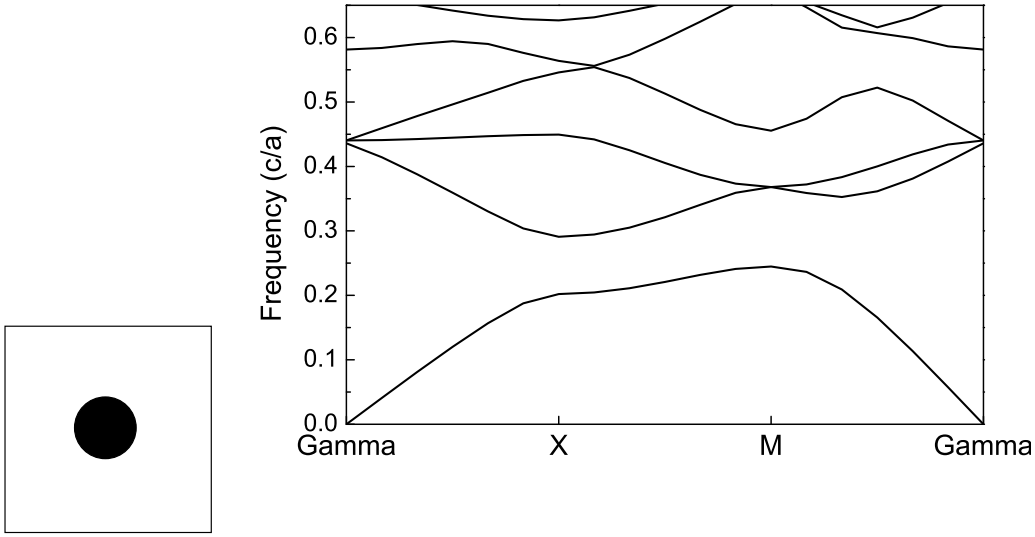

(a) Geometry (b) Band diagram

Figure 5.4: Geometry and band diagram of the stage 1 Sierpinski carpet structure.

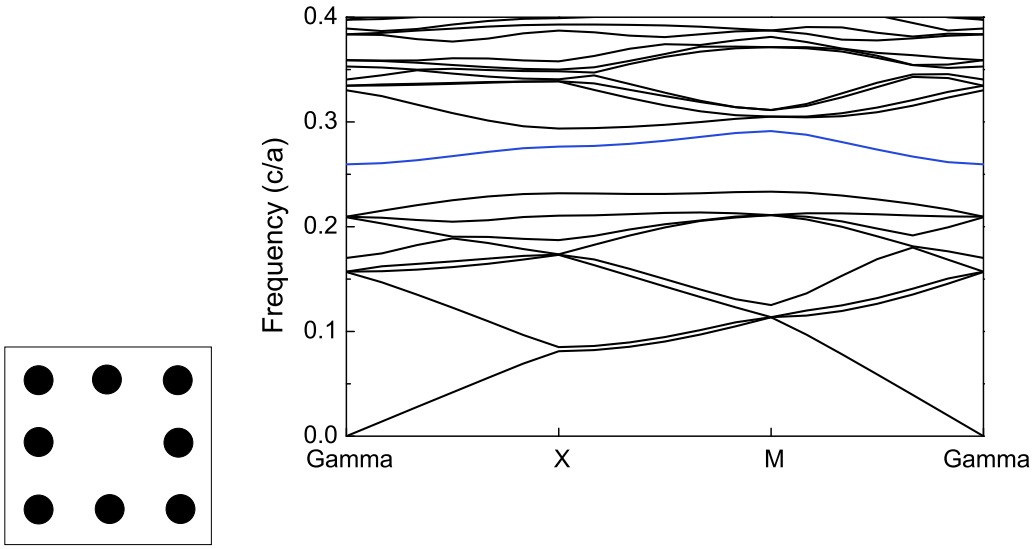

(a) Geometry (b) Band diagram

Figure 5.5: Geometry and band diagram of the stage 2 Sierpinski carpet structure. Blue band represent the defect state.

the Fig. 5.4(a). This geometry is actually equivalent to a unit cell for the square lattice photonic crystal, so it should have the dispersion similar to the dispersion of square lattice. The dispersion calculations were performed by varying different values of the rod width for TE and TM polarizations. The band gap was found only for the TM polarization(see Fig. 5.4(b)), and the maximum gap width was obtained for the rod width equals to 0.25(no units since normalized with the size of the unit cell). In subsequent calculations, cylinder is chosen that of infinite height and radius 0.25.

Approximant 2 The geometry of the stage 2 Sierpinski carpet structure is illustrated in the Fig. 5.5(a) and its the band structure is shown in the Fig. 5.5(b). The approximant 2 is also a photonic crystal with a single defect in the center of the unit cell. The computational cell size of the approximant 2 was thrice larger than cell used for the stage one Sierpinski carpet. As the size of the cell becomes larger, the bands fold back proportionately into the Brillouin zone. Which is the reason for the appearance of more number of bands in the same frequency range as that of the band structure of approximant 1. Fig 5.5(b), shows the presence of band gap with the mid frequency 0.26(c/a) due to the underlying square lattice geometry, and the defect state due to the cavity in the middle of the structure.

The concepts demonstrated in photonic crystals with cavities can be directly translated to explain the properties of defect states in the dispersion of fractal structures. Similar to the photonic crystal cavities, light coupled to a defect state stays confined in xy-plane for a short time in the cavity and eventually leak in to the out-of-plane [14]. Light from out-of-plane can easily couple to such defect states of the cavity or light can leak from it to external medium efficiently.

Approximant 3 The geometry of the stage 3 Sierpinski carpet structure is shown in the Fig. 5.6(a)(in the region drawn with the red line), and its band structure is shown in the Fig. 5.6(b). In the Fig 5.6, as can be observed that the number of defect states increased in comparison to the number of defect states in the band gap of approximant 2, which can be attributed to the increase in the number of cavities.

Approximant 4 The geometry of the stage 4 Sierpinski carpet is shown in the Figure 5.6(a) and its band structure is shown in the Fig. 5.7. Since the computational cell to define the approximant 4 demands huge computational power, therefore dispersion is chosen to be calculated only at a single K-vector i.e Gamma point. It can be observed in the band diagram that number of

defect states is increased many more times than in case of smaller approximants. Having so many defect states inside the band gap would allow the light to couple in to the configuration very easily and over a broad range of frequencies. And, it is worth to note that, light coupled to defect states stays confined in the cavities which are present all around the geometry. Cavities are regions supposed to be occupied with material of small refractive index as that of polymer 1.5, hence incorporating fluorescent molecules in polymer occupied regions would greatly increase their absorption efficiency in comparison to fluorescent molecules in an unperturbed configuration. Analysis of the dispersion diagram of stage 4 Sierpinski carpet gives a positive indication that the coupling from the out-of-plane can be increased by fractal geometries. However, the maximum absorption enhancement can occur only if both out-of-plane coupling and good field confinement occurs at a same time in a balanced way, hence there is need to verify whether the fields are confined.

5.4 Electric fields analysis

Increase in out-of-plane coupling with the slab configuration is not just enough to enhance the light-matter interaction, light should also spend sufficient time in the slab before it escapes out of the slab. In order to investigate whether light is confining in the cavities of the Sierpinski structure, electric fields were calculated using a MPB program.

The propagation and confinement of modes inside a Sierpinski carpet structure can be better inferred from the maps of the fields. The MPB program is also capable of calculating the fields, time average energy densities at any given K-vector for any polarization of the field. The maps of electric field(Ez) in the third and fourth stage Sierpinski carpet structures were calculated for TM polarization at the K-vector gamma point, and the summarized plot of the field maps at few selected frequencies is presented in the Figure. 5.8.

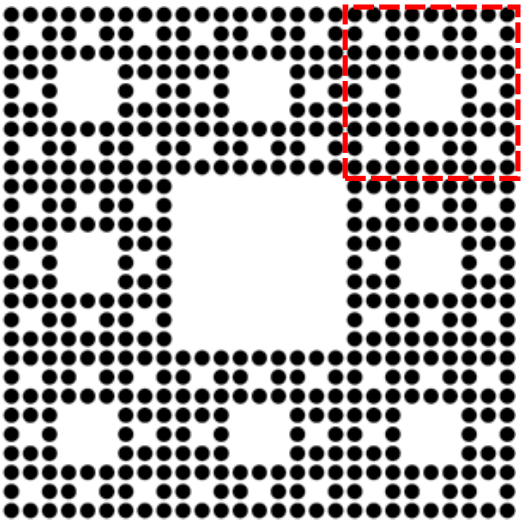

(a) Illustration of the stage 3 Sierpinski carpet(shown in the red squared region) and stage 4 Sierpinski carpet

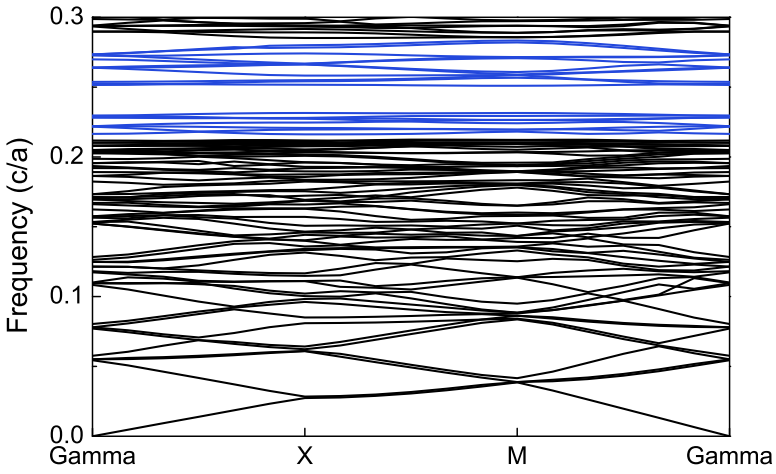

(b) The band diagram of the stage 3 Sierpinski carpet structure. Blue bands represent the defect states in the band gap.

Figure 5.6

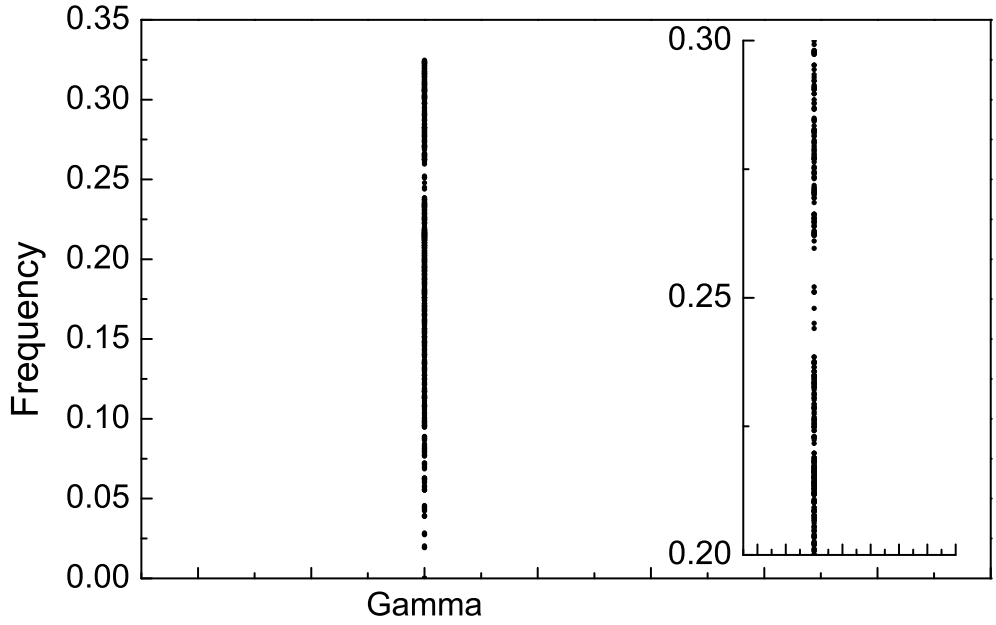

Figure 5.7: The band diagram of the stage 4 Sierpinski carpet structure. Inset shows a close view of the band gap and defect states present in the band gap

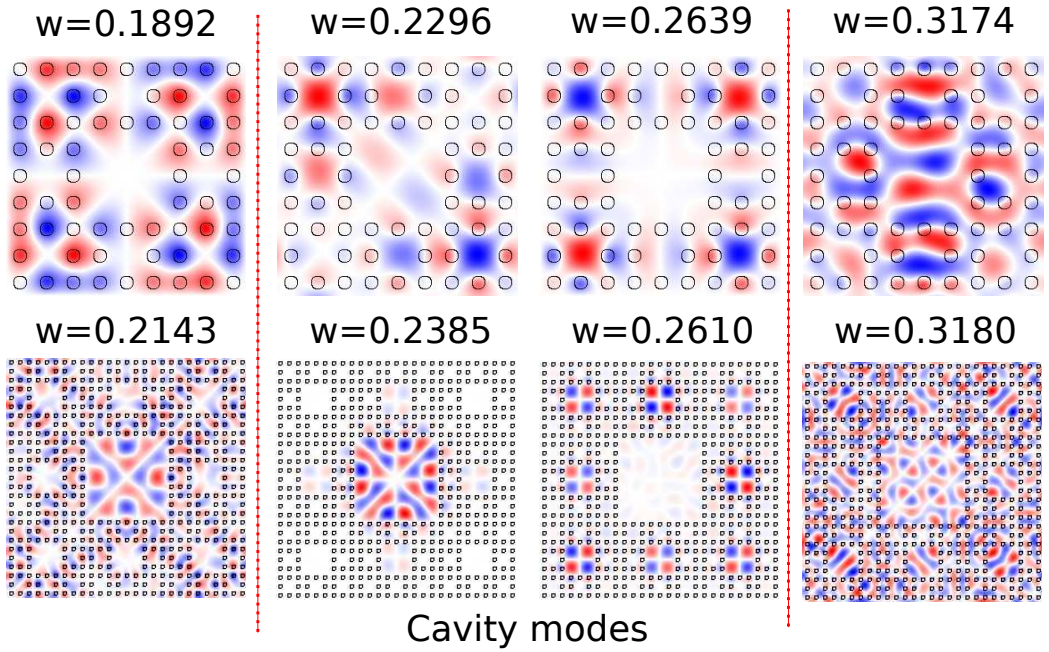

Figure 5.8: The maps of electric field(Ez) acquired in the stage 3 Sierpinski carpet(first row) and stage 4 Sierpinski carpet(second row). Dashed lines separate the maps of different frequencies in the dispersion: frequencies below the band gap, frequencies correspond to defect states in the band gap, and frequencies above the gap.

The maps of fields for frequencies corresponding to the defect states in the band gap clearly confirm that the fields are strongly confined in the cavities of the structure. From the Figure. 5.8, it can be observed that the fields at frequencies below the gap are occupying in large index cylinders to minimize their frequency. While the fields at frequencies above the band gap are occupying in lower index regions in order to be orthogonal to the lower bands. These both behaviours below and above the gap are very similar to what is typically known in photonic crystals [14].

As discussed in the beginning that one of our primary interest is to enhance the absorption of fluorescent molecules in a slab patterned with Sierpinski carpet structure. In the proposed configuration, fluorescent molecules can be added to the polymer which is occupying the space around the high index cylinders. Since the field confinement occurs in those cavities which are occupied by the fluorescent polymer, hence an increase in excitation due to enhanced fields would significantly enhance the absorption of fluorescent molecules.

5.5 K-Space analysis

The dispersion calculations of the Sierpinski carpet structures provided valuable information about the modes supported by the structure. However, information of modes obtained from the maps of fields is hidden and coupled. In general, each one of the modes supported by the photonic structure is associated with an amplitude, direction and a wave vector($\mathbf{k}$). Since many modes of the fractal structure are excited at a same time, and probably they propagate in the same direction or localized in the real space and time, hence it would be impossible to decouple the information of individual modes. However, it is possible to uncover the information of individual modes in the Fourier space, which contains the information of wave vectors corresponding to each mode. K-space investigations of the modes inside a direction coupler in photonic crystal [15], two dimensional random structures [6] have already provided the insights of the dynamics of modes in those structures. Resolution in K-space is given by the simple relation

$$\triangle \mathbf{k} = \left(\frac{-\mathbf{k}}{a} \right) \triangle a, \tag{5.1}$$

where $\mathbf{k}$ is the wave vector of the mode and a is the size of the unit cell in real space. It is clear from the expression (5.1) that the resolution in $\mathbf{k}$-space can be increased by increasing the size of the unit cell(a) of the lattice in real space. Hence, to have a high resolution in K-space, stage 4 Sierpinski

carpet structure of size 81×81 is chosen, which is larger than the size used in dispersion and field calculations.

K-space investigation of modes was implemented with a Finite Difference Time Domain(FDTD) free program called meep [16]. FDTD is a numerical approach to calculate the propagation of fields with time in any kind of geometry using the Maxwell equations, defined with certain boundary conditions. FDTD calculations can give a exact picture of the fields inside the geometry at any instant of time. In FDTD calculations, at first a two dimensional unit cell of stage 4 Sierpinski carpet was defined, and periodic boundary conditions were imposed. Three thousand Ez point dipoles were placed randomly across the structure of dimensions 81×81 to excite all the modes supported by the structure at a particular frequency. All the point dipoles were allowed to excite with different phases, thus fields emanating from dipoles across the structure propagate and superpose in a complicated manner and generate a speckle. Images of the fields were acquired for long time after the evolution of the fields inside the structure. Each map of the field contains a real and imaginary components of the field. Two dimensional maps of the electric field(Ez) acquired for different frequencies were Fourier transformed twice and then shifted back such that zero wave vector component moves to center of the array.

Summarized plot of k-space analysis is shown in the Figure. 5.9 for various frequencies. In a single k-plot(norm of the Fourier transform of the electric field components in the z-direction) at any frequency, x and y axes represent the direction of wave propagation in x and y directions respectively. Since the structure is anisotropic, so different anisotropic dynamics of wave vectors for different modes is expected, and hence a summarized plot of wave vectors for all frequencies in a one graph may loose certain information, hence individual k-plots for each frequency are plotted. Wave vector for free space propagation is evaluated for the refractive index of the air medium and drawn as a white color circle in k-plots, which is so called as radiation zone. Position of each pixel on the k-plot represent the wave vector amplitude, and location of pixel with respect to the circle tells whether the mode is a leaky mode or guided mode, and the color of each pixel represents the norm of the Fourier transform of the electric field component in the z-direction. The pixels which lie with in the circle represent the leaky modes or cavity modes which can couple to out-of-plane/air, while the modes which lie above the circle represents the guided modes of the configuration.

It can be observed in k-plots for the frequencies below the band gap(0.22-0.28), light is propagating as a general mode with an equal amplitude$|k|$, since those wavelengths are larger than the geometrical features of the structure, hence modes propagate as if in a unperturbed slab. The k-plots for

frequencies in the band gap display defect states/leaky modes inside the circle associated to light line. The k-plots for frequencies(0.3 and 0.32) above the band gap clearly do not display modes inside the radiation zone. The k-plot for the frequency 0.34 displays some defect states in the circle, which indicates the presence of another band gap at higher frequencies, while fractals are known to display multiple band gaps. However, it was hard to recognize the second band gap from the band diagram of stage 4 Sierpinski carpet. And, macroscopically it can be observed that, there are two different regimes, where in the first regime for frequencies corresponding to band gap, leaky modes are present, which can felicitate the light coupling from free space into the slab. While in the second regime at lower frequencies, modes propagate as a general mode, and find no leaky mode to escape out of the slab, which would enable an efficient light transport inside the slab. The presence of two regimes one after the other suggest the role of fractal geometries in the modification of dispersion. Henceforth, it is possible to modify the dispersion in such a way to enhance the light-matter interaction and transport light efficiently.

It is worth to note that some k-plots have anisotropic k distribution, such as shown in the Figure. 5.9 for the frequency 0.24, which has only two possible directions of propagation. If the emission of dye is coupled to such anisotropic modes, then it would be possible to direct the light propagation only in x and y directions, hence fluorescence will avoid to take longer paths such as diagonal paths, in this manner losses due to scattering and re-absorption can be minimized.

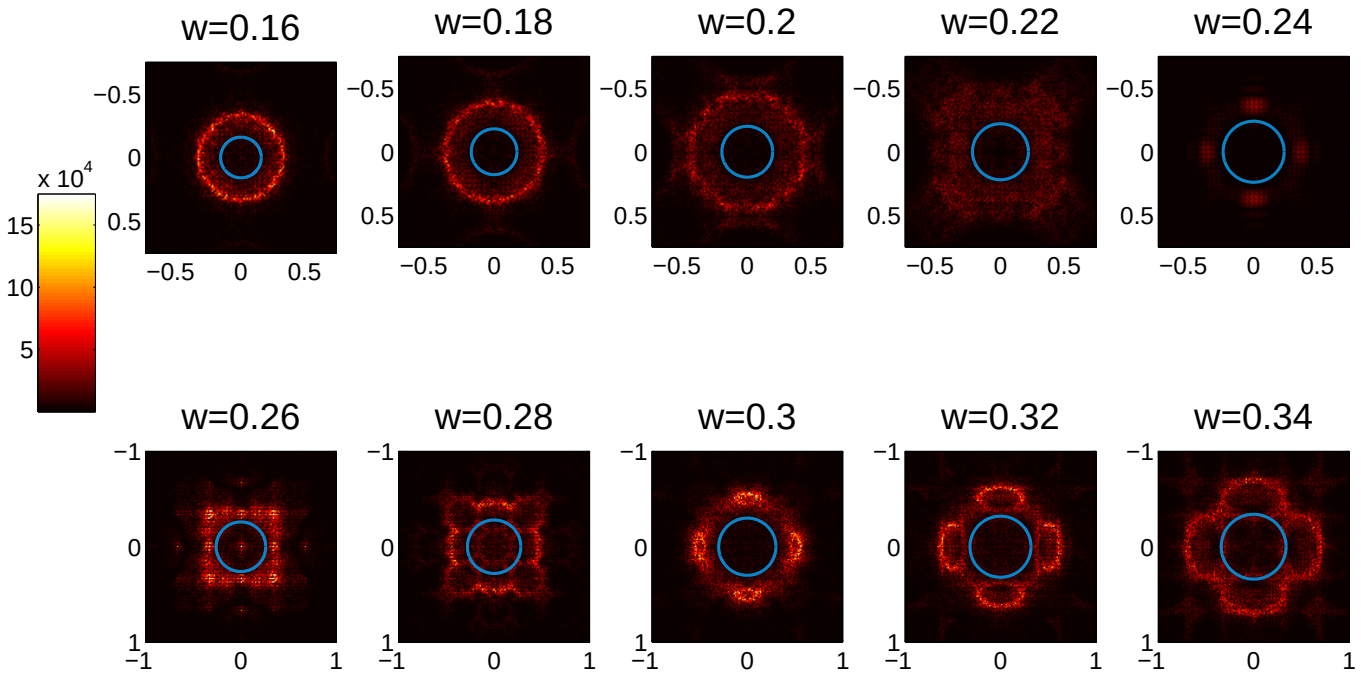

Figure 5.9: Summarized figure of norms of the Fourier transform of the electric field(Ez) distribution for various frequencies. The modes lying within the radiation zone(blue circle) for frequencies 0.26 and 0.28 represent the leaky modes of the geometry. Each k-plot is a representation of wave vectors associated to modes, where x and y axes represent the direction of propagation. Frequencies of respective maps of fields are written above their k-plots.

5.6 Conclusions

Patterning a slab can modify the dispersion of the slab in such a way to have two different spectral regimes, where in one regime defect states are created, and the other regime where modes propagate as a general mode and find no leaky mode to escape out of the slab. These two regimes can be matched with the absorption and emission bands of fluorescent molecules in an LSC, to improve the LSCs efficiency. Presence of localized fields all around the fractal patterned structure at frequencies in the band gap can facilitate an enhancement of of light-matter interaction over the bulk volume, which is a necessary aspect to realize an efficient LSC.

REFERENCES

[1] Renata Reisfeld, Viktoria Levchenko, and Tsiala Saraidarov. Interaction of luminescent dyes with noble metal nanoparticles in organic-inorganic glasses for future luminescent materials. *Polymers for Advanced Technologies*, 22(1):60–64, January 2011.

[2] I. Wayan Sudiarta and Petr Chylek. Mie-scattering formalism for spherical particles embedded in an absorbing medium. *J. Opt. Soc. Am. A*, 18:1275–1278, 2001.

[3] Rajeshkumar Mupparapu, Kevin Vynck, Iacopo Malfanti, Silvia Vignolini, Matteo Burresi, Petra Scudo, Roberto Fusco, and Diederik S Wiersma. Enhanced downconversion of UV light by resonant scattering of aluminum nanoparticles. *Optics Letters*, 37(3):368–370, February 2012.

[4] Yeonsang Park, Emmanuel Drouard, Ounsi El Daif, Xavier Letartre, Pierre Viktorovitch, Alain Fave, Anne Kaminski, Mustapha Lemiti, and Christian Seassal. Absorption enhancement using photonic crystals for silicon thin film solar cells. *Optics Express*, 17(16):14312–14321, August 2009.

[5] Linyou Cao, Justin S. White, Joon-Shik Park, Jon A. Schuller, Bruce M. Clemens, and Mark L. Brongersma. Engineering light absorption in semiconductor nanowire devices. *Nature Materials*, 8(8):643–647, 2009.

[6] Kevin Vynck, Matteo Burresi, Francesco Riboli, and Diederik S. Wiersma. Photon management in two-dimensional disordered media. *Nature Materials*, 11:1017–1022, 2012.

[7] C. Puente, J. Romeu, R. Pous, X. Garcia, and F. Benitez. Fractal multiband antenna based on the sierpinski gasket. *Electronics Letters*, 32(1):1 –2, January 1996.

[8] F. Frezza, L. Pajewski, and G. Schettini. Fractal two-dimensional electromagnetic band-gap structures. In *Microwave Symposium Digest, 2003 IEEE MTT-S International*, volume 2, pages 825 – 828 vol.2, June 2003.

[9] Mitsuo Wada Takeda, Soshu Kirihara, Yoshinari Miyamoto, Kazuaki Sakoda, and Katsuya Honda. Localization of electromagnetic waves in three-dimensional fractal cavities. *Physical Review Letters*, 92(9):093902, March 2004.

[10] W. Kim, V. P. Safonov, V. M. Shalaev, and R. L. Armstrong. Fractals in microcavities: Giant coupled, multiplicative enhancement of optical responses. *Physical Review Letters*, 82(24):4811–4814, June 1999.

[11] Giorgio Volpe, Giovanni Volpe, and Romain Quidant. Fractal plasmonics: subdiffraction focusing and broadband spectral response by a sierpinski nanocarpet. *Optics Express*, 19(4):3612–3618, February 2011.

[12] Steven Johnson and John Joannopoulos. Block-iterative frequency-domain methods for maxwell's equations in a planewave basis. *Optics Express*, 8(3):173–190, January 2001.

[13] Weining Man. *Photonic Quasicrystals and Random Ellipsoid Packings: Experimental Geometry in Condensed Matter Physics*. PhD thesis, Princeton University, 2005.

[14] John D. Joannopoulos, Steven G. Johnson, Joshua N. Winn, and Robert D. Meade. *Photonic Crystals: Molding the Flow of Light (Second Edition)*. Princeton University Press, February 2008.

[15] Rob J. P. Engelen, Yoshimasa Sugimoto, Henkjan Gersen, Naoki Ikeda, Kiyoshi Asakawa, and L. (Kobus) Kuipers. Ultrafast evolution of photonic eigenstates in k-space. *Nature Physics*, 3(6):401–405, 2007.

[16] Ardavan F. Oskooi, David Roundy, Mihai Ibanescu, Peter Bermel, J.D. Joannopoulos, and Steven G. Johnson. Meep: A flexible free-software package for electromagnetic simulations by the FDTD method. *Computer Physics Communications*, 181(3):687–702, March 2010.

A

Appendix

A.1 Algorithm of Monte Carlo simulation of a random walker in a thin slab with absorbing boundary conditions

The definitions of parameters used in the algorithm are as follows: x1, y1, z1, x2, y2, z2 are the Cartesian coordinates of a photon, ux1, uy1, uz1, ux2, uy2, uz2 are the directional cosines of a photon, s is the step length, p is the path length, L is the slab thickness, λ is the scattering mean free path, γ is the random number between [0,1] and d is the distance to the edge of the slab.

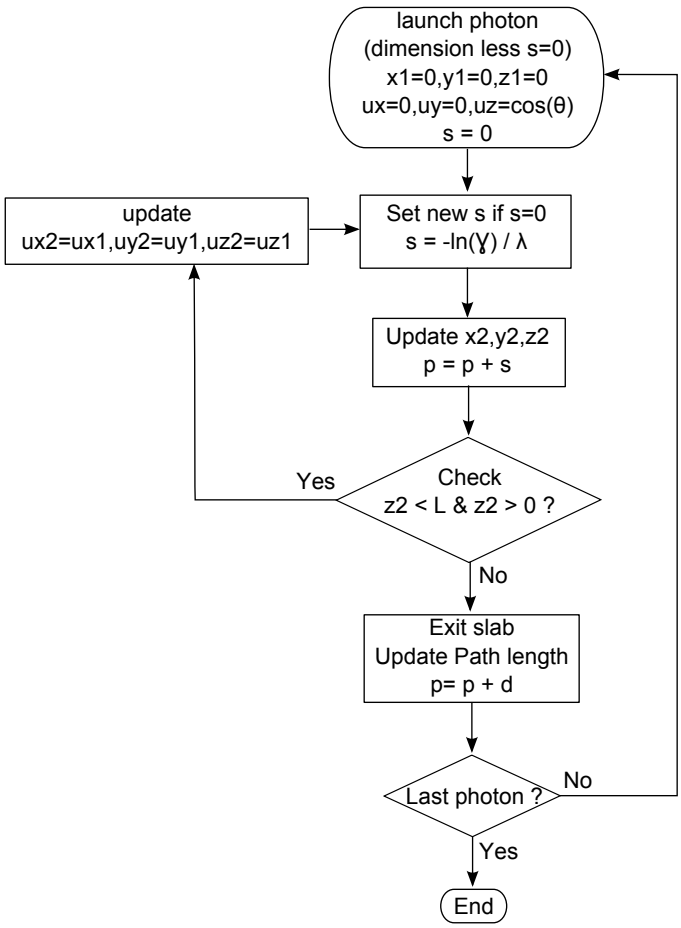

Figure A.1: Schematic diagram of the algorithm followed in Monte Carlo simulations of a random walker in a thin slab dispersed with point scatterers. Absorbing boundary conditions are imposed on the edges of the slab, thereby all the random walkers touching or crossing the slab edges are considered as absorbed.

A.2 Algorithm of Monte Carlo simulation of a random walker in a thin slab with reflecting boundary conditions

The definitions of parameters used in the algorithm are as follows: x1, y1, z1, x2, y2, z2 are the Cartesian coordinates of a photon, ux1, uy1, uz1, ux2, uy2, uz2 are the directional cosines of a photon, s is the step length, p is the path length, L is the slab thickness, λ is the scattering mean free path, γ is the random number between [0,1], r is the Fresnel reflection coefficient at an angle Φ, and d is the distance to the edge of the slab.

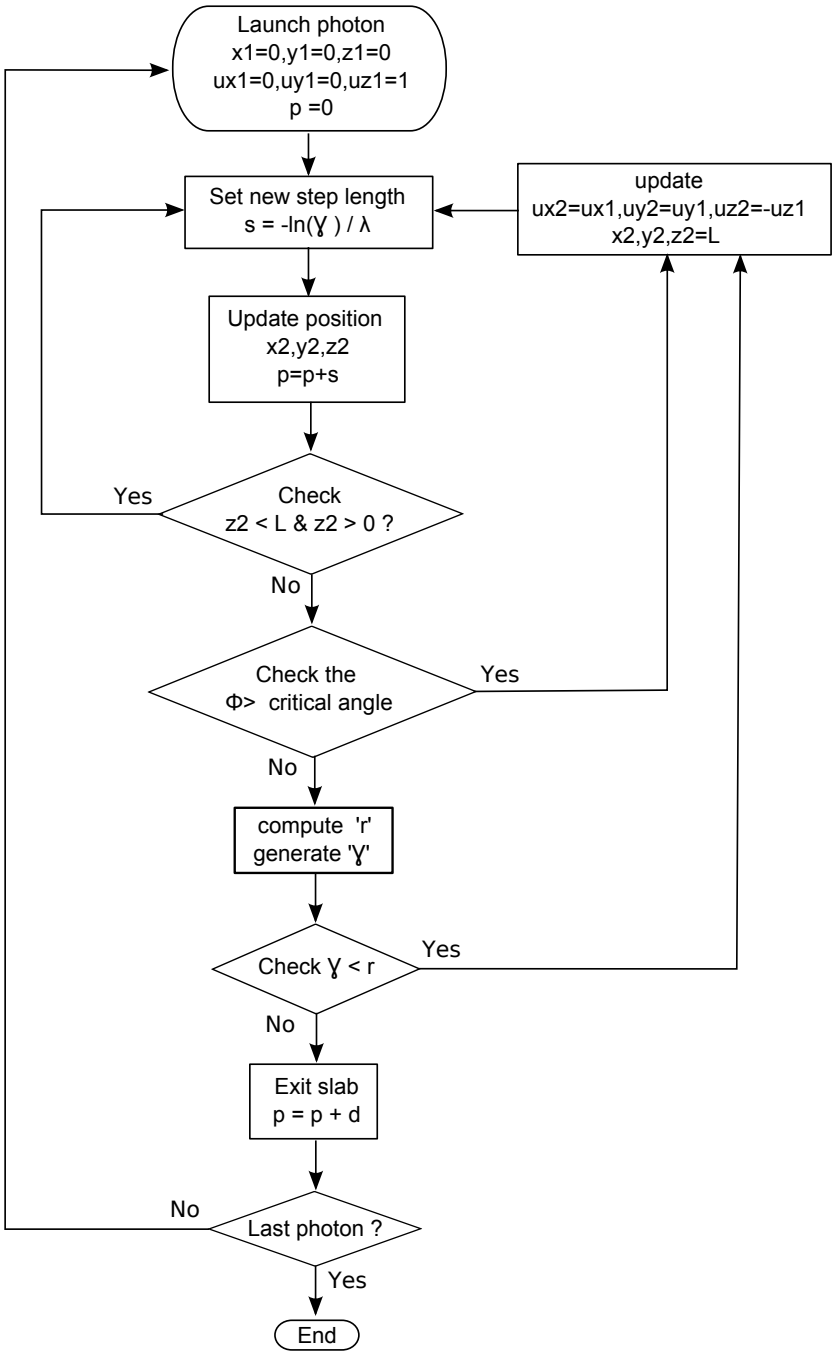

Figure A.2: Schematic diagram of the algorithm followed in Monte Carlo simulations of light propagation in a thin slab dispersed with point scatterers. Reflective boundary conditions are imposed on the edges of the slab, thereby all the random walkers touching or crossing the slab edges are either reflected internally or transmitted based on their angle of incidence with the edges.

A.3 Analytical solutions of time resolved transmission and reflection in a diffusive slab medium

Interaction of wave phenomenon is at best explained by the radiative transfer equation(RTE). RTE is defined by the balance of specific intensity in a volume element of a scattering medium, propagating in space, per unit time, per unit solid angle, per unit area, in a certain direction, with the variation of specific intensity due to the scattering and absorption in that volume element. There are so many models which provide analytical solutions to the RTE, among them diffusion approximation is the most popular approach. It was described in [1], about the mathematical formulation to obtain the diffusion equation. Diffusion equation for the non-absorbing medium is given by the equation

$$\left(\frac{1}{v}\frac{\partial}{\partial t} - Dv^2\right) U_d(\mathbf{r},t) = Q(\mathbf{r},t), \tag{A.1}$$

where $Q(\mathbf{r},t)$ is the isotropic source, D is the diffusion coefficient, U_d is the specific intensity, and v is the velocity of light in the diffusive medium.

Considering the scattering in the medium as isotropic, hence we have

$$D = \frac{1}{3\mu_s}, \tag{A.2}$$

where μ_s is a scattering coefficient (inverse of the scattering mean free path). The diffusion coefficient independent of absorption coefficient works very well for small values of μ_a, otherwise $D = 1/3(\mu_s + \mu_a)$ should be considered. For an isotropic source that emits a pulse of unit energy in an infinitely extended absorbing medium with an absorption coefficient $\exp(-\mu_a vt)$, the general solution of diffusion equation is given by:

$$U_d(\mathbf{r},t) = \frac{v\, exp\left(\frac{|\mathbf{r}-\mathbf{r}'|^2}{4Dvt} - \mu_a vt\right)}{4\pi(4\pi Dvt)^{3/2}}. \tag{A.3}$$

Refractive index contrast can play a critical role in determining the path length distribution inside the diffusive medium, particularly in thin samples. Zhu *et al* [2] have demonstrated that the effect of internal reflection can be accounted with a single parameter i.e refractive index ratio of the medium to the external medium. Considering the internal reflections, diffusion equation can be solved by considering extrapolated boundary conditions, equivalent to specific intensity becomes zero at an extrapolated length z_e outside the

sample. Using the formulations used in the [3], we obtain the extrapolation length $z_e = 2AD$, where A is given by much simplified expression

$$\begin{aligned} A = {} & 504.332889 - 2641.00214n + 5923.699064n^2 - \\ & 7376.355814n^3 + 5507.531041n^4 - 2463.357945n^5 \\ & + 610.95654n^6 - 64.8047n^7, \end{aligned}$$

and n is the relative refractive index of the diffusive medium with the external medium. The source is placed at a depth $z_o = 1/\mu_s$ below the surface where incident photons would have randomized if illuminated normally with the surface. Apart from the source placed at z_o, in order to achieve the extrapolated boundary conditions, infinite pairs of positive and negative dipole sources have to be placed at different positions given by

$$\begin{aligned} z_{+,m} &= 2m(s + 2z_e) + z_o && \text{for positive sources,} \\ z_{-,m} &= 2m(s + 2z_e) - 2z_e - z_o && \text{for negative sources,} \\ m &= (0, \pm 1, \pm 2, ...). \end{aligned}$$

Contribution of positive sources $U_{d+}(\mathbf{r}, t)$ and negative sources $U_{d-}(\mathbf{r}, t)$ together gives the average diffusion intensity:

$$U_d(z, \rho, t) = U_{d+}(z, \rho, t) + U_{d-}(z, \rho, t), \tag{A.4a}$$

$$U_{d+}(z, \rho, t) = \frac{v\ exp(-\mu_a vt - \frac{\rho^2}{4Dvt})}{4\pi(4\pi Dvt)^{3/2}} \times \sum_{m=-\infty}^{m=\infty} exp\left[-\frac{(z - z_{+,m})^2}{4Dvt}\right], \tag{A.4b}$$

$$U_{d-}(z, \rho, t) = -\frac{v\ exp(-\mu_a vt - \frac{\rho^2}{4Dvt})}{4\pi(4\pi Dvt)^{3/2}} \times \sum_{m=-\infty}^{m=\infty} exp\left[-\frac{(z - z_{-,m})^2}{4Dvt}\right], \tag{A.4c}$$

here ρ is the distance of an arbitrary point either on front or on rear surface of the slab from the injection point of the source($z = 0$) or at a position on the z axis($z = L$) at the rear surface. The time resolved reflectance $R(t)$, i.e the power crossing the surface $z = 0$ per unit area is given by

$$R(t) = \int_0^{+\infty} (4\pi D \frac{\partial}{\partial z} U_d(\rho, z = 0, t)) 2\pi\rho \mathrm{d}\rho, \tag{A.5}$$

similarly for the transmittance we have

$$T(t) = \int_0^{+\infty} (-4\pi D \frac{\partial}{\partial z} U_d(\rho, z = L, t)) 2\pi\rho \mathrm{d}\rho. \tag{A.6}$$

Substituting the $U_d(\rho, z = 0, t)$ from eq.(A.4a) in eq.(A.5) and $U_d(\rho, z = L, t)$ from eq.(A.4a) in eq.(A.6), we finally get the time resolved reflectance and transmittance terms, which are

$$R(t) = -\frac{exp(-\mu_a vt)}{2(4\pi Dv)^{1/2}t^{3/2}} \times \sum_{m=-\infty}^{m=\infty} \left(z_{3,m} exp(\frac{z_{3,m}^2}{4Dvt}) - z_{4,m} exp(\frac{z_{4,m}^2}{4Dvt}) \right) \tag{A.7a}$$

$$T(t) = \frac{exp(-\mu_a vt)}{2(4\pi Dv)^{1/2}t^{3/2}} \times \sum_{m=-\infty}^{m=\infty} \left(z_{1,m} exp(\frac{z_{1,m}^2}{4Dvt}) - z_{2,m} exp(\frac{z_{2,m}^2}{4Dvt}) \right) \tag{A.7b}$$

The functions $R(t)$ and $T(t)$ represent the probability density function of reflection and transmission at a time t. Time resolved transmission and reflection in equations (A.7a) and (A.7b) can be simply converted into path length distribution by multiplying with the speed of light in the diffusive medium.

REFERENCES

[1] Akira Ishimaru. *Wave propagation and scattering in random media*. Wiley-IEEE Press, 1999.

[2] J. X. Zhu, D. J. Pine, and D. A. Weitz. Internal reflection of diffusive light in random media. *Physical Review A*, 44(6):3948–3959, September 1991.

[3] Daniele Contini, Fabrizio Martelli, and Giovanni Zaccanti. Photon migration through a turbid slab described by a model based on diffusion approximation. i. theory. *Applied Optics*, 36(19):4587–4599, July 1997.

Conclusions of this thesis

In sum, this thesis has discussed comprehensively about luminescent solar concentrators, their issues, and novel approaches using light scattering to improve their efficiency. Though there have been numerous approaches to enhance absorption/fluorescence of molecules using different kind of systems such as disordered, ordered, and plasmonic structures, and some how they could address particularly poor absorption of the molecules, and only in small volumes, however they fail to address the loss of light in escape cone in the slab or vice versa. In this context, approaches suggested in this thesis simultaneously try to address two basic goals: stronger absorption of fluorescent molecules and efficient fluorescent light transport inside the slab. The conclusions of this thesis can be explained in terms of following points

- The strategy of path length enhancement using aluminum nanoparticles tries to enhance absorption of UV-absorbing molecules, at the same time their emission is allowed to propagate freely inside the slab without any hindrance.

- Though weakly scattering is enhancing optical path length enhancement significantly, but it is not directly translated into significant absorption enhancement. The maximum absorption enhancement for any finite amount of absorption found to occur in a intermediate scattering regime but not diffusive enough. Choosing resonant dielectric nanoparticles, it is possible avoid any effect on fluorescence propagation inside the slab.

- And finally, engineering dispersion of a slab by fractal patterning is suggested as another approach, which rightly addresses the above mentioned goals. Engineering dispersion enables to have two different spectral regimes for the slab, where in one regime, absorption of fluorescent molecules is enhanced over the bulk medium due to leaky modes originated from the fractal pattern and strong confinement of fields in fractal cavities, while in the second regime, fluorescence is is coupled to guided modes of the slab and absence of leaky modes in this regime allow fluorescent light to propagate freely inside the slab.

List of publications and patents

1. Rajeshkumar Mupparapu, Kevin Vynck, Iacopo Malfanti, Silvia Vignolini, Matteo Burresi, Petra Scudo, Roberto Fusco, and Diederik S Wiersma. Enhanced downconversion of UV light by resonant scattering of aluminum nanoparticles. *Optics Letters*, 37(3):368-370, February 2012.

2. Kevin Vynck, Rajeshkumar Mupparapu, Diederik Wiersma. Wavelength converters and luminescent compositions [Patent](deposited).

3. Rajeshkumar Mupparapu, Matteo Burresi, Kevin Vynck, Diederik Wiersma. Luminescent Solar Concentrators [Patent](in process).

Acknowledgements

First and foremost, I would like to express my deep gratitude to my PhD supervisor Diederik, for giving me an opportunity to work in his research group, and for his patient guidance, enthusiastic encouragement throughout the PhD. Under his supervision, I enjoyed complete independence in choosing the topics to work, ideas to implement, I think which really nurtured me to become an independent researcher. I was fortunate to work with various *incredible* post-docs during last four years. I am really grateful to Silvia, for her help and support in the initial period of my PhD and life in Italy. I would like to thank my friend Iacopo Malfanti for his guidance in direct laser writing and Aluminum nanoparticles experiments, and making me aware of *Beetles*. I am particularly grateful to Kevin, who was immensely helpful and offered invaluable assistance, guidance in all my research activities of the PhD, without his help the message delivered in this thesis would not have been complete. I would like extend my gratitude to Matteo for his support in experiments in the lab, I have been quite motivated with his enthusiasm in the lab, building experimental set-ups, handling projects, fun on the whiteboard.

I would like thank all the researchers in the group: Francesca Intonti, Francesco Riboli, and Tomas Svensson for their assistance and valuable suggestions. Special thanks also to all my graduate friends, especially group members: Jean-Christophe (JC), Radha, Romolo, Lorenzo, Filippo, Sepideh, Joyce, Sara, Hao, Giacomo, Marco, and Gora for their friendship and support. I would like to thank all my friends in Florence: Deepa, Vaishali, Malini, Radha, Shashank, Shilesh, Basheer, Bhushan, Vasanth, Avinash, Arka, Sowmya, Polish Tomas, and Spanish Gliarmo. I could live happily in Florence only through their companionship, which made me feel like being with family.

I would also like to convey my sincere acknowledgement to *Regione Toscana* for providing the financial means for initial three years of my PhD. I would like to extend my gratitude to funding agencies "ENI" and "Nanophotonics for energy" for providing the grants for supporting my research activities at LENS. I am very grateful to our collaborators Dr. Roberto Fusco and Dr. Petra Scudo at ENI Novara, for their continuous assistance in implementation of smart window project.

I would also like to extend my thanks to all the technicians in the mechanical workshop, electronic workshop of LENS for their help in building the sample stage(*Chinese tower*), diode laser, sample mounts, solving various other technical issues. I would like to thank Ricardo Tani for his cordial and constant help during last four years.

This PhD journey of incredible four years at LENS have taught me immense number of things in science and life, and have given me chance to meet so many warm hearted people, made me to feel at *home away from home*. I would like to whole heartedly thank each one of them.

Finally, I wish to thank my parents and all my family members for their support and encouragement throughout my study.

Grazie a tutti gli amici, alle persone del Lens e all'ospitalita' italiana. Che bella vita a Firenze ed al Lens!.